

**DEVELOPMENT OF A REGISTRATION FRAMEWORK  
FOR ECHOCARDIOGRAPHY AND COMPUTED  
TOMOGRAPHY CARDIOVASCULAR IMAGE FUSION**

**AZIRA BINTI KHALIL**

**FACULTY OF ENGINEERING  
UNIVERSITY OF MALAYA  
KUALA LUMPUR**

**2018**

**DEVELOPMENT OF A REGISTRATION  
FRAMEWORK FOR ECHOCARDIOGRAPHY AND  
COMPUTED TOMOGRAPHY CARDIOVASCULAR  
IMAGE FUSION**

**AZIRA BINTI KHALIL**

**THESIS SUBMITTED IN FULFILMENT OF THE  
REQUIREMENTS FOR THE DEGREE OF DOCTOR OF  
PHILOSOPHY**

**FACULTY OF ENGINEERING  
UNIVERSITY OF MALAYA  
KUALA LUMPUR**

**2018**

**UNIVERSITY OF MALAYA**  
**ORIGINAL LITERARY WORK DECLARATION**

Name of Candidate: Azira Binti Khalil

Matric No: KHA140008

Name of Degree: Doctor of Philosophy

Title of Project Paper/Research Report/Dissertation/Thesis (“this Work”):

Development of a Registration Framework for Echocardiography and Computed Tomography Cardiovascular Image Fusion

Field of Study: Biomedical Engineering

I do solemnly and sincerely declare that:

- (1) I am the sole author/writer of this Work;
- (2) This Work is original;
- (3) Any use of any work in which copyright exists was done by way of fair dealing and for permitted purposes and any excerpt or extract from, or reference to or reproduction of any copyright work has been disclosed expressly and sufficiently and the title of the Work and its authorship have been acknowledged in this Work;
- (4) I do not have any actual knowledge nor do I ought reasonably to know that the making of this work constitutes an infringement of any copyright work;
- (5) I hereby assign all and every rights in the copyright to this Work to the University of Malaya (“UM”), who henceforth shall be owner of the copyright in this Work and that any reproduction or use in any form or by any means whatsoever is prohibited without the written consent of UM having been first had and obtained;
- (6) I am fully aware that if in the course of making this Work I have infringed any copyright whether intentionally or otherwise, I may be subject to legal action or any other action as may be determined by UM.

Candidate’s Signature

Date:

Subscribed and solemnly declared before,

Witness’s Signature

Date:

Name:

Designation:

## ABSTRACT

Echocardiography and Cardiac CT images are important imaging modalities in diagnosing the cardiac diseases. The image registration and fusion could offer the solution to the physician where the integrated image from these two modalities provide complementary information. This study proposed a registration framework to register 2D echocardiography images with 3D cardiac CT images. The registration facilitates the fusion of CT and echocardiography to aid the diagnosis of aortic and mitral valves diseases. It provides surgical guidance during transcatheter valve replacement (TVR) and implantation (TVI). The developed image registration framework consists of three major steps: temporal registration, noise reduction and spatial registration. Temporal registration allows time stamping of echocardiography time series data to identify frames that are at a similar cardiac phase as the cardiac CT volume data. Next, in the preprocessing phase, the noise of echocardiography image is reduced using the speckle reducing anisotropic diffusion (SRAD) technique. For the spatial registration, an intensity-based normalized mutual information (NMI) method is applied with pattern search optimization algorithm to produce an interpolated cardiac CT image. This registration framework however does not utilize the optical tracking information. The proposed registration method has been applied on the short axis "Mercedes Benz" sign, long parasternal axis and four chamber views of cardiac images from ten patients. The accuracy of the fully automated registration method is  $0.81 \pm 0.08$  and  $1.30 \pm 0.13$  mm in terms of the Dice Similarity Coefficient (DSC) and the Hausdorff distance (HD) for aortic valve respectively. Besides that, for the long body of aorta, the DSC and HD are  $0.79 \pm 0.02$  and  $1.19 \pm 0.11$  mm respectively. DSC and HD for the left atrium assessments are  $0.87 \pm 0.04$  and  $1.23 \pm 0.32$  mm respectively, whereas for left ventricle are  $0.82 \pm 0.07$  and  $1.14 \pm 0.18$  mm respectively. These accuracies are comparable to gold standard manual registration by expert. There was no significant difference in aortic and mitral

annulus diameter measurements between the automatically and manually registered CT images. The transformation parameters showed small deviation (RMSE  $\leq 2.12$  mm deviation in translation and  $<3^\circ$  for rotation) between manual and automatic registration. Without the use of optical tracking, the registration method has shown its applicability for effective fusion of echocardiography with preoperative CT volume data to potentially facilitate catheter-based surgery. Thus, the proposed method enables to aid the physician in diagnosing the aortic and mitral valves disease as well as providing surgical guidance during the treatment procedure of TVR or TVI.

University of Malaya

## ABSTRAK

Imej ultrabunyi dan Tomografi pengkomputeran (CT) adalah modaliti pengimejan yang penting dalam memberi maklumat diagnosis berkaitan penyakit jantung. Imej pendaftaran merupakan satu teknik pemrosesan imej secara digital yang mampu menawarkan penyelesaian kepada pakar perubatan dimana proses imej pendaftaran ini dapat menggabungkan maklumat perubatan dari dua atau lebih modaliti pengimejan. Pakar perubatan boleh mendapatkan maklumat diagnosis penyakit jantung yang lebih lengkap dari integrasi maklumat dari modaliti yang terlibat. Kajian tesis ini mencadangkan satu rangka kerja imej pendaftaran yang dapat mengintegrasikan maklumat dari modaliti ultrabunyi jantung dan CT. Tujuan imej pendaftaran ini, bukan hanya dapat menghasilkan satu gabungan maklumat yang lengkap dari kedua-dua modaliti ini, tapi ia juga dapat memudahkan pakar perubatan dalam perancangan dan bimbingan ketika pembedahan penggantian injap (TVR atau TVI) untuk pesakit injap jantung (injap aortik dan injap mitral). Terdapat tiga langkah utama dalam rangka kerja imej pendaftaran ini iaitu: pemilihan imej melalui pendaftaran temporal, pengurangan artifak dalam imej ultrabunyi dan pendaftaran spatial. Pendaftaran temporal membolehkan imej ultrabunyi dipilih dari rakaman ultrabunyi berdasarkan fasa jantung yang sama dengan pengambilan imej CT. Selepas imej ultrabunyi ini dipilih, proses mengurangkan artifak dilakukan menggunakan teknik "*Speckle Reducing Anisotropic Diffusion*" atau SRAD. Kemudian, imej ultrabunyi didaftarkan ke imej CT melalui pendaftaran spatial. Pendaftaran spatial pula menggunakan kaedah berasaskan "*Normal Mutual Information*" (NMI) yang menggunakan algoritma corak carian imej interpolasi CT jantung yang optimum atau yang sepadan dengan imej echocardiography tersebut. Kaedah imej pendaftaran ini telah diaplikasi terhadap imej paksi pendek "*Mercedes Benz*", paksi panjang parasternal dan imej empat ruang jantung (*four chamber view*) oleh 10 pesakit. Keputusan validasi pekali persamaan dadu (DSC) dan jarak Hausdorff (HD)

telah digunakan keatas empat struktur jantung iaitu injap aortik, badan aorta, atrium kiri dan ventrikel kiri. Bagi injap aortik, keputusan DSC dan HD adalah  $0.81 \pm 0.08$  dan  $1.30 \pm 0.13$  mm masing-masing. Bagi struktur badan aorta pula, keputusan DSC dan HD adalah  $0.79 \pm 0.02$  dan  $1.19 \pm 0.11$  mm masing-masing. Manakala, bagi struktur atrium kiri, keputusan DSC dan HD adalah  $0.87 \pm 0.04$  and  $1.23 \pm 0.32$  mm masing-masing. Struktur ventrikel kiri pula, keputusan DSC dan HD mencatatkan  $0.82 \pm 0.07$  and  $1.14 \pm 0.18$  mm masing-masing. Keputusan ini adalah berdasarkan perbandingan dengan keputusan imej pendaftaran secara manual oleh pakar perubatan dan didapati tidak ada perbezaan yang signifikan. Selain itu, tidak ada perbezaan yang signifikan antara ukuran diameter annulus injap aortik dan mitral antara imej-imej interpolasi CT melalui kaedah yang dicadangkan dengan imej pendaftaran manual oleh pakar perubatan. “*Root Mean Square Error*” atau RMSE juga dihitung untuk membandingkan perbezaan antara parameter dalam transformasi spatial antara teknik yang dicadangkan dengan secara manual oleh pakar perubatan. RMSE yang tercatat adalah kecil ( $RMSE \leq 2.12$  mm untuk translasi dan  $<3^\circ$  untuk sudut dalam tiga paksi). Ini dapat disimpulkan bahawa tanpa menggunakan pengesanan optik, kaedah yang dicadangkan telah menunjukkan imej pendaftaran 2D ultrabunyi dan 3D CT yang berkesan dan berpotensi memudahkan pakar perubatan dalam pembedahan melibatkan pengantian injap aortik dan mitral jantung.

## ACKNOWLEDGEMENTS

Foremost, I would like to express my gratitude to God Almighty, ALLAH SWT for the blessing and mercy he bestowed upon me, so I can accomplish my thesis entitled *“Development of a Registration Framework for Echocardiography and Computed Tomography Cardiovascular Image Fusion”* as the requirement for the Degree of Doctor of Philosophy. This thesis becomes a reality with the kind help and support of many individuals. I would like to extend my sincere thanks to all of them.

Firstly, I would like to express my sincere gratitude to my supervisors, Dr. Lai Khin Wee, Dr. Liew Yih Miin and Dr. Ng Siew Cheok, for the continuous support of my Ph.D study and related research, for their patience, motivation, and immense knowledge. Their guidance helped me in all the time of research and writing of this thesis. I could not have imagined having better advisors and mentors for my Ph.D study.

I would also like to thank Dr. Ahmad Khairuddin from the National Heart Institute, Kuala Lumpur, Malaysia for his valuable discussions and explanations on the medical sciences, which helped me understand various cardiac diseases and treatment procedures. I would also like to express my gratitude to Norfaniza Zabidi from the clinical research department of the institute for the assistance of data collection used in this thesis.

I greatly appreciate the financial support from the University of Malaya Postgraduate Research Grant (PG027-2014B), Ministry of Science, Technology and Innovation Science Fund (01-01- 03-SF0973), and Islamic Science University of Malaysia (USIM/SLAB) for the last three years.

I would also like to thank my colleagues and friends at the University of Malaya for their help and support over the course of my study. I would like to especially thank Amir

Faisal, Fatima Azzahra, Goh Choon Hian and Hanum for the numerous discussions on both research and non-research related matters.

Last, but never least, I would like to express my gratitude towards my family for the encouragement which helped me in the completion of this research and thesis. My beloved and supportive husband, Mohd Azizudin who is always by my side when times I needed him most and helped me a lot in making this study and my loving son, Eiman El Zaeem, who served as my inspiration to pursue this undertaking. Special thanks go to my beloved aunts, Shafia Bibi, Subedah and Shafariyah for continuous support during my Ph.D journey.

This thesis is dedicated to my grandmother and the memory of my beloved grandfather. Thank you for raising me and it is your shining example that I try to emulate in all that I do.

Thank you for everything.

## TABLE OF CONTENTS

Abstract .....	iii
Abstrak .....	v
Acknowledgements .....	vii
Table of Contents .....	ix
List of Figures .....	xiii
List of Tables.....	xv
List of Symbols and Abbreviations.....	xvi
List of Appendices .....	xix
<b>CHAPTER 1: INTRODUCTION.....</b>	<b>1</b>
1.1 Background.....	1
1.2 Problem statement .....	4
1.3 Thesis objectives.....	7
1.4 Thesis contributions.....	8
1.5 Thesis overview.....	9
<b>CHAPTER 2: LITERATURE REVIEW.....</b>	<b>10</b>
2.1 Cardiovascular system.....	10
2.1.1 Anatomy and physiology.....	10
2.1.2 Blood circulation in the heart .....	14
2.1.3 Cardiac cycle and electrical activation .....	15
2.2 Cardiovascular imaging .....	17
2.2.1 Overview of various cardiovascular imaging systems .....	17
2.2.2 Echocardiography.....	22
2.2.3 Cardiac CT .....	25

2.3	Image registration and fusion .....	28
2.3.1	Theory on image registration and fusion.....	28
2.3.2	Multimodal image fusion on cardiac structures .....	31
2.3.2.1	Intramodal cardiac image registration and fusion .....	31
2.3.2.2	Intermodal cardiac image registration and fusion .....	33
2.3.2.3	Image registration of echocardiography and CT .....	35
2.3.2.4	Summary .....	39
<b>CHAPTER 3: METHODOLOGY .....</b>		<b>40</b>
3.1	Data acquisition .....	40
3.1.1	Demographic information .....	41
3.1.2	Cardiac CT acquisition .....	42
3.1.3	Echocardiography acquisition .....	43
3.2	Image registration .....	43
3.2.1	Temporal registration .....	45
3.2.2	Echocardiography noise reduction .....	47
3.2.3	Spatial registration.....	49
3.2.3.1	Spatial transformation .....	51
3.2.3.2	Linear interpolation .....	52
3.2.3.3	Normalized Mutual Information (NMI).....	53
3.2.3.4	Optimization.....	54
3.3	Validation of registration accuracy.....	55
3.3.1	Qualitative assessment of registration accuracy.....	55
3.3.1.1	Defining the gold standard alignment .....	55
3.3.1.2	Overall cardiac CT image quality .....	56
3.3.2	Quantitative assessment of registration accuracy.....	56

3.3.2.1	Manual segmentation .....	57
3.3.2.2	Dice Similarity Coefficient (DSC).....	57
3.3.2.3	Hausdorff distance (HD) .....	58
3.3.2.4	Diameter of aortic and mitral valve annulus measurement.....	58
3.3.2.5	Root mean square error (RMSE).....	59
<b>CHAPTER 4: RESULTS.....</b>		<b>60</b>
4.1	Automatic registration results.....	61
4.2	Comparison between automatic registration and manual registration results .....	62
4.3	DSC and HD results.....	63
4.4	Bland-Altman analysis.....	65
4.5	Transformation analysis.....	66
4.6	Echocardiography and cardiac CT fusion image.....	67
4.7	Registration computation time.....	69
<b>CHAPTER 5: DISCUSSION .....</b>		<b>70</b>
5.1	Major findings of the study.....	70
5.2	Comparison with previous similar studies.....	72
5.3	Clinical relevance of the study .....	73
5.4	Study limitations and suggestion for improvement.....	75
5.4.1	The heart as rigid body structure .....	75
5.4.2	Seed position .....	76
5.4.3	Computation speed .....	77
5.5	Suggestions to improve the current technique.....	77
<b>CHAPTER 6: CONCLUSION AND FUTURE WORK .....</b>		<b>80</b>
6.1	Thesis contribution .....	80

6.2	Conclusions .....	81
6.3	Future work.....	82
6.3.1	Intraoperative guidance of cardiac treatment using echocardiography and cardiac CT fusion .....	82
6.3.2	Comparison of echocardiography-cardiac CT fusion with echocardiography-MRI fusion .....	83
6.3.3	US-CT image fusion for other anatomical structures.....	83
	References .....	85
	List of Publications and Papers Presented .....	97
	Appendix A.....	98

University of Malaya

## LIST OF FIGURES

Figure 1.1: (left) Image of the heart with the position of aortic valve labelled. (right) Comparison between normal and stenotic aortic valve (Healthwise-Incorporated, 2016). .....	2
Figure 1.2: (left) Image of heart with the position of mitral valve labelled. Arrow shows correct flow of blood. (right) Image shows mitral valve prolapse causing blood regurgitation from left ventricle to left atrium. (Healthwise-Incorporated, 2016). .....	3
Figure 2.1: Location of the heart in the thorax (Alexander et al., 1998). .....	11
Figure 2.2: Cross section of the heart walls showing the lining of the cardiac wall (Korpas, 2013) .....	12
Figure 2.3: Anatomy of heart (Kenny, 2013). .....	13
Figure 2.4: Blood circulation in the heart (Kenny, 2013). .....	15
Figure 2.5: ECG signal with PQRST waves and cardiac cycle information. .....	17
Figure 2.6: M-mode imaging along aortic valve structure plane with AO (aorta) and LA (left atrium) locations indicated (García-Fernández & Caso, 2009). .....	22
Figure 2.7: Tomographic planes used in a 2D echocardiographic study. (A) long parasternal axis view; (B) short parasternal axis view; (C) four chamber view (García-Fernández & Caso, 2009). .....	23
Figure 2.8: (a) Long parasternal axis view. Aortic valve (AO); right ventricle (RV); left atrium (LA); mitral valve (MV); (b) left ventricle as visualized in the echo image on the right (García-Fernández & Caso, 2009). .....	23
Figure 2.9: (a) Short parasternal axis view through the base of the heart. Aortic valve (AO), right atrium (RA), right ventricle (RV), left atrium (LA), tricuspid valve (TV), pulmonary valve (PV) and right ventricular outflow tract (RVOT) are visualized in the echo image on the right (b) (García-Fernández & Caso, 2009). .....	24
Figure 2.10: (2) Apical four chamber view. Right ventricle (RV), mitral valve (MV), left ventricle and tricuspid valve (TV) are visualized in the echo images (b) (García-Fernández & Caso, 2009). .....	25
Figure 2.11: Parasternal long-axis view with color flow Doppler during (a) diastolic frame and (b) systolic frame. Aortic valve (AO), right ventricle (RV), left atrium (LA), mitral valve (MV) and left ventricle can be visualized in the figures (García-Fernández & Caso, 2009). .....	25

Figure 2.12: (a) A normal aortic valve with thin, non-calcified cusps (arrows). (b) An oblique view thickening and aortic valve calcifications as well as left ventricular hypertrophy (*). (c) A four chamber view obtained during diastole with an open mitral valve (arrowhead)(Budoff & Shinbane, 2016)).	27
Figure 2.13: $T(x)$ maps the point $x$ in the moving image $R$ to its corresponding position in the fixed image $S$ .	29
Figure 2.14: Basic image registration pipeline (Ibanez et al., 2015).	30
Figure 3.1: Overall registration workflow	44
Figure 3.2: Temporal registration method.	46
Figure 3.3: Spatial registration pipeline.	50
Figure 3.4: Drawing of the estimated seed plane for three different views, which is used to initialize the registration search.	51
Figure 4.1: Automatic registration result. (a) “Mercedes Benz”, (b) long parasternal axis, (c) four chamber views.	61
Figure 4.2: Comparison between automatic registered CT and manually registered CT of three different views. (a) “Mercedes Benz”, (b) long parasternal axis, (c) four chamber views.	62
Figure 4.3: Difference of aortic valve diameter measurement between CT plane from automatic and manual registration method, with 95% limits of agreement (black dotted line) and bias (blue line).	65
Figure 4.4: Difference of mitral valve diameter measurement between CT plane from automatic and manual registration method, with 95% limits of agreement (black dotted line) and bias (blue line).	66
Figure 4.5: Fusion of echocardiography frame and cardiac CT at (a) short axis “Mercedes Benz” sign, (b) long axis parasternal and (c) four chamber views.	68
Figure 5.1: New registration scheme to improve temporal registration.	78
Figure 5.2: New registration scheme to improve spatial registration.	79

## LIST OF TABLES

Table 2.1: Comparison between different cardiovascular imaging procedures .....	21
Table 3.1: Demographic information of patient recruited for this study. ....	41
Table 4.1: Registration accuracy as measured using DSC and HD. ....	64
Table 4.2: RMSE of transformation parameter between automatic and manual registration method.....	67
Table 4.3: Average Computation Time for Automatic Registration of Different Views	69
Table 5.1: Comparison of distance errors in related studies on multimodality registration. .....	73

University of Malaya

## LIST OF SYMBOLS AND ABBREVIATIONS

$\vec{n}$	:	outer normal to the $\partial\Omega$
$p_A(a)$	:	marginal probabilities of cardiac CT
$p_{AB}(a, b)$	:	joint probability of the two images
$p_B(b)$	:	marginal probabilities of echocardiography
$\overline{z(t)}$	:	mean over a region at t.
$ \overline{\eta}_s $	:	number of pixels in the window which amounts to number of neighboring pixels
$\partial\Omega$	:	$\Omega$ border
$\Delta t$	:	time step
$C$	:	diffusion coefficients
$c(q)$	:	a constant value over the entire image
$C_E$	:	east diffusion coefficients
$C_S$	:	south diffusion coefficients
$H(A)$	:	Shannon-Wiener entropies of cardiac CT image
$H(A,B)$	:	joint entropy of the two images
$H(B)$	:	Shannon-Wiener of echocardiography image
$I(A, B)$	:	mutual information metric
$I_{in}(x,y)$	:	input image
$I_{out}(x,y;t)$	:	output image
$n$	:	number of echocardiography frames
$q(x,y;t)$	:	instantaneous coefficient of variation
$q_0(t)$	:	speckle scale function
$R_A$	:	contoured ROI in the 2D CT plane
$R_B$	:	contoured ROI in the echocardiography frames
$R_x$	:	rotation in $x$ -direction
$R_y$	:	rotation in $y$ -direction
$R_z$	:	rotation in $z$ -direction
$S_x$	:	scaling in $x$ -dimension
$S_y$	:	rotation in $y$ -dimension
$T_a$	:	transformation parameter resulted from the proposed algorithm.

$T_m$	:	transformation parameter resulted from expert's manual registration
$t_x$	:	translation in $x$ -direction
$t_y$	:	translation in $y$ -direction
$t_z$	:	translation in $z$ -direction
$u$	:	input image coordinate in $x$
$u'$	:	output image coordinate in $x$
$v$	:	input image coordinate in $y$
$v'$	:	output image coordinate in $y$
$w$	:	input image coordinate in $z$
$w'$	:	output image coordinate in $z$
$\alpha$	:	rotation angle about $x$ axes respectively
$\beta$	:	rotation angle about $y$ axes respectively
$\gamma$	:	rotation angle about $z$ axes respectively
$\Omega$	:	image support
2D	:	two dimensional
3D	:	three dimensional
AV	:	atrioventricular node
CAD	:	coronary artery disease
CoR	:	correlation ratio
CT	:	computed tomography
CXR	:	chest X-ray
DC	:	diverging circle
DS	:	diverging square
DSC	:	dice similarity coefficient
DTW	:	dynamic time warping
E	:	energy of histogram
ECC	:	entropy correlation coefficient
ECG	:	electrocardiogram
EF	:	ejection fraction
GPS	:	generalized pattern search

HD	:	Hausdorff distance
HIFU	:	high intensity focused ultrasound
ICOV	:	instantaneous coefficient of variation
ICP	:	iterative closest point
IVC	:	inferior vena cava
LA	:	left atrium
LV	:	left ventricle
MI	:	mutual information
MPI	:	myocardial perfusion imaging
MRI	:	magnetic resonance imaging
NCC	:	normalized cross correlation
NMI	:	normalized mutual information
PET	:	Positron Emission Tomography
PSMI	:	point similarity measure based on MI
RA	:	right atrium
RMSE	:	root mean square error
ROI	:	region of interest
RV	:	right ventricle
SA	:	sinoatrial node
SM	:	self-adaptive masking
SPECT	:	Single Photon Emission Computed Tomography
SRAD	:	Speckle Reducing Anisotropic Diffusion
SVC	:	superior vena cava
TEE	:	transesophageal echocardiography
TRE	:	target registration error
TVI	:	transcatheter valve implantation
TVR	:	transcatheter valve replacement
US	:	ultrasound
WC	:	Woods criterion

## LIST OF APPENDICES

Appendix A: Ethics Approval Letter.....	98
---	----

University of Malaya

## CHAPTER 1: INTRODUCTION

This chapter provides a brief overview of aortic and mitral valve diseases that require the use of medical imaging for the purpose of the diagnosis, surgical planning and treatment procedure of the diseases. An overview of valve diseases and standard treatment procedures are discussed in Section 1.1. The problem statement of this research is stated in Section 1.2. The motivation behind this research along with research objectives are listed in Section 1.3. Section 1.4 summarizes the contribution of this thesis. The detailed layout of this thesis is provided in Section 1.5.

### 1.1 Background

Heart valve diseases are “mystery killers.” They advance gradually and indistinctly yet are equipped for bringing about sudden and startling demise. In America, more than five millions people are affected by moderate or severe heart valve diseases, and the numbers are expected to increase ("Heart Valve Society of America," 2017). In Asia, heart valve disease is an epidemic (Nobuyoshi et al., 2009) with 0.14 cases per 1000 population in Japan (Kawakita, 1986), 1.86 cases per 1000 population in China (Zhimin et al., 2006), 0.5 cases per 1000 population in Korea (Yoon et al., 1995), 4.54 cases per 1000 population in India (Ahemad et al., 1999) and 1.3 cases per 1000 population in Bangladesh (Ahmed et al., 2005) were reported. A patient can succumb to single or multiple valve diseases. Aortic and mitral valves diseases are the most common heart valve diseases found to affect mankind to date.

The function of the aortic valve is to allow unidirectional flow of blood carrying oxygen from the left ventricle (F. Li et al.) (F. P. Li et al., 2015) to the aorta (Figure 1.1). During ventricular diastole, the aortic valve is closed to prevent the backflow of blood from the aorta to the left ventricle. Whereas during ventricular systole, the aortic valve opens to allow sufficient cardiac output to be channeled from the LV to the aorta for

circulation around the body (Driscoll, 2016). The leakage of blood into the LV (aortic regurgitation) and narrowing of the valve opening (aortic stenosis) are common malfunctions of the aortic valve. Aortic regurgitation could be due to aging, high blood pressure or injury. Aortic stenosis, by contrast, occurs due to the buildup of calcium and scarring (Carabello, 2007; Nishimura, 2002). Both conditions can cause the increase of volume and pressure in the LV, resulting in ventricular hypertrophy and eventually heart failure in untreated cases. The overall burden of disease due to severe aortic stenosis and regurgitation is substantial among the elderly above 70 years old, with estimated 12.4% and 14.6% respectively of this age group (Osnabrugge et al., 2013; Singh et al., 1999).

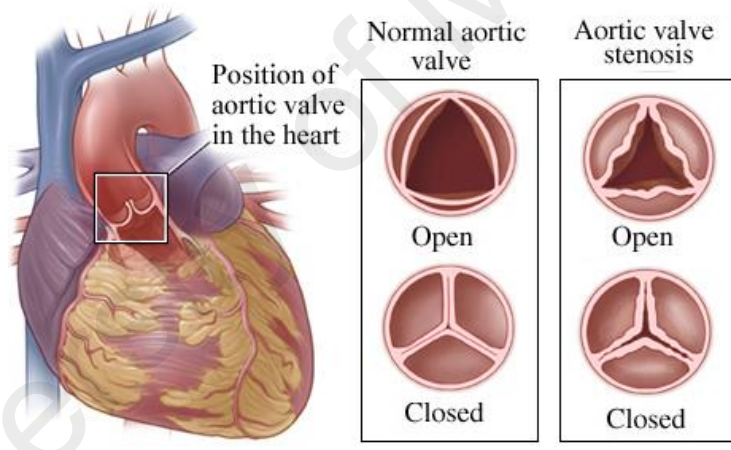


**Figure 1.1: (left) Image of the heart with the position of aortic valve labelled. (right) Comparison between normal and stenotic aortic valve (Healthwise-Incorporated, 2016).**

The mitral valve, on the other hand, is located between the left chambers of the heart, allowing unidirectional blood flow control between the left atrium (LA) and left ventricle (F. Li et al.) (see Figure 1.2) (Ho, 2002) . The performance of the mitral valve can be hampered by stenosis (narrowing of the valve), prolapse (bulging of flaps on the valve) and regurgitation (leakage and backward flow of blood from LV into the LA during LV

contraction at ventricular systole) (Enriquez-Sarano et al., 2007; Turi, 2004). Approximately 10% of the patients in Europe are affected by the mitral valve disease, and the disease remains frequent in developing countries (Iung et al., 2003; Marijon et al., 2007).

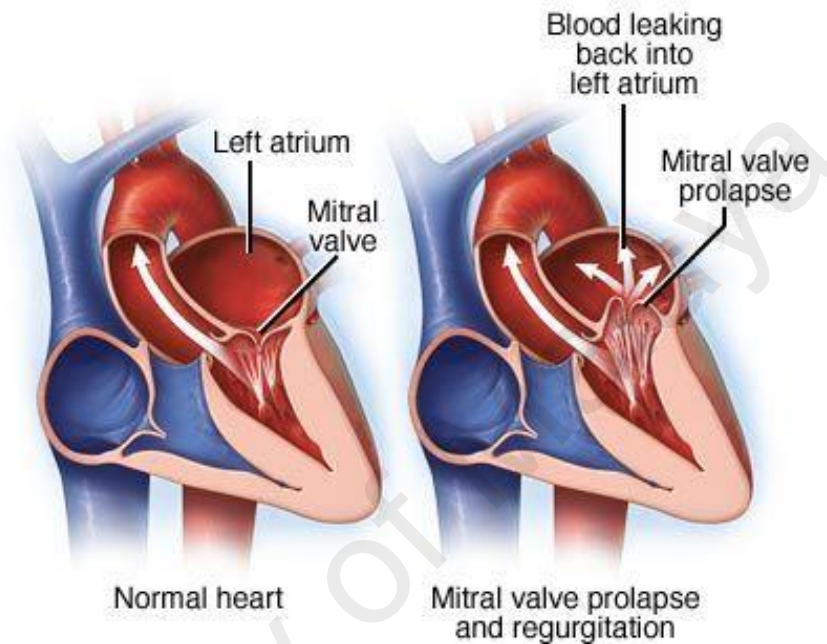


**Figure 1.2: (left) Image of heart with the position of mitral valve labelled. Arrow shows correct flow of blood. (right) Image shows mitral valve prolapse causing blood regurgitation from left ventricle to left atrium. (Healthwise-Incorporated, 2016).**

Catheterization by balloon valvotomy or valve repair surgery are the standard treatment strategies for aortic and mitral valve diseases (Acker et al., 2014; Leon et al., 2010; Slogoff et al., 1990). For many cases, balloon valvuloplasty procedure can treat the valve disease. It is done as part of a cardiac catheterization, which is less invasive than general surgery or open heart surgery. During a balloon valvuloplasty, a small catheter holding an expandable balloon is threaded into the heart and placed into the opening of the stenotic valve which has become stiff due to calcium buildup. The balloon is then expanded to widen the opening of the valve and separate the leaflets. In cases where the valve cannot be successfully treated by balloon valvuloplasty, a different surgical

treatment such as open heart surgery may be used to open the valve and allow better blood flow. During open heart surgery, the physician opens the patient's chest and heart to repair the defective heart valve. This invasive procedure, however, is more risky and may lead to morbidity such as renal injury and stroke (Gardner et al., 1985; Newman et al., 2006).

As an alternative, patients with severe stenosis and at high surgical risk for abovementioned treatment can be prescribed with transcatheter valve replacement (TVR) or implantation (TVI) (Leon et al., 2010). During TVR or TVI, a prosthetic valve is inserted through a catheter and implanted within the affected valve. These minimally invasive treatment procedures have shown to reduce risk and morbidity associated with the open heart surgery (Gardner et al., 1985; Newman et al.).

## **1.2 Problem statement**

Imaging modalities such as echocardiography and cardiac CT are important to diagnose heart valve diseases and to guide treatment procedures. Two-dimensional echocardiography is the primary preoperative imaging modality for assessing valve pathology. Echocardiography can be used to provide anatomical details of aortic and mitral valves, rule out valve regurgitation, as well as measure systolic ejection performance and the extent of wall hypertrophy (Tsang et al., 2015). Other clinical indices provided by this modality include the degree of mitral valve regurgitation and stenosis, annular size, defects of anterior or posterior leaflets, chordal and papillary muscle structural integrity, as well as overall LV size and systolic function (Omran et al., 2010).

Echocardiography has also been used as an intraoperative imaging modality to provide surgical guidance to clinician owing to its real-time *in vivo* functionality. Echocardiography uses high frequency sound wave to probe body tissue, and therefore is not associated with ionizing radiation. It is low cost as compared to other real-time imaging modalities such as fluoroscopy (Hahn, 2013; Omran et al., 2010; Tsang et al.,

2015). Additionally, replacing fluoroscopy with echocardiography for intraoperative image guidance reduces the amount of ionizing radiation received by both patient and clinicians. Another advantage for using echocardiography is that no specialized facilities or room design are required to limit scattered radiation in order to protect the public as in the use of cardiac CT or fluoroscopy for heart examination and intervention. (Hahn, 2013). Echocardiography imaging can be performed in any location suitable for cardiac intervention including the operation theatre. Despite the aforementioned advantages, image quality of echocardiography is confounded by speckle noise and a limited field of view. Therefore it appears inferior as compared to other modalities such as CT or MRI (Grau et al., 2007). Besides, 2D echocardiography provides only planar images. Issues associated with maintaining both the surgical tool and the anatomical targets in the same view during surgery have also been reported (F. P. Li et al., 2015).

Cardiac CT, by contrast, is commonly applied for pre-procedural assessment of valvular dysfunction to select candidate patients for TVR and TVI (Hahn, 2013). The modality provides essential information critical in treatment planning. It allows quantitative assessments of the valve morphology and severity of valvular dysfunction (Messika-Zeitoun et al., 2006). CT has been reported to be useful for identifying complications in patients who have undergone aortic or mitral valve surgery (Morris et al., 2010). However, due to the use of high dose of ionizing radiation, cardiac CT is infeasible to be utilized during the treatment procedure as surgical guidance modality. Cardiac CT is also limited in providing functional information on hemodynamics such as transvalvular pressure gradients and the presence of regurgitation (Chun et al., 2008), which is essential for surgical guidance.

Both echocardiography and CT provide complementary information. These information would benefit the patients if they could be combined to aid cardiac diagnosis and treatment. Multimodality imaging can be achieved by establishing a direct spatial correspondence between both modalities for complementary fusion of anatomical and functional information. Such fusion has good potential to increase the diagnostic accuracy of aortic and mitral valve pathology, as well as facilitating preprocedural planning and intraprocedural guidance for surgical procedures of TVR and TVI. The principle step in this fusion process is to bring the different modalities images into spatial alignment, a procedure called image registration (Mäkelä et al., 2002). However, both imaging modalities uses very different imaging principles and protocols, therefore produce very different images of the same anatomical structure. For example, cardiac CT utilizes x-ray to acquire volumetric images of the patient's heart. Intensities of each tissue types appear homogenous and tissue boundaries are easily identified. On the other hand, echocardiography utilized ultrasound waves to produce 2D cross-sectional images of the heart's structure and functions. Echocardiography images are inherently full of speckle and are acquired at very specific chest locations as the ultrasound transducer has to be carefully angled between patient's ribs for useful imaging. With the target being a dynamic organ, it is very challenging to register 3D cardiac CT and 2D echocardiography images of the moving heart for the purpose of surgical guidance.

### 1.3 Thesis objectives

The main aim of this thesis is to develop an automated 2D to 3D registration framework for the fusion of echocardiography and CT data, specifically targeting to guide aortic and mitral valve surgery. The technique should simultaneously address the issues of temporal synchrony and spatial alignment of moving heart images from intraoperative transthoracic echocardiography and preoperative CT data, offering opportunities for novel ways to display composite structural and functional information from both modalities. .

The specific objectives of this thesis include:

- i. To develop image registration and fusion techniques for the alignment of echocardiography and CT data to aid diagnosis and guide intraprocedural treatment of aortic and mitral valves disease.
- ii. To develop an automatic 2D to 3D registration and fusion framework for three different cardiac views, “*Mercedes Benz*” sign, long parasternal axis and four chamber views, without optical tracking information.
- iii. To validate the accuracy of the registration framework for the guidance of aortic and mitral valve surgery using real clinical data in a retrospective study.

#### **1.4 Thesis contributions**

The main goal of this thesis is to develop an automatic 2D to 3D registration framework for the fusion of intraoperative echocardiography and preoperative CT data. The registration technique targets to improve the diagnostic accuracy of aortic and mitral valves dysfunction, as well as facilitate preprocedural planning and provide intraprocedural guidance during cardiac interventions.

The contribution of this thesis includes:

- i. Introducing a multimodality registration framework for intraprocedural navigation during TVR and TVI treatments of aortic and mitral valve diseases.
- ii. Creating a registration framework for the fusion of preoperative cardiac CT and intraoperative echocardiography images with no optical tracking information provided to aid the process.
- iii. Validating the performance of the proposed registration approach on clinical data sets qualitatively and quantitatively.

## 1.5 Thesis overview

The outline of the thesis is as follows:

Chapter 2 provides a brief overview of cardiac anatomy and physiology. It continues with describing imaging properties of Echocardiography and cardiac CT as well as underlying theories behind medical image registration techniques. This chapter also discusses previous works on echocardiography to CT registration for cardiovascular imaging and other variety of image-guided surgical applications.

Chapter 3 presents information on image acquisition and proposes a novel registration method for echocardiography and cardiac CT fusion. The methods described in this chapter were published in (Khalil et al., 2016, 2017).

Chapter 4 offers various qualitative and quantitative results generated by the automatic registration pipeline presented in Chapter 3. The registration workflow was validated on ten patient data sets.

Chapter 5 contains the discussion on the results of the proposed technique and its clinical impact. This chapter also includes a discussion on the comparison with previous studies. Various limitations of the study are acknowledged and suggestions to improve the current technique are presented in this chapter.

Chapter 6 summarizes the thesis and highlights the main conclusions that can be drawn from this research. Contributions of current research and potential directions for future work are provided.

## **CHAPTER 2: LITERATURE REVIEW**

This chapter discusses basic anatomy and function of the heart as well as describes the main clinical modalities to image the cardiovascular system. This chapter also reviews published works on image registration and fusion related to the heart as well as previous research involving echocardiography and CT.

Understanding of the fundamentals of cardiac anatomy and physiology is essential for the exploration of cardiac imaging. In Section 2.1, the anatomy and physiology of the heart is presented. This will allow a better understanding of the significance of the imaging procedure as well as helpful in the interpretation of the imaging results. In Section 2.2, various cardiovascular imaging modalities are discussed, particularly echocardiography and cardiac CT. Finally, in Section 2.3, image registration and fusion techniques involving multimodality imaging for cardiovascular are presented. In this Section, a critical review on image fusion technology for echocardiography and CT are discussed.

### **2.1 Cardiovascular system**

For a better understanding of this study, a brief review of the heart's anatomy and physiology is presented in the next subsections, including the blood circulation, as well as cardiac cycle and electrical activation of the heart.

#### **2.1.1 Anatomy and physiology**

The heart is a muscular organ in which its function is to pump blood throughout the body via the circulatory system. The weight of an adult heart is approximately 230 – 340 g, depending on the volume of the heart muscle, which varies individually. The heart is positioned between the lungs, located behind the body's thickest bones-the sternum, and the bottom of the heart rests on the diaphragm muscle (see Figure 2.1). About one third

of the heart structure is located to the right of the middle, and the remaining two thirds are located to the left. The average dimensions of the heart are 130 mm in length, 90 mm in width and 60 mm in thickness (Korpas, 2013; Lazo, 2014). The rib cage protects the heart. The lungs, stomach, liver and the intestines (colon) are among structures which are located in close vicinity to the heart (Kenny, 2013).

The heart is encased in a sac or lining, with the opening of the sac adhering to the great vessels entering and exiting the heart. The lining which is the pericardium is composed of two layers: the outermost layer or fibrous pericardium and the innermost layer or serous pericardium. The serous pericardium itself has two layers, the external parietal layer and the internal visceral layer. The visceral layer, or the epicardium, is in direct contact with the actual heart muscle or the myocardium itself. The endocardium lines the inside of the heart (see Figure 2.2) (Applegate, 2013).

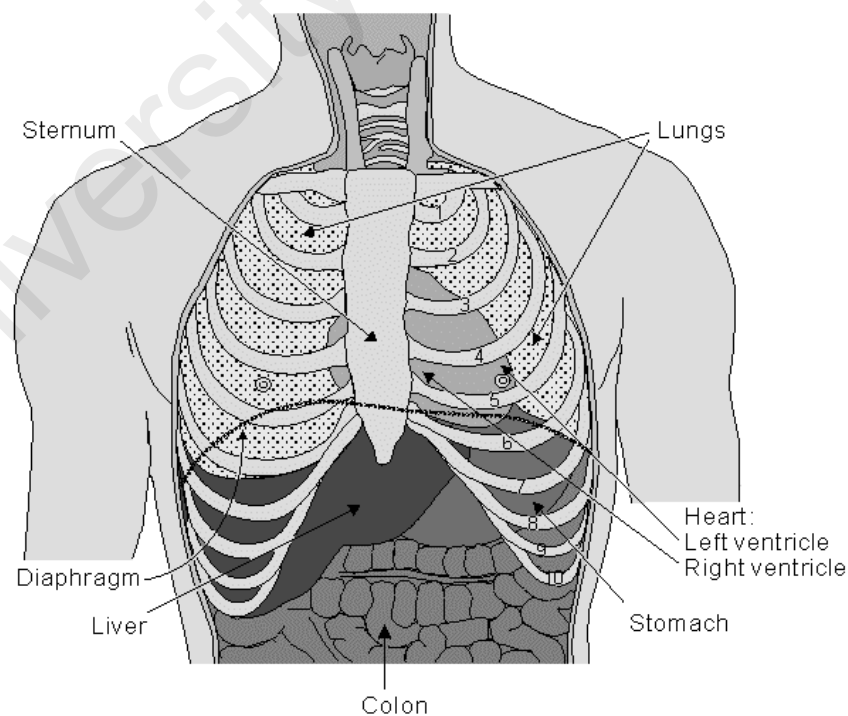


**Figure 2.1: Location of the heart in the thorax (Alexander et al., 1998).**

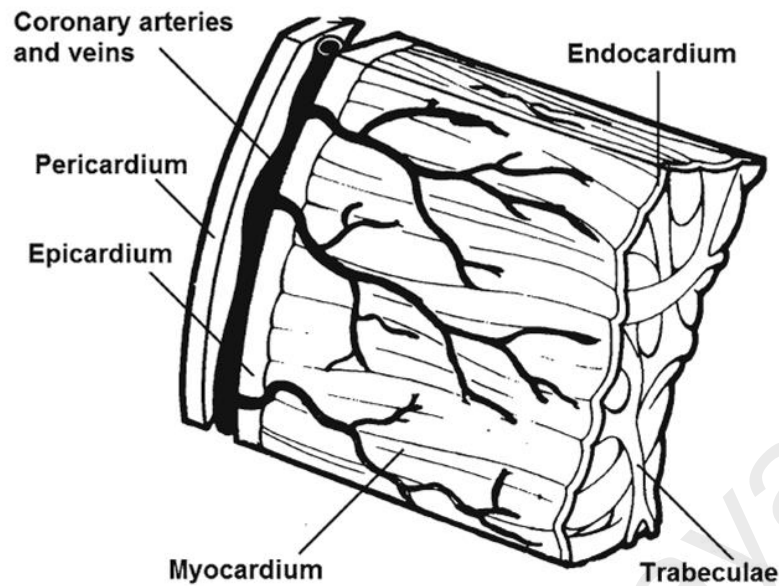


**Figure 2.2: Cross section of the heart walls showing the lining of the cardiac wall (Korpas, 2013)**

The heart consists of four chambers, two upper atria and two lower ventricles (see Figure 2.3). The upper chambers are smaller than lower chambers. Septa separate the right chambers from the left chambers. There are four valves in the heart: the tricuspid, mitral, pulmonary and aortic valves. The tricuspid valve is located between the right atrium (RA) and right ventricle (RV), while the mitral valve is located between left atrium (LA) and left ventricle (F. Li et al.). The pulmonary valve is located between the RV and the pulmonary artery, while the aortic valve is located in the outflow tract of the LV (Kenny, 2013).

The great vessels of the heart can be divided into two categories, i.e. blood vessels that enter the heart and exit the heart (see Figure 2.3). There are three important vessels entering to the RA of the heart which are the coronary sinus, superior vena cava (SVC) and inferior vena cava (IVC). These three vessels contain deoxygenated blood. The coronary sinus is the vessel that brings the deoxygenated blood from the heart itself. The SVC brings the deoxygenated blood from body parts above the level of the heart while

IVC returns the blood from body parts below the level of the heart. The blood that enters the RA is passes through the tricuspid valve into the RV. In contrary, there are four pulmonary veins that enter the LA of the heart. These veins carry oxygenated blood from the lungs to LA, where the blood emptied through the mitral valve into the left ventricles (Levick, 2013).

The great vessel that exits the superior part of the RV is the pulmonary trunk. This trunk branches into right and left pulmonary arteries, which function to supply the deoxygenated blood to the right and left lungs. The great vessel that exits the heart from the left ventricle is the aorta. Aorta supplies the heart muscle with oxygenated blood for its normal pumping function through the coronary arteries. Portion of the oxygenated blood is also supplied through a branch from the aorta, known as ascending aorta, to the entire body (Levick, 2013)

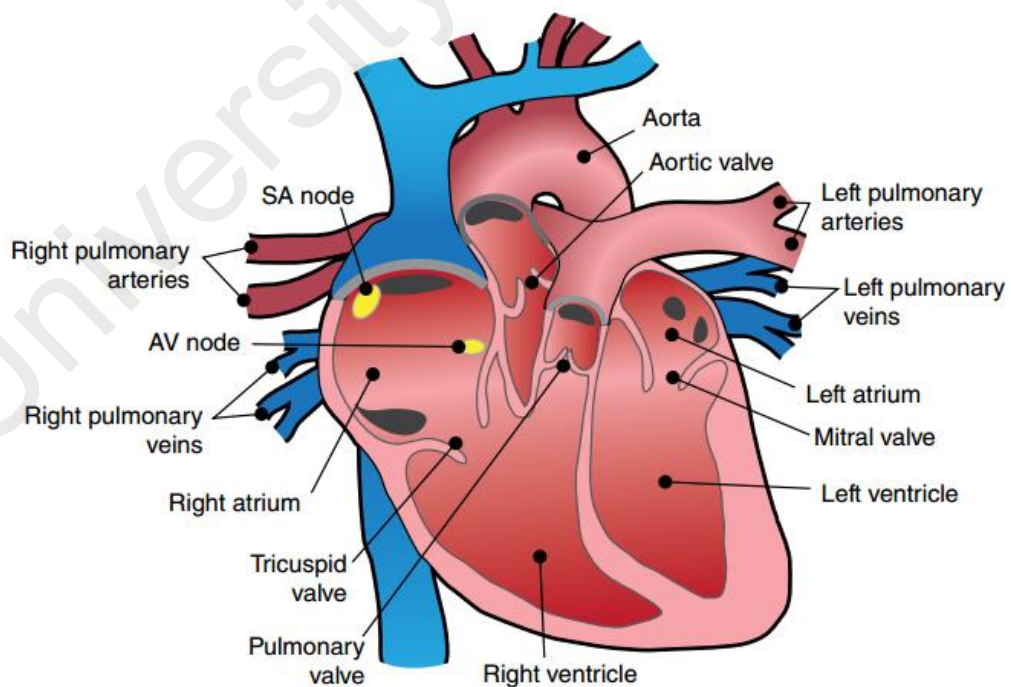


**Figure 2.3: Anatomy of heart (Kenny, 2013).**

### **2.1.2 Blood circulation in the heart**

The primary function of the heart is to pump blood cells throughout the body. Gas exchange occurs between lung and blood cells, whereby oxygen is transferred from the lungs to the blood cells while carbon dioxide is transferred in reverse. Circulation of the blood throughout the entire body is accomplished by the heart which forces the blood through the blood vessels. This blood circulation composed of two types: the pulmonary circulation and the systemic circulation. During the pulmonary circulation, the blood is pumped out from the heart to the lungs for oxygen replenishment. In the lungs, oxygen is absorbed and carbon dioxide is removed from the blood. On the other hand, during the systemic circulation, the blood is pumped by the heart to the rest of the body to nourish the tissue (Welsh, 2013).

Deoxygenated blood enters the RA via SVC, IVC and coronary sinus. The blood passes through tricuspid valve to enter the RV and then exits the RV through the pulmonary trunk. The pulmonary trunk bifurcates into two branches: the left and right pulmonary arteries that supply the deoxygenated blood to the lungs. The oxygenated blood from the lungs return to the heart through left and right pulmonary veins which are connected to the LA. From LA, the oxygenated blood passes through the mitral valve into the LV. Finally the oxygenated blood flow through the aortic valve to ascending aorta where the blood will be supplied to the entire body (see Figure 2.4) (Korpas, 2013; Lazo, 2014; Welsh, 2013).

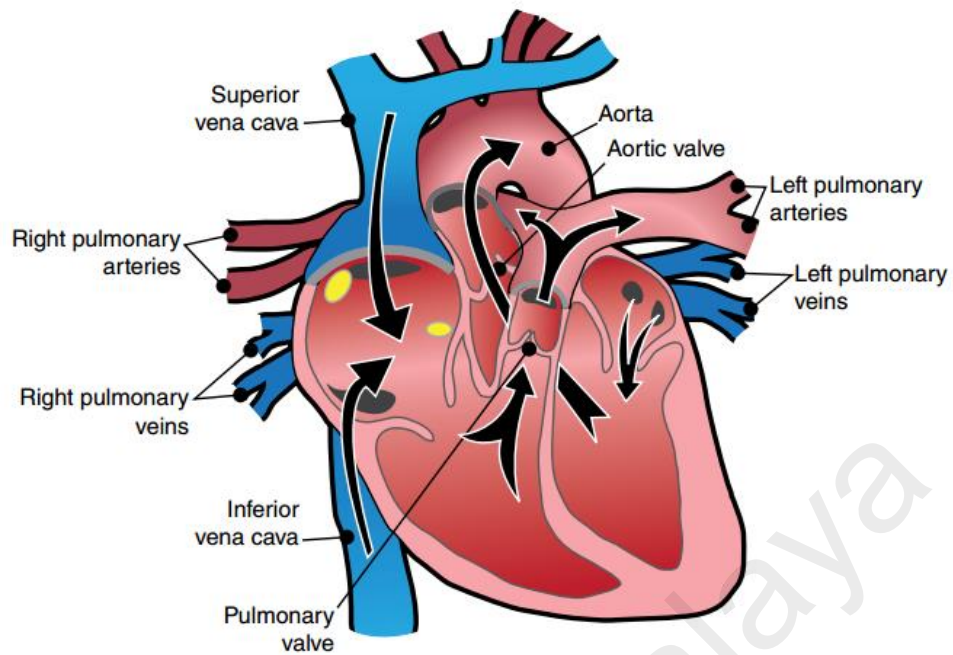


**Figure 2.4: Blood circulation in the heart (Kenny, 2013).**

### 2.1.3 Cardiac cycle and electrical activation

Cardiac cycle comprises of systole and diastole. Systole represents the period of ventricular contraction while diastole represents the period of ventricular relaxation. During diastole, both atria and ventricles are relaxed. The pressure of atrial is slightly higher than ventricular pressure. The tricuspid and mitral valves are open allowing blood to pass from the atria into the ventricles. During this time, the aortic and pulmonic valves are closed because pressures of pulmonary artery and aortic are higher than ventricular pressures. The coronary flow is high during this cycle. During the end of diastole, atria contract, adding 10 – 20% more volume to ventricles (Alraies et al., 2017; Fung, 2013; Marzullo et al., 2016).

Meanwhile during systole, myofibrils of the ventricular myocardium shorten, coronary blood flow is reduced, and ventricular pressure rises. The mitral and tricuspid valves close at early systole cycle. This is followed by the interval of isovolumetric contraction, when continued shortening of the myofibrils causes ventricular pressure to exceed pulmonary

artery and aortic pressure. Then, the pulmonic and aortic valves open, and ejection of ventricular begins. During systole, the tricuspid and mitral valves are closed, allowing the blood returning to atria, causes atrial volume and pressure to increase. At the end of ventricular ejection, the myofibrils rapidly relax causing the ventricular pressure to drop. The pulmonic and aortic valves are then close, while tricuspid and mitral valves open, allowing the blood from atria to fill the ventricles. During early diastole, the filling of the blood occurs rapidly and slows down as atrial pressure and volume decrease (Marzullo & Mariani, 2016).

The myocardial muscle has an intrinsic rhythm of contraction. The sinoatrial (SA) node, a small mass of specialized cells embedded in the wall of the RA near the entrance of the SVC, has the fastest inherent rhythm and serves as the impulse generator for the remainder of the heart. The electrical depolarization wave spreads to the surrounding atrial muscle cells and mechanical contraction is stimulated. There is no specialized conduction fibers within atria, and the impulse spreads from cell to cell to cover the entire atria within 0.08 s. Mechanical contraction requires approximately 0.1 s, longer than the spread of the electrical signal (Fox et al., 2013).

There is a delay in electrical signal transmission from atria to ventricles. As the signal enters the atrioventricular (AV) node, it is held for about 0.1 s before entering the specialized conduction system (the bundle of His) in the interventricular septum. This delay allows atria to empty prior to ventricular systole onset. Propagation of the electrical signal from the AV node through the bundle of His to the ventricular myocardium is followed by mechanical systole onset, which requires about 0.3 s (Fox et al., 2013).

The electrical activity is reflected by the Electrocardiogram (ECG) (see Figure 2.5). The ECG signal typically consists of a P wave, QRS complex, and T wave. The P wave represents the electrical signal that starts atrial contraction. The QRS complex serves the

same function in the ventricles (depolarization) whereas the T wave identifies an electrical reset of ventricles for the next cardiac cycle (repolarization). During much of diastole, the heart is electrically silent (Fox et al., 2013; Fung, 2013).

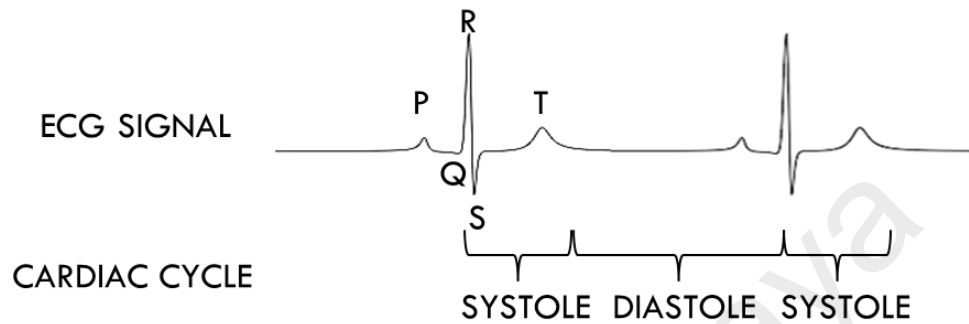


**Figure 2.5: ECG signal with PQRST waves and cardiac cycle information.**

## 2.2 Cardiovascular imaging

The imaging options for the cardiovascular system include: chest X-Ray, Nuclear Medicine, Echocardiography, Cardiac CT and Cardiac Magnetic Resonance Imaging (MRI). Each imaging modality provides unique information to the physician and is used for different purposes. (Suetens, 2017) and (Bushberg, 2002) provide detailed description of each of these imaging procedures.

### 2.2.1 Overview of various cardiovascular imaging systems

Chest X-ray (CXR) examination is almost often prescribed as the first imaging procedure for a patient in suspected cases of heart or lung disease. It is a noninvasive imaging procedure where a small amount of X-ray radiation was used to expose the chest in creating static projection image on the detector (Bushberg, 2002). A CXR shows structural information, including the location, size and shape of the heart as well as the lungs and bones of the chest. However, the CXR cannot resolve the internal heart structure due to the loss of depth information. Therefore, heart disease cannot be

accurately diagnosed based on CXR alone. The use of radiation in the imaging procedure also confound the use of this modality for real-time imaging, therefore no functional information of the heart can be obtained.

Other imaging procedures such as angiography also utilize ionizing radiation to image the heart. This procedure requires injection of a radiocontrast agent into the blood vessel and low dose x-ray beam is used to create real-time images of the heart based on fluoroscopy technique (Moscucci, 2013). This procedure provides 2D assessment of coronary arteries in ischemic heart disease, cardiac valves function, the congenital heart lesions and the great vessels abnormalities. However, this procedure is contraindicated for patients who are allergy to contrast agent and is high risk to patient with hypertension. Furthermore, due to the radiation exposure over an extended period of time during the procedure, it is also not recommended for using during intervention for treatment purposes.

Myocardial perfusion imaging (MPI) is another noninvasive type of heart examination which uses nuclear medicine imaging technique such as Single Photon Emission Computed Tomography (SPECT) and Positron Emission Tomography (PET) (Cremer et al., 2014) . These imaging procedures use small quantity of radioactive materials (radiotracer) that are typically injected into the blood vessel, inhaled or swallowed. The radiotracer travels to the target area and gives off gamma rays which are detected by a gamma camera and a computer to process the images of the examined structure. MPI provides information on blood flow and heart function for the detection of coronary artery disease as well as the extent of coronary stenosis. It also allows assessment of the damage to the heart following a heart attack. However, MPI is limited by poor system resolution and localization of the affected anatomical site has been reported to be difficult (Ballinger, 2015).

Echocardiography is the ultrasound (US) imaging of the heart. It is a vital imaging examination for diagnosing the heart disease. It has been used as an *in vivo* imaging modality during minimally invasive surgical procedure (Hahn, 2013). Basic working principle of echocardiography imaging involves generation of high frequency sound wave by an US probe, which is directed towards the tissue. Portion of the sound waves that penetrates the tissue get reflected back towards the transducer when the waves encountered boundaries of tissues with different reflective indices. The reflected signals are detected and processed by echocardiography system to reconstruct images of the heart structures. Currently, 2D echocardiography is the main preoperative imaging modality for assessing valve pathologies. This modality allows clinician to estimate the degree of valve regurgitation or stenosis, valve annular size, involvement of the leaflets, chordal and papillary muscle structural integrity, and overall LV size and LV systolic function (Omran et al., 2010).

Echocardiography can also be used as an intraoperative image guidance to facilitate physician in surgery due to its real-time capability without the use of ionizing radiation. It is also a low cost option as compared to other imaging modalities (Grewal et al., 2009). However, the quality of echocardiography images is inferior as compared to other imaging modalities such as cardiac CT and MRI due to the presence of speckle noise and limited field of view (FOV) (Grau et al., 2007). Three-dimensional echocardiography have shown the potential to provide real time 3D visualizations of the heart structure and overcome some of the limitations of conventional 2D echocardiography (Chan et al., 2004). Unfortunately, such technology is not widely available and expensive as compared to 2D echocardiography.

Cardiac CT is commonly applied as preoperative imaging tool. Cardiac CT produces cross-sectional images of the heart structure. It represents the X-Ray attenuation properties of the tissue being imaged (Mahesh et al., 2007). Thin X-Ray radiations are used to scan the FOV and yield line attenuation measures at all possible angles of the body being imaged. The line attenuation measures are used to reconstruct the 3D attenuation map of the body with each point on the map carries the value of X-Ray attenuation coefficient. Spiral or sequential technique can be used to reconstruct the 3D image of the heart. Additionally, contrast agents could also be used to enhance the visualization of blood vessels and identify the presence of tumors because of the difference in contrast uptake between tumours and the surrounding normal tissue. Volumetric CT scans provide essential information critical in treatment planning, including morphology of the valves and the stenosis severity (Messika-Zeitoun et al., 2006). However, cardiac CT is impracticable to be utilized as a real-time intraprocedural guidance due to the use of high dose ionizing radiation. It is also lacking in providing information on hemodynamics such as transvalvular pressure gradients, and for the detection of valve regurgitation (Chun et al., 2008).

Similar to cardiac CT, cardiac MRI can provide 3D cross-sectional images of the heart. MRI examination utilizes strong magnetic field to produce maps of atomic nuclei (hydrogen atoms in water or fat molecules in the body) (Dymarkowski et al., 2005). The atomic nuclei spin could be considered as a magnetic vector, causing the proton to behave like a magnet. The image acquisition involves an initial sequence of exciting pulses and the recording of the emitted signal. The amplitude of the signal is then used to generate maps showing the heart structures. MRI produces images with high resolution as well as high tissue contrast useful for the assessment and measurement of different cardiac structures. However, compared to cardiac CT, this examination are much more expensive and it is contraindicated for patient with metallic implant such as graft stents, cardiac

pacemaker device or hemodynamics support devices (Manning et al., 2002). Despite MRI is a gold standard for cardiac assessment, its resolution is still insufficient to resolve valve leaflets. Therefore infeasible for surgical planning of valve diseases.

Table 2.1 compares and contrasts the properties of the aforementioned imaging procedures. Echocardiography and cardiac CT stand out as excellent choices for real-time image guidance in intraoperative procedure and for preoperative planning, respectively. Due to the inferior image quality of echocardiography, the ability to spatially correlate the structural and haemodynamic features in echocardiography with 3D structural information in cardiac CT is envisioned to bring significant improvement to the diagnostic accuracy of cardiac disease, as well as the efficiency of minimally invasive interventions. A further discussion on Echocardiography and cardiac CT are presented in next subsections.

**Table 2.1: Comparison between different cardiovascular imaging procedures**

<b>Properties</b>	<b>CXR</b>	<b>Angiography</b>	<b>Nuclear Medicine</b>	<b>Echocardiography</b>	<b>Cardiac CT</b>	<b>MRI</b>
<b>2D images</b>	YES	YES	YES	YES	NO	NO
<b>3D images</b>	NO	NO	NO	YES	YES	YES
<b>Diagnostic information</b>	YES	YES	YES	YES	YES	YES
<b>Functional information</b>	NO	YES	YES	YES	NO	NO
<b>Preoperative examination</b>	YES	YES	YES	YES	YES	YES
<b>Intraoperative examination</b>	NO	NO	NO	YES	NO	NO

### 2.2.2 Echocardiography

The echocardiography procedure can be performed in M-mode, B-mode (2D Echocardiography) and Doppler-mode (Evangelista et al., 2010; Otto, 2012). In M-mode, the scanning is based on echo transmission in a single line (see Figure 2.6). The graph shows the reflected echoes in which structural depth and movement in time are reliably represented. This M-mode procedure provides the physician with information on the motion of cardiac structure such as valves (García-Fernández et al., 2009).

2D echocardiography or B-mode imaging provides real-time high resolution images of cardiac anatomy and function. There are three basic imaging planes used for imaging the heart which include long parasternal axis view (imaging from the aorta to the apex), short parasternal axis view, and apical four chamber views (see Figure 2.7).

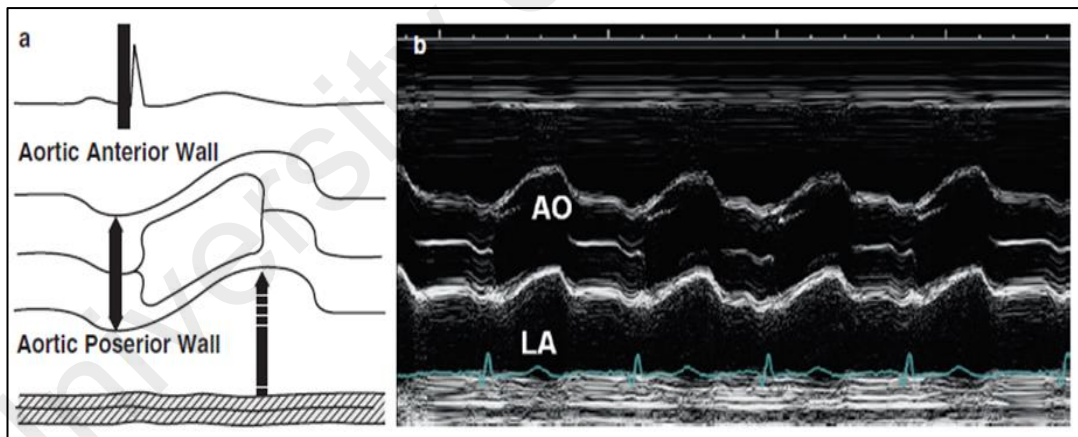


**Figure 2.6: M-mode imaging along aortic valve structure plane with AO (aorta) and LA (left atrium) locations indicated (García-Fernández & Caso, 2009).**

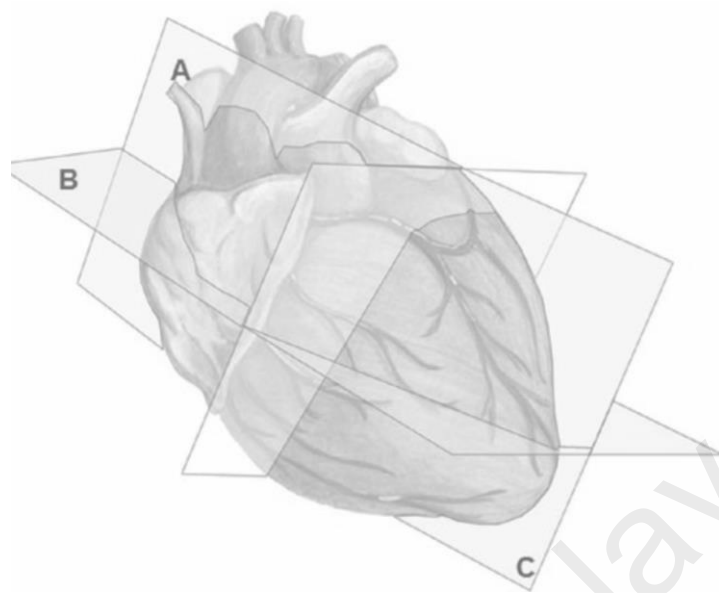


**Figure 2.7: Tomographic planes used in a 2D echocardiographic study. (A) long parasternal axis view; (B) short parasternal axis view; (C) four chamber view (García-Fernández & Caso, 2009)**

The long parasternal axis view (see Figure 2.8) is the first echocardiographic imaging plane performed for most adult patients. This plane is used to assess aortic and mitral valve diseases. In this view, the thickness of valve leaflets and their motion during the cardiac cycle can be evaluated. The dimension of the left atrium, which can be affected by mitral valve pathology, is evaluated in this view as well.

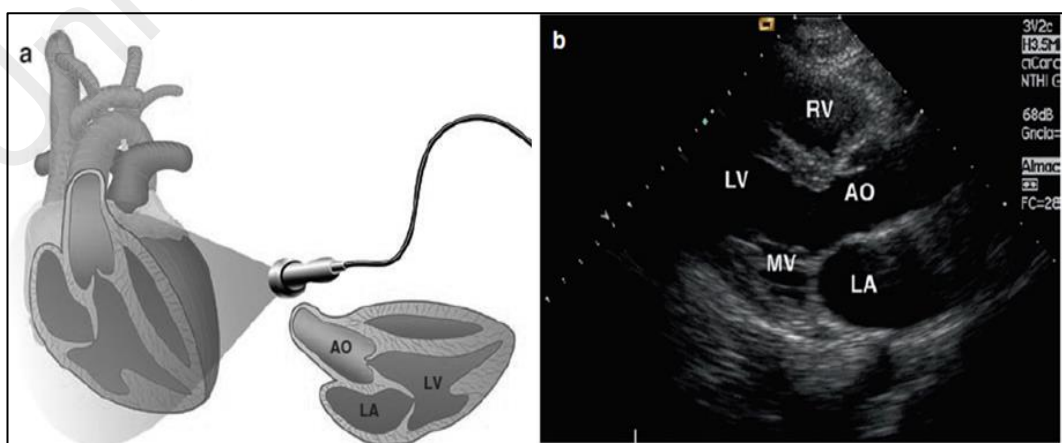


**Figure 2.8: (a) Long parasternal axis view. Aortic valve (AO); right ventricle (RV); left atrium (LA); mitral valve (MV); (b) left ventricle as visualized in the echo image on the right (García-Fernández & Caso, 2009).**

Besides that, the short parasternal axis view (see Figure 2.9) can be acquired by rotating the US probe 90 degrees from the long parasternal axis view and swept from the cranial to caudal position. The most cranial view provides a view on the aortic valve, atria, right ventricular outflow tract, and proximal pulmonary arteries. The three coronary cusps of the aortic valve can be viewed with possible imaging of the proximal right coronary artery arising from the right coronary cusp and the left main coronary artery originating from the left coronary cusp depending on manipulation of transducer on patient chest.

In addition, the apical four chamber view (see Figure 2.10) allows the visualization of all four chambers of the heart, the tricuspid and the mitral valves. Other 2D echocardiography imaging views include the Doppler imaging. Doppler imaging utilizes Doppler Effect to provide blood flow velocity and direction measurements in the heart and great vessels (Figure 2.11). Doppler ultrasound measures changes in the reception of sound wave when objects reflecting the sound waves are in motion with respect to the transducer (either moving away or moving towards the transducer).

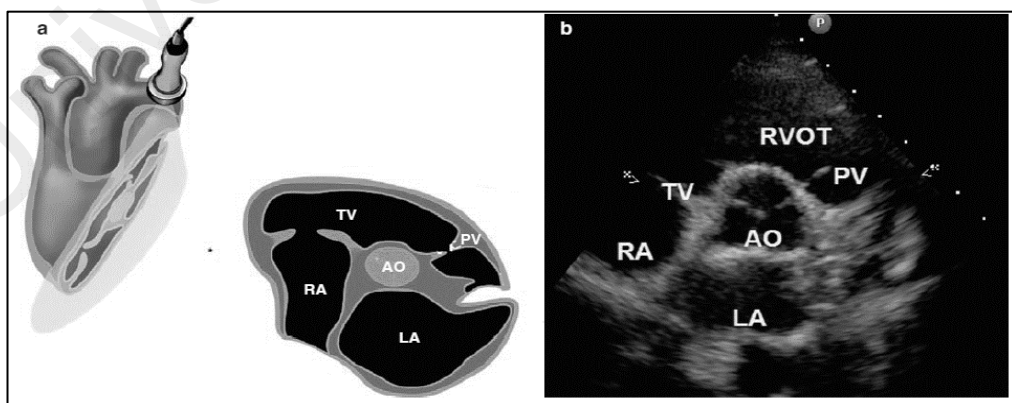


**Figure 2.9:** (a) Short parasternal axis view through the base of the heart. Aortic valve (AO), right atrium (RA), right ventricle (RV), left atrium (LA), tricuspid valve (TV), pulmonary valve (PV) and right ventricular outflow tract (RVOT) are visualized in the echo image on the right (b) (García-Fernández & Caso, 2009).

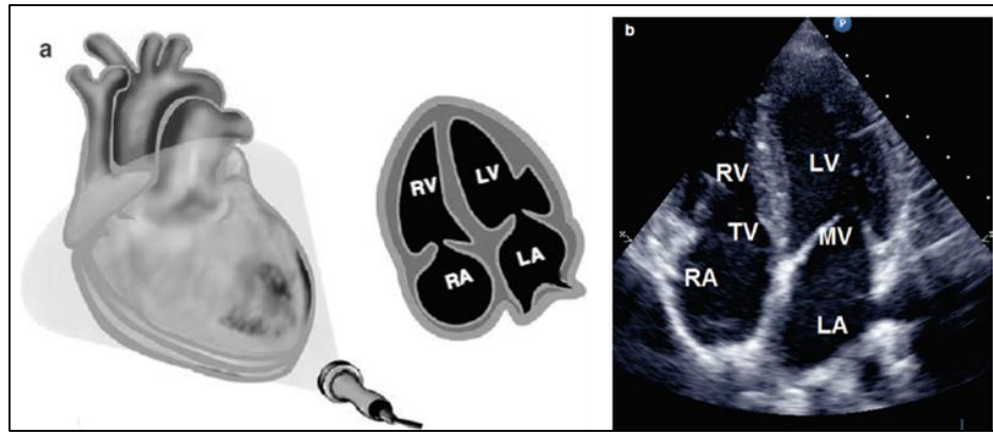


**Figure 2.10: (2) Apical four chamber view. Right ventricle (RV), mitral valve (MV), left ventricle and tricuspid valve (TV) are visualized in the echo images (b) (García-Fernández & Caso, 2009).**

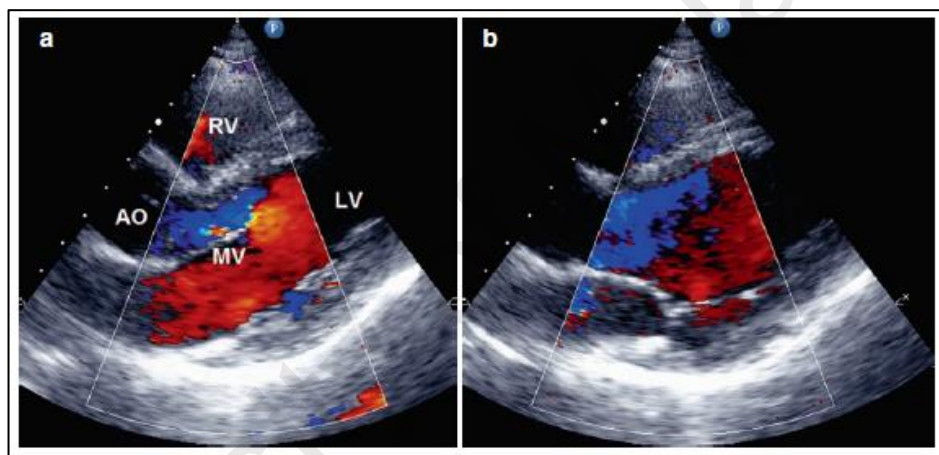


**Figure 2.11: Parasternal long-axis view with color flow Doppler during (a) diastolic frame and (b) systolic frame. Aortic valve (AO), right ventricle (RV), left atrium (LA), mitral valve (MV) and left ventricle can be visualized in the figures (García-Fernández & Caso, 2009).**

### 2.2.3 Cardiac CT

Cardiac CT is a noninvasive preoperative imaging examination that utilized x-ray radiation to take cross-sectional images of the heart and its blood vessels. This imaging procedure provides a three dimensional (3D) image of the whole heart to help physician in detecting or evaluating coronary heart diseases (Mahesh & Cody, 2007). Cardiac CT also provides information on calcium buildup in the coronary arteries, alteration of cardiac structures such as aorta and valves under disease conditions, and pericardial

disease. Advances in the recent technology of multi-array detector CT with retrospective cardiac gating allows for improved visualization and detailed anatomic evaluation of the heart valves (Feuchtner, 2013).

As described in the last section, CT contrast is indicative of the amount of x-ray attenuation by different tissue types (Bushberg, 2002). This difference in attenuation coefficients depends on the density of the tissues and body structures. Blood and soft tissue have similar tissue density and similar ratio of hydrogen, oxygen, carbon atoms. These tissues therefore have similar x-ray attenuation properties and appear dark in the image. Bone contains calcium and attenuates more X-rays than both blood and soft tissue, hence appears brighter in CT images. Fat consists of hydrogen whereas lung consists of air, which is of extremely low physical density and appears black. The higher the density, the brighter the structure appears. The appearance of calcium, air, and muscle/blood are bright white, black, and gray, respectively. CT images consist of over 5,000 shades of gray centered on zero (water). Therefore, CT image can distinguish blood from air, fat, and bone, but not readily from muscle or other soft tissue (Budoff et al., 2016).

To differentiate blood and soft tissue such as the LV, where there is no air or fat to act as a natural contrast agent, the injection of a radiocontrast agent is required. Likewise, contrast enhancement is also required to distinguish the lumen and wall of the coronary artery. The accentuated absorption of X-rays by elements of high atomic number like calcium and iodine allows excellent visualization of small amounts of coronary calcium as well as the contrast-enhanced lumen of medium-size coronary arteries. Furthermore, the cardiac CT images are excellent in visualizing cardiac valves (Budoff & Shinbane, 2016). Figure 2.12 shows a few cardiac CT images of cardiac valves and surrounding structures.

Currently, cardiac CT is not the main imaging modality for the assessment of cardiac valves. It is used as a supplement to echocardiography and MRI (Chen et al., 2009), and in general has higher resolution than cardiac MRI to allow visualization of the movement of valve leaflets. The notable limitation of retrospective ECG-gated CT is the use of ionizing radiation in the evaluation of valve morphologic features and function. Instead of being performed prospectively at a specific point in the cardiac cycle, as is now often possible for coronary artery evaluation, the imaging assessment of valve function must be performed throughout the cardiac cycle, resulting to a substantial radiation dose penalty. Thus, only selected patients could undergo cardiac CT of the heart valves, such as those with contraindications for MRI (such as patient with metal implant or pacing device). In particular, patients who are undergoing a cardiac valve procedure may benefit from preoperative CT of the valves, which allows simultaneous coronary artery evaluation for the purpose of excluding significant arterial stenosis. Postoperative patients with prosthetic valves may also benefit from undergoing CT angiography if echocardiography and MRI are suboptimal (Chen et al., 2009; Feuchtner, 2013).

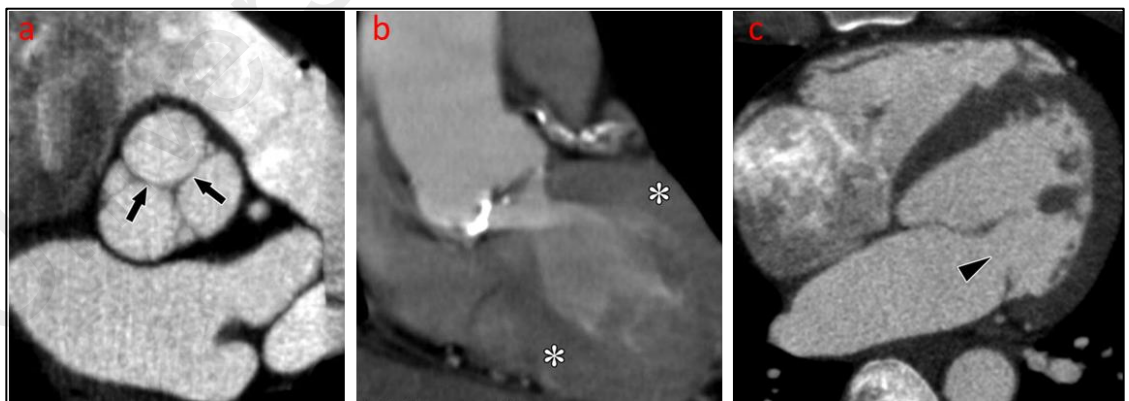


**Figure 2.12: (a) A normal aortic valve with thin, non-calcified cusps (arrows). (b) An oblique view thickening and aortic valve calcifications as well as left ventricular hypertrophy (\*). (c) A four chamber view obtained during diastole with an open mitral valve (arrowhead)(Budoff & Shinbane, 2016)).**

## **2.3 Image registration and fusion**

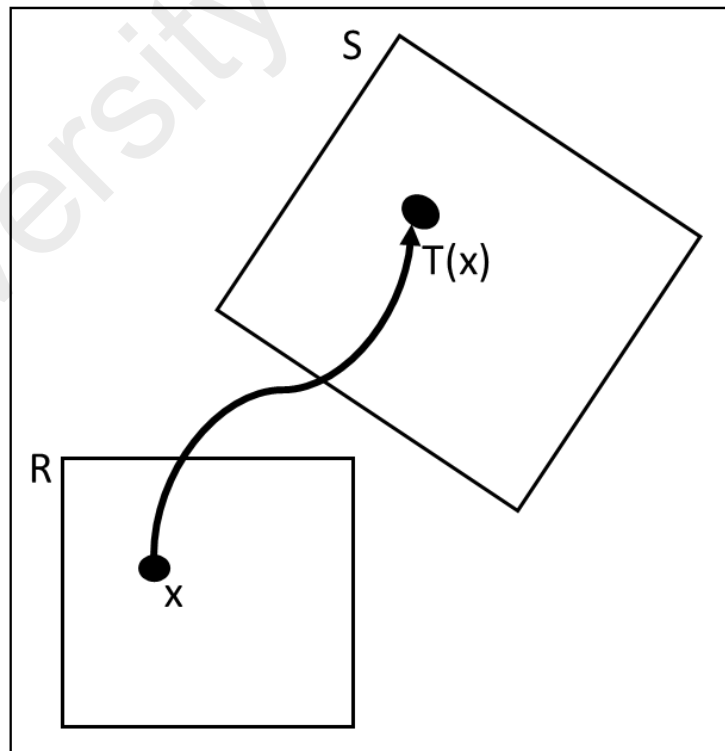
The acquisition and analysis of medical images is crucial to clinical applications. In many cases, medical imaging plays an integral part of the entire clinical work flow including diagnosis, planning and the final execution of the interventional procedure. It is especially important in minimally invasive treatment procedure because medical imaging provides physician visual of structures that they otherwise could not see. A specific clinical case often has multiple images acquired at different time points or from different viewpoints. It can also have images taken with differing imaging modalities. Thus, for the integration of the various sources of information, image fusion is often useful.

Image fusion of the same or different modalities plays an important role in providing physician with additional information they could not get from a single modality alone. The fusion of images helps the physician to integrate the information from multiple modalities and provides them with a second opinion in diagnosing and treating diseases. The principal step in the fusion process involves bringing both imaging modalities into spatial alignment through image registration.

### **2.3.1 Theory on image registration and fusion**

Image registration is a process that finds a transformation that maps features in one coordinate space to their location in another coordinate space (Rafael Gonzalez et al., 2002). It allows one to transfer information between both coordinate spaces. The basic steps in image registration procedures often involve feature extraction, geometrical transformation definition, similarity measure and optimization. First, feature space extracts the selected feature to be used for mapping. Second, search space determines the degree of transformation that brings alignment between the fixed and moving images.

Let us assume there are two images to be spatially registered, the moving image,  $R(x)$ , which is defined over a domain  $x \in V_R$ , and a fixed image,  $S(x)$ , which is defined over a domain  $x \in V_S$ . The transformation,  $T(x)$  is used to transform points in  $R(x)$ , to their corresponding positions in  $S(x)$  (see Figure 2.13). The commonly used transformations include rigid, affine, projective, and curved transformations. A similarity measure is used to estimate the similarity merit of the fixed image and transformed moving image. The search for optimal transformation parameters to register the images spatially can be accomplished by optimizing (maximizing or minimizing) a similarity measure derived from features in the image, e.g. the intensities of voxels in the images. The search process continues according to the optimization strategy until convergence, i.e. transformation parameters, which minimize or maximize the similarity measure are found (Ibanez et al., 2015; Rafael Gonzalez & Woods, 2002).



**Figure 2.13:**  $T(x)$  maps the point  $x$  in the moving image  $R$  to its corresponding position in the fixed image  $S$ .

Figure 2.14 shows a pipeline of a basic image registration workflow and its main components. The inputs to the registration algorithm are a fixed image, a moving image and initial transform estimates that need to be optimized. During the registration process, points in the fixed image are transformed into the moving image before the similarity measure or metric is evaluated. As the transformed points may not lie exactly on the discrete grid positions defining the moving image, an interpolator is needed to estimate the voxel intensities at those points (Ibanez et al., 2015; Rafael Gonzalez & Woods, 2002).

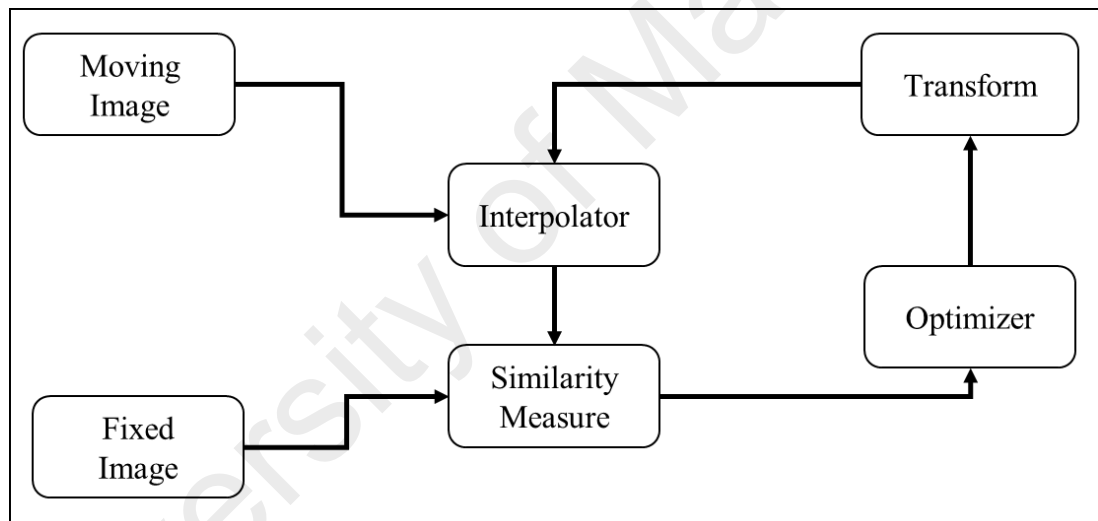


**Figure 2.14: Basic image registration pipeline (Ibanez et al., 2015).**

Image registration is an area of ongoing research. In 1992, (Brown, 1992) provided a comprehensive survey on different registration methods. This was followed by thorough reviews describing the state-of-the-art registration algorithms and applications by Audette et al. (2000); D. L. Hill et al. (2001); Maintz et al. (1998) and Zitova et al. (2003). Lester et al. (1999) and D. L. Hill et al. (2001) provided reviews focusing on image registration in medical field whereas Mäkelä et al. (2002) and (Zitova & Flusser, 2003) provided a review on cardiac image registration.

### **2.3.2 Multimodal image fusion on cardiac structures**

Multimodal image fusion of cardiac structures is a complicated process as compared to the fusion of other body parts, such as brain or kidney, due mainly to the heart and thorax motions as well as the deformable nature of the heart. Two types of image registration have been proposed to date, the intramodal and intermodal cardiac image registration. Intramodal cardiac image registration is an image registration between the same imaging modalities, e.g. registering images taken at different times or from different viewpoints of a modality. Intermodal cardiac image registration, by contrast, is an image registration between different types of imaging modalities, e.g. echocardiography with CT, which is investigated in this research.

#### **2.3.2.1 Intramodal cardiac image registration and fusion**

To date, intramodal image registration techniques have been proposed for echocardiography (Grau et al., 2007), cardiac MRI (Liew et al., 2015), PET (Pallotta et al., 1995) and SPECT (O'Connor, 2000).

Grau et al. (2007) present a registration algorithm to register 3D echocardiography images acquired from two different acoustic windows (apical and parasternal). The objective of their research was to improve the accuracy and robustness of 3D cardiac functional analysis. Their image registration algorithm is based on local phase and orientation of the image, calculated at each voxel, and is applied in a multiresolution framework to improve speed and robustness. Despite the excellent accuracy, the use of 3D echocardiography has not been adopted fully as a routine imaging method in the clinical practice due to the difficult image acquisition, inferior image quality and laborious manual data analysis (Kühl et al., 2004).

Liew et al. (2015) proposed an intramodal motion correction algorithm to realign multislice cine MRI data. Cine MRI is a standard clinical reference for quantitative assessment for LV functions, but it is limited by motion artifacts caused by a movement of the valvular plane during contraction and partial volume effects along slice thickness dimension. Liew et al. proposed a multislice image registration method to register cine short axis and radial long axis MRI stack, in order to correct displacement in the multi-breath-hold cine images due to inconsistent breath hold positions. Although the proposed framework has shown reduced misalignment between slices, the usage of MRI is only limited for the diagnosis of valve diseases as its resolution is still insufficient to resolve the movement of valve leaflets to guide surgical planning and treatment. As mentioned before, MRI is also limited as compared to cardiac CT in terms of cost as well as contraindications for patients with a metallic implant.

In nuclear medicine field, Tabrizi et al. (2001) proposed an intramodality image registration method for SPECT data. During myocardial perfusion imaging using SPECT, the patient being imaged is requested to remain static, just so the spatial location and distribution activity of the radiopharmaceuticals remains localized at the target region for the entire period of the image acquisition. However, motion artifacts arise between the transmission images due to the changes in the position of the heart and the voluntary patient motion. Their study focused on the evaluation of the performance and accuracy of three different motion correction algorithms used in nuclear cardiac imaging, including diverging square (DS), diverging circles (DC) and self-adaptive masking (SM) methods. Based on the results, DC and SM algorithms perform better when compared with the DS algorithm.

Klein et al. (2007) proposed an affine 4D registration algorithm for PET data. The purpose of the registration framework was to compensate the motion artifacts of gated cardiac PET emission images in order to better estimate the perfusion and metabolic parameters. They presented a technique to register emission images from different time frames with the end diastolic time frame. The algorithm was based on a non-uniform elastic material model with 12 parameters of global affine motion model. The algorithm iteratively calculates registration parameters of the model using a cost function that combines a least squares voxel difference measure with penalty terms assuming constant velocity and an affine model. The method does not require the precise a priori segmentation of the object.

The above findings suggest that significant work has been conducted in the cardiovascular imaging field. The importance of imaging for treatment procedure as well as for application in cardiac valves pathology, however, has not been adequately addressed. These registration frameworks were introduced to address primarily the issue of motion artifacts to enable quantitation of cardiac wall and fluid dynamics within a single modality.

### **2.3.2.2 Intermodal cardiac image registration and fusion**

Efforts to fuse images from different modalities can be divided into two categories, 3D to 3D (3D/3D) registration and 2D to 3D (2D/3D) registration. Research in 3D/3D registration focused mainly on CT-MR (Betancur et al., 2012), CT-PET (Marinelli et al., 2012), SPECT-PET (Gilardi et al., 1998), MR-PET (Sinha et al., 1995) and MR-SPECT (Aladl et al., 2004).

Betancur et al. (2012) proposed a registration framework to align inpatient dynamic CT and short axis view of cine MRI. The purpose of this registration is to provide physician a better visualization of the heart. Cardiac MRI has been widely used to assess

cardiac function, morphology, and myocardial perfusion/viability, whereas computed tomography (CT) systems image the dynamic morphology of the heart with higher spatial resolution and is preferred to assess the coronary veins for cardiac resynchronization therapy (CRT) as compared to MRI. To align the images of both modalities, the registration technique utilize normalized cross correlation curves computed from each image sequence to describe the global cardiac dynamics together with an adapted dynamic time warping (DTW) procedure. The spatial registration utilized rigid transformation that maximizes the normalized mutual information of DTW synchronized images. Their 3D/3D registration algorithm has shown good accuracy for aligning CT and MRI images for better visualization of cardiac structure.

Besides, Aladl et al. (2004) developed an image registration approach to align gated cardiac SPECT and MR images. This study focused to register both modalities in order to allow direct comparison for physiological assessment of the LV (F. Li et al.), e.g. to detect coronary artery disease, to assess wall thickening, abnormality in regional motion, ejection fraction (EF), and myocardial perfusion and viability. The registration algorithm utilized rigid-body transformation and mutual information (MI) similarity metric. The registration results of 20 patients were compared against manual registration. The reported translation and rotation error were 0.9 to 1.5 pixels and 2.7 to 5.4, respectively.

Marinelli et al. (2012) proposed an automatic method to register functional PET and cardiac CT. Their algorithm is based on rigid transformation and mutual information as the similarity metric. A multiresolution optimization scheme was implemented to reduce the registration time. Khurshid et al. (2008) is another research group that has also proposed a registration algorithm to register CT and PET. Their technique involved prior extraction of the heart from PET data through windowing and c-mean clustering, and separate segmentation of heart geometry from the CT scans. The heart geometries from

both modalities were then registered and a motion correction vector was calculated such that the alignment error of the two modalities was minimized. Both methods in registering CT and PET scans allow for joint assessment of CT which is capable in defining coronary artery disease (CAD) and PET which is good in measuring the myocardial perfusion. The modalities used in Aladl et al. (2004), Marinelli et al. (2012) and Khurshid et al. (2008) studies, however, cannot be utilized for minimally invasive procedure. Therefore, the issue of image guidance for interventional procedure, which was not critical for their application, was not addressed.

On the other hand, 2D to 3D image registration is a more challenging task as compared to 3D to 3D image registration. It is because a 2D image contains less information than a 3D image. Precisely, the 2D image is a scan imaged from a 3D tissue volume with an arbitrary position and orientation, and is equivalent to a slice extracted from a 3D volume of the object. There are two main methodologies for 2D to 3D registration. The first approach involves correspondence between the 2D image with the projections of 3D volumes (Szpala et al., 2005; Turgeon et al., 2005). The second method involves developing a transformation that aligns the 2D image within the 3D volumetric data. 2D to 3D registration can be grouped into several categories, including feature based (Guéziec et al., 1998), intensity based (Hipwell et al., 2003; Weese et al., 1997), and hybrid methods (Turgeon et al., 2005). Very limited studies on 2D echocardiography to 3D CT volume registration are reported. The review of existing studies is provided in the next subsection.

### **2.3.2.3 Image registration of echocardiography and CT**

A few registration frameworks have been proposed to fuse echocardiography and CT volumetric data. Huang et al. (2009) have proposed and demonstrated a registration fusion of intraoperative 2D echocardiography with preoperative 3D CT. The study was

performed on a beating heart phantom and an animal study. They used rigid transformation and mutual information bringing together complementary anatomical information of the heart phantom from both imaging modalities. To reduce speckle noise in echocardiography images, they utilized a median filtering technique. A fiducial marker (bead glass target) was attached to the surface of the heart phantom to evaluate the target registration error (TRE). Although the TRE was small ( $1.7 \pm 0.4$  mm), this method can only be utilized for testing and evaluating the registration algorithm, as the fiducial marker cannot be attached on the human heart surface before preoperative images are acquired.

Besides, Zhong et al. (2006) presented a feature-based technique known as virtual touch which was implemented by collecting the intraoperative surface points of the heart from 3D echocardiography catheter. The aim of this study was to guide LA endocardium ablation intervention. The registration algorithm implemented an iterative closest point (ICP) method to register the surface points of the LA to the surface model derived from CT images. Although the technique shows a quality surface point registration with TRE of 1.2 mm and is more than 700 times faster than current methods, the utilization of 3D echocardiography as a guidance modality in clinical practice is still limited in comparison to 2D echocardiography.

Sun et al. (2007) presented an intensity-based method for registering 3D gated intracardiac echocardiography to preoperative 3D CT images. The motivation of this study was to assist the physician in diagnosing cardiac disease and in guiding electrophysiology ablation procedures. Their registration algorithm utilized normalized cross correlation (NCC) as the similarity measure and best neighbor method as the optimizer. The study showed good registration accuracy in an animal study without the need of additional segmentation in US images. The proposed techniques, however, still

requires human expert to manually choose appropriate threshold value and perform initial alignment before applying the image registration algorithm.

Sandoval et al. (2013) evaluated similarity measures for intensity-based rigid and elastic registration between preoperative computed tomography (CT) and transesophageal ultrasound (US) images of the LA and the pulmonary veins. This registration aimed to guide physician for high intensity focused ultrasound (HIFU) ablation therapy in patients with atrial fibrillation. They compared the performance of eight similarity measures namely mutual information (MI), normalized mutual information (NMI), entropy correlation coefficient (Hahn), joint entropy (H), point similarity measure based on MI (PSMI), energy of histogram (E), correlation ratio (CoR) and Woods criterion (WC). The results showed that WC and MI gave better performance as compared to others in rigid registration. Whereas for elastic registration, NMI gave higher performance than MI.

Lang et al. (2011) have demonstrated two different methods in registering TEE echocardiography and CT images: (1) the feature and surface-based registration, and (2) image-based registration. The first technique employed iterative closest point (ICP) to align the preoperative surface model with homologous surfaces extracted from the intraoperative TEE images. Whereas the second technique is an intensity-based technique which uses MI for registration which has been found useful when landmark points could not be reliably extracted from the images. Their experiments were conducted on small preliminary data sets and results showed that both registration techniques have the potential to be used in real-time image navigation environment for minimally invasive cardiac interventions.

Meanwhile, F. Li et al. (2012) from the same research group have developed a hybrid method to register 3D intraoperative echocardiography and preoperative CT images. The method consists of two stages. In the first stage, anatomical features are segmented from the first frame of echocardiography images and the CT images. A feature-based registration based on ICP techniques is used to align those features and serve to initialize the second stage. In second stage, the intensity-based mutual information technique is implemented with Powell's optimization method to register images from both modalities. The technique, however, requires a manual segmentation procedure prior to surgery.

F. P. Li et al. (2013) introduced a method to register 4D synthetic cardiac CT with 4D US images. The 4D synthetic cardiac CT was generated from a static CT and a 3D TEE series through nonrigid registration technique. The synthesized CT images were found comparable to real dynamic CT images. Although the results provide similar anatomical representation of the ROI and the registration accuracy is close to that obtained using real dynamic CT images, the results however suffered from inconsistency due to the different image acquisition protocols for CT and echocardiography. During standard CT scanning, the patient's heart rate was intentionally reduced by using  $\beta$ -blockers while the patient stays fully conscious. On the other hand, TEE procedure does not apply  $\beta$ -blockers and patient is sedated using general anesthesia. These different approaches potentially induce changes to patient's cardiac motion and heart rate, causing misalignment of intraoperative echocardiography and preoperative CT images. In addition, the correct visualization of deformable anatomical structure is only restricted to within the FOV of TEE images. Structures outside of the imaging region of the TEE scan cannot be deformed for registration, as the deformation fields of the synthetic CT images were derived from the TEE images.

#### 2.3.2.4 Summary

An observation of the trend of current literature suggests that very limited studies were introduced to spatially align 2D echocardiography and cardiac CT volumetric data. Previous studies are similar in the aspect that optical tracker device is mandatory to track the US probe position and orientation during echocardiography and CT registration. These techniques are currently limited by the coarse resolution and the availability of the optical tracker device for clinical application, but merely tested on the phantom and animal studies. Image fusion between 3D echocardiography and CT has also been studied (Kiss et al., 2013; Maffessanti et al., 2014), but this specialized ultrasound technology is quite new, requires additional user training and therefore has yet to be widely adopted. In addition, there is an additional procedure cost associated with 3D echocardiography imaging and the limited access to 3D streaming make it poorly suited for real-time fusion with other modalities (Huang et al., 2009). Moreover, little studies have been conducted to study the use of image fusion to assess aortic and mitral valve disease and for surgical navigation during TVR and TVI.

## CHAPTER 3: METHODOLOGY

This chapter presents materials and methods used in this research to register 2D echocardiography images to cardiac CT volume. This chapter starts by introducing the data acquisition protocol in Section 3.1. The method of image registration is presented in Section 3.2. The proposed method consists of three major steps: temporal registration, echocardiography noise reduction and spatial registration. The details of each major steps are presented in Section 3.2.1 to 3.2.3. The accuracy of proposed method was validated based on comparison with gold standard manual registration as presented in Section 3.3. The error analysis includes qualitative and quantitative analysis as discussed in Section 3.3.1 and 3.3.2.

### 3.1 Data acquisition

Ten patients with indicated heart valve disease (aortic or mitral valve diseases) were recruited to undergo multimodality imaging. The data collected were anonymized. For each patient, a 2D time series echocardiography scan and a retrospectively gated cardiac CT volumetric scan were acquired preoperatively on the same day. All data used in the experiments were collected retrospectively under a protocol approved by the Research Ethics Board of National Heart Institute, Kuala Lumpur, Malaysia. The ethics approval letter is attached in Appendix A.

The demographic information of the patients recruited for this research is presented in Section 3.1.1. An overview of the properties of cardiac CT and echocardiography acquisitions are discussed in Section 3.1.2 and 3.1.3, respectively.

### 3.1.1 Demographic information

The demographics of the ten recruited patients are shown in Table 3.1.

**Table 3.1: Demographic information of patient recruited for this study.**

PATIENT #	AGE	SEX
1	78	Male
2	73	Female
3	81	Male
4	76	Female
5	79	Female
6	85	Female
7	80	Male
8	73	Male
9	72	Female
10	70	Female

As mentioned previously in Chapter 1, the aortic and mitral valves diseases is substantial among the elderly above 70 years old (Osnabrugge et al., 2013; Singh et al., 1999).

### 3.1.2 Cardiac CT acquisition

The preoperative cardiac CT data were collected at the National Heart Institute, Kuala Lumpur, Malaysia. An ethical approval was obtained from the Institutional Research Ethics Board. CT images were provided as anonymized DICOM files from the hospital archiving systems. Patients were in the supine position during image acquisition. All patients underwent retrospectively-gated cardiac CT scan using a 64-slice dual source CT scanner (Somatom Definition, Siemens Medical Solutions, and Germany). The properties of the cardiac CT data are as follow:

Tube voltage	:	120 kVp
Tube current	:	Depending on patient size
Gantry rotation time	:	0.33s
Pitch	:	0.2–0.43 (automatically adapted to the heart rate)
Spatial resolution	:	$0.4 \times 0.4 \times 0.4$ mm at single frame per cardiac cycle
Data reconstruction	:	40-70% of the R-R interval
Slice thickness	:	0.75mm
Matrix size	:	512×512 pixels

### 3.1.3 Echocardiography acquisition

The echocardiography data from the same patients were also collected retrospectively and were provided as anonymized DICOM files from the hospital archiving systems. The 2D time series echocardiography scans were performed by using a Philips IE33 ultrasound system equipped with an S5-1 (1.0–3.0 MHz) transducer on the same day of cardiac CT examination. The images acquired include short axis “Mercedes Benz” sign views of the aortic valve plane, long parasternal axis and four chamber views. The properties of the cardiac CT data are as follow:

Frame rate	:	30 to 100 Hz
Cardiac cycle	:	cover four to five cardiac cycles
Spatial resolution	:	0.3 x 0.3mm
Image size	:	800 x 600 pixels

### 3.2 Image registration

The proposed registration method consists of three major steps: temporal registration, noise reduction and spatial registration. Temporal registration was performed to synchronize echocardiography and cardiac CT images in time. Next, in the preprocessing, the noise of echocardiography image was reduced using speckle reducing anisotropic diffusion (SRAD) technique. The spatial registration used a rigid geometrical transformation to the selected 2D planar echocardiography image to spatially align it with the static cardiac CT volume using intensity-based registration algorithm. This image registration framework was implemented in MATLAB (vR2014a, Mathworks, Natick, USA) on an Intel(R) Xeon (R) CPU E5-26200 @ 2.00 GHz computer. Figure 3.1 shows overall proposed registration workflow of this study and the detailed description on each of these stages are given in subsequent sections.

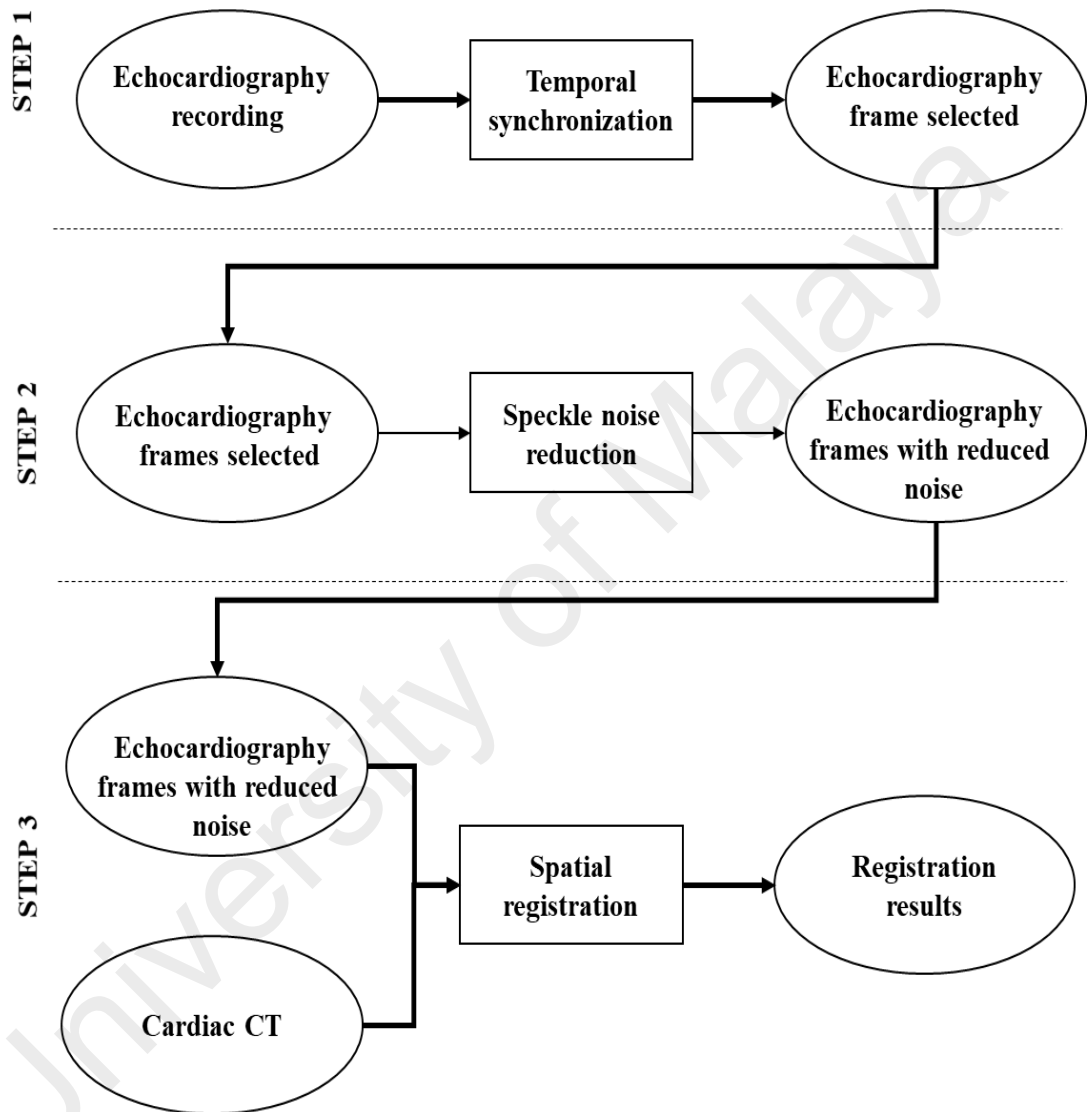


**Figure 3.1: Overall registration workflow**

### 3.2.1 Temporal registration

Temporal registration was performed to synchronize echocardiography and cardiac CT images in time because both modalities produce images of different sampling latencies and temporal resolution (Tavard et al., 2014). Depending on the heart rate and frame rate, echocardiography typically depicts a pumping heart moving through systolic and diastolic phases during surgical navigation. Cardiac CT volume data was captured at a single time point, typically at the diastolic phase, during preoperative assessment. Since the shape of the heart varies over diastole and systole, it is critical to correctly select the 2D planar echocardiography images to ensure the success of spatial registration with the CT volume.

In this study, temporal registration of both imaging modalities was achieved by time stamping using ECG gating signals that were obtained concurrently during echocardiography imaging. In the ECG signal, the R peaks were automatically detected based on the amplitude of the signal. In order to select echocardiography images with similar cardiac phases to the preoperative cardiac CT volume, the ECG signal was linearly interpolated within the R-R interval. In this study, three frames located within 40-70% of the interval were chosen for spatial registration (see Figure 3.2). This interval was determined from the capturing time delay recorded in the CT header file and was found to reside close to the end-diastolic phase of the cardiac cycle.

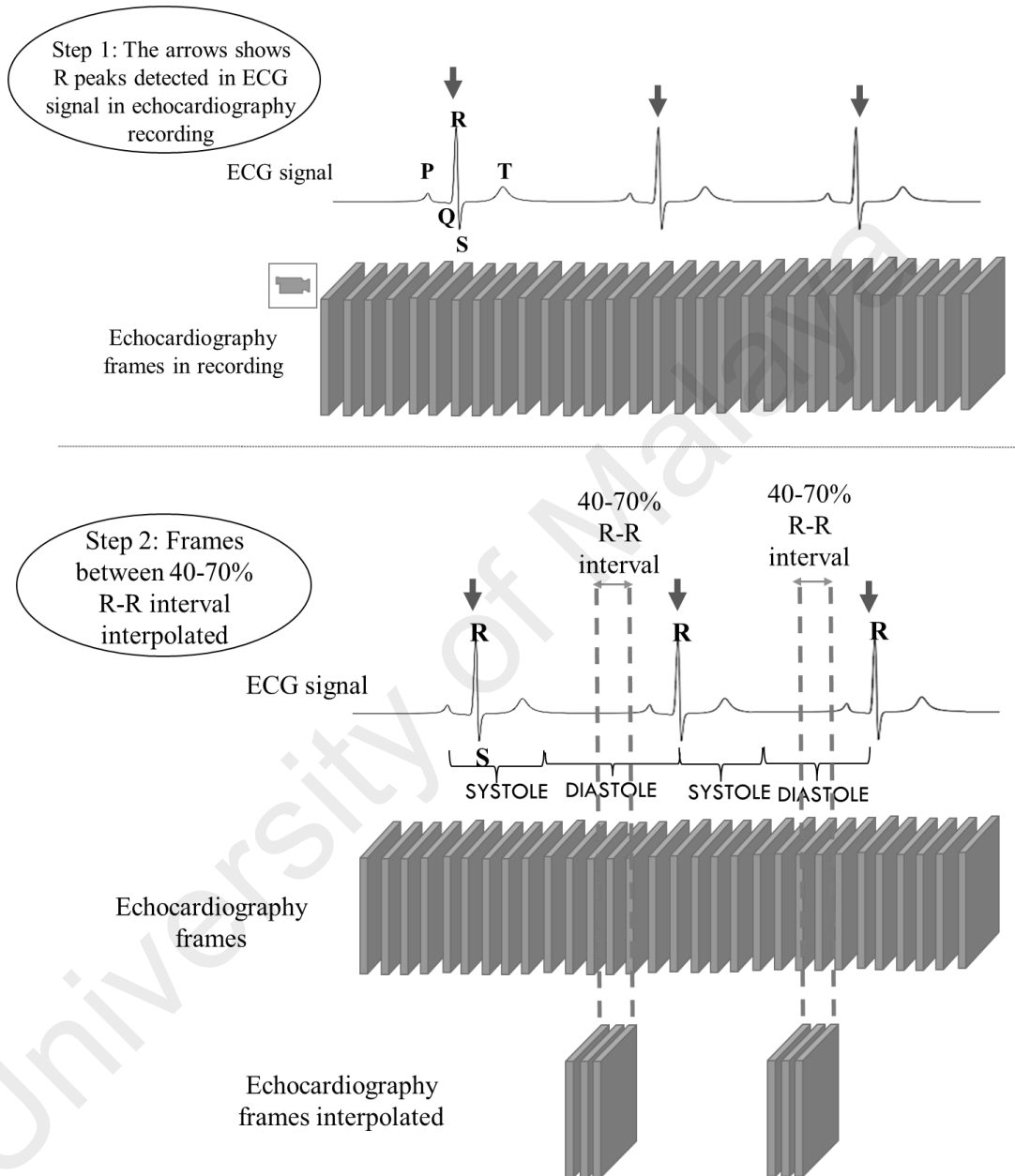


**Figure 3.2: Temporal registration method.**

### 3.2.2 Echocardiography noise reduction

To succeed in registration, a voxel similarity measure such as the mutual information function, should be quasi convex and contains a minimum number of local maxima. The inherent undesired property of echocardiography image, i.e. speckle noise artifacts, impedes the above mentioned condition by affecting the mutual information value (Shekhar et al., 2002). Removing speckle noise, hence, is significant to improve the registration accuracy. Median filtering is often adopted to suppress noise, aiming to smooth the mutual information function for improved registration, however this filtering undesirably blur the boundaries of the anatomical structure. Instead of median filtering, Speckle Reducing Anisotropic Diffusion (SRAD) is adopted to reduce the speckle noise in echocardiography images. This approach is based on both additive noise reduction's anisotropic diffusion (Perona et al., 1990) and multiplicative noise reduction's Lee and frost filters (Frost et al., 1982; Lee, 1980). SRAD confers one main advantage over conventional filtering methods, i.e. it preserves and enhances edges while suppressing the speckle noise. Despite being computationally more demanding, implementing SRAD remains feasible in the registration process since only a single selected echocardiography image is used throughout the entire registration process in our case. Involving only a single echocardiography image also indicates that the quality of this echocardiography image forms the key factor to define the image registration outcome. Therefore, it is worth to perform a complex preprocessing, such as SRAD, for acquiring the improved image quality.

The following partial differential equations (Equation 3.1 and Equation 3.2) transforms the input image  $I_{in}(x,y)$  with finite power and no zero values over the image support,  $\Omega$ , to the output image  $I_{out}(x,y;t)$

$$\frac{\partial I_{out}(x,y;t)}{\partial t} = \text{div}[c(q)\nabla I_{out}(x,y;t)] \quad (3.1)$$

$$I_{out}(x, y, 0) = I_{in(x,y)}, \left( \frac{\partial I_{out}(x, y; t)}{\partial \vec{n}} \right) \Big|_{\partial \Omega} \quad (3.2)$$

where  $\partial \Omega$  indicates the  $\Omega$  border and  $\vec{n}$  indicates the outer normal to the  $\partial \Omega$ . The diffusivity tensor function characterizing type of diffusion,  $c(q)$  is defined by Equation 3.3.

$$c(q) = e^{-\frac{[q^2(x, y; t) - q_0^2(t)]}{q_0^2(t)(1 + q_0^2(t))}} \quad (3.3)$$

If  $c(q)$  represents a constant value over the entire image, then isotropic diffusion is taking place; here, the  $c(q)$  is a function depending on the targeted area to determine the strength of diffusion in different areas depending on  $q_0(t)$  and  $q(x, y; t)$ ; where  $q_0(t)$  denotes the speckle scale function and  $q(x, y; t)$  denotes the instantaneous coefficient of variation defined in Equation 3.4 and Equation 3.5.

$$q(x, y; t) = \sqrt{\frac{\alpha \left( \frac{|\nabla I|}{I} \right)^2 - \beta \left( \frac{\nabla^2 I}{I} \right)^2}{\left[ 1 + \delta \left( \frac{\nabla^2 I}{I} \right)^2 \right]}} \quad (3.4)$$

$$q_0(t) = \frac{\sqrt{\text{var}[z(t)]}}{z(t)} \quad (3.5)$$

The parameters,  $\beta$  and  $\delta$  serve as weighting parameters, empirically set as 1/2, 1/4 and 1/16 (Wu et al., 2006).

The instantaneous coefficient of variation,  $q(x, y; t)$ , governs the diffusion intensity or amount of smoothing. In regions of edges,  $q(x, y; t)$ , returns high values and hence induces diffusion flow in edge directions. While in homogenous region,  $q(x, y; t)$ , returns low values and hence induces isotropic diffusion. Whether a region is considered

homogeneous is controlled by the speckle scale function,  $q_0(t)$  in  $c(q)$  relative to  $q(x,y;t)$ , where  $\text{var}[z(t)]$  denotes intensity variance at  $t$  and  $\overline{z(t)}$  denotes mean over a region at  $t$ .

At a given location  $(i,j)$ , the discrete-domain and discrete-time implementation of update rule for SRAD introduced by Yu (Yu et al., 2002) is represented as follow:

$$I_{i,j}^{t+\Delta t} = I_{i,j}^t + \frac{\Delta t}{|\overline{n_s}|} \left[ C_E (I_{i+1,j}^t - I_{i,j}^t) + C_S (I_{i,j-1}^t - I_{i,j}^t) + C (I_{i,j+1}^t - I_{i,j}^t) + C (I_{i-1,j}^t - I_{i,j}^t) \right] \quad (3.6)$$

where  $|\overline{n_s}|$  represents the number of pixels in the window which amounts to number of neighboring pixels that are taken into account. Similar to Yu (Yu & Acton, 2002), four pixels were adopted in the process.  $C_E$ ,  $C_S$ , and  $C$ , represent diffusion coefficients (in which its value amounts to '0' as it approaches edge; amounts to unity as it approaches homogenous regions) at the east pixel, south pixel and center pixel respectively. The time step is denoted by  $\Delta t$ , while the subscripts 'E' and 'S' in  $C_E$  and  $C_S$  represent eastern and southern diffusion direction. This update rule assumes the same diffusion strength in both northern and western direction with the center pixel, whereas, the diffusion strength in both southern and eastern pixels are associated with their corresponding diffusion coefficients. For each iteration, instantaneous coefficient of variation (ICOV) and diffusion coefficient are computed based on the pixel intensities in the sliding window. The image in the next iteration is computed based on the current image; the final image is the last image after applying the diffusion for several iterations. The parameters of SRAD such as the step size and number of iterations are determined by experts with the goal of smoothening echocardiography image to resemble CT image.

### 3.2.3 Spatial registration

To perform spatial registration of each 2D planar echocardiography image frame to the corresponding preoperative cardiac CT volume, a rigid 2D to 3D intensity-based registration scheme was employed, utilizing mutual information as the similarity metric

and pattern search algorithm as the underlying optimizer. The echocardiography image frame was selected from the temporal registration process and underwent speckle noise reduction. In the registration process, the 2D planar echocardiography image was spatially maneuvered within the vicinity of the cardiac CT volume to search for the best matching cardiac CT plane. The overall proposed spatial registration framework is presented in Figure 3.3 and the details of each step are presented in the following subsections.

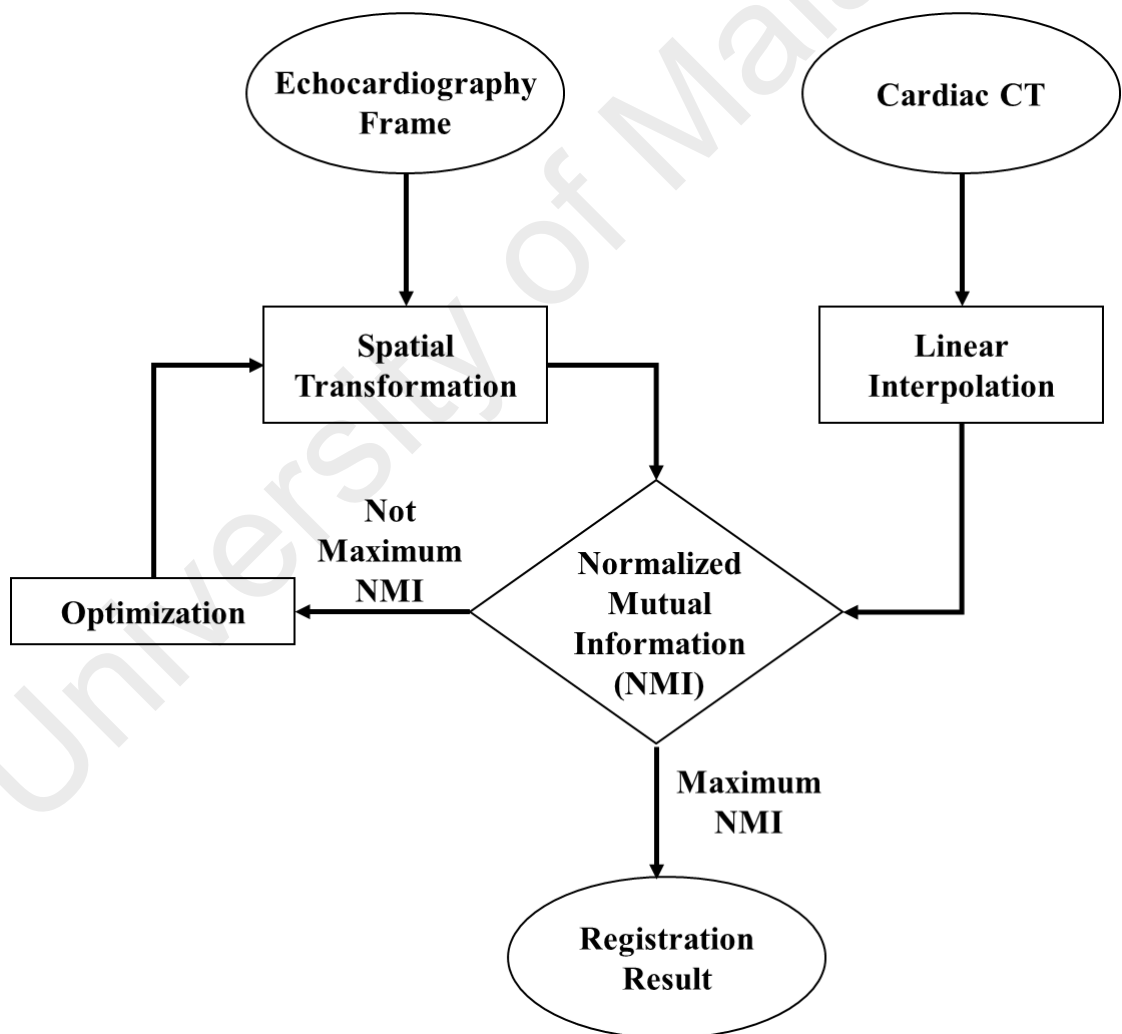


**Figure 3.3: Spatial registration pipeline.**

### 3.2.3.1 Spatial transformation

The search for best matching plane of CT started off by assigning and placing the echocardiography image at the seed position. The seed position provided is dependent on the selected views for registration with cardiac CT (see Figure 3.4). This seed position includes the orientation and position of the valves plane, which were estimated and provided by the expert during preprocedural planning on CT volume with respect to 3D axes of the patient's body (see Figure 3.4).

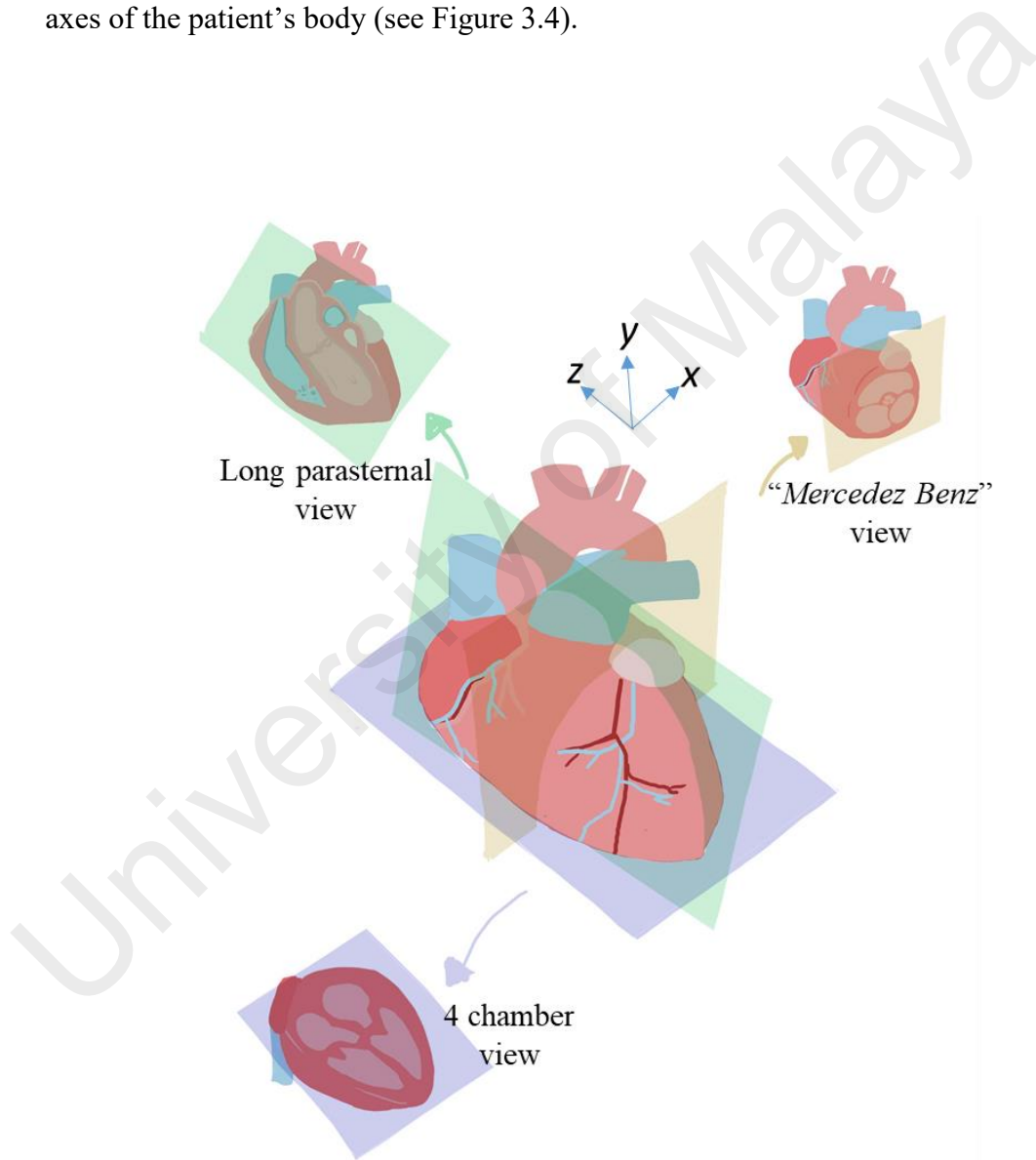


**Figure 3.4: Drawing of the estimated seed plane for three different views, which is used to initialize the registration search.**

A rigid spatial transformation,  $T$ , consisting of 8 degrees of freedom was applied to the 2D planar echocardiography images, consisting of 3D translation ( $t_x$ ,  $t_y$ , and  $t_z$ ), 3D rotation ( $R_x$ ,  $R_y$  and  $R_z$ ) and 2D scaling ( $S_x$  and  $S_y$ , i.e. along both dimensions of the planar image). Equation 3.7- 3.9 shows the transformation matrix and its components used for this study.

$$\begin{bmatrix} u' \\ v' \\ w' \\ 1 \end{bmatrix} = T \times \begin{bmatrix} u \\ v \\ w \\ 1 \end{bmatrix} \quad (3.7)$$

$$T = 2D \text{ Scaling} \times 3D \text{ Rotation} \times 3D \text{ Translation} \quad (3.8)$$

$$T = \begin{bmatrix} S_x & 0 & 0 & 0 \\ 0 & S_y & 0 & 0 \\ 0 & 0 & 1 & 0 \\ 0 & 0 & 0 & 1 \end{bmatrix} \times \begin{bmatrix} 1 & 0 & 0 & 0 \\ 0 & \cos \alpha & -\sin \alpha & 0 \\ 0 & \sin \alpha & \cos \alpha & 0 \\ 0 & 0 & 0 & 1 \end{bmatrix} \times \begin{bmatrix} \cos \beta & 0 & -\sin \beta & 0 \\ 0 & 1 & 0 & 0 \\ \sin \beta & 0 & \cos \beta & 0 \\ 0 & 0 & 0 & 1 \end{bmatrix} \times \begin{bmatrix} \cos \gamma & -\sin \gamma & 0 & 0 \\ \sin \gamma & \cos \gamma & 0 & 0 \\ 0 & 0 & 1 & 0 \\ 0 & 0 & 0 & 1 \end{bmatrix} \times \begin{bmatrix} 1 & 0 & 0 & 0 \\ 0 & 1 & 0 & 0 \\ 0 & 0 & 1 & 0 \\ t_x & t_y & t_z & 1 \end{bmatrix} \quad (3.9)$$

where  $u, v, w$  are the input image coordinate,  $u', v', w'$  are the transformed coordinate and  $\alpha, \beta, \gamma$  are the rotation angle about  $x, y, z$  axes respectively.

### 3.2.3.2 Linear interpolation

A linear interpolation was implemented on the cardiac CT volume to sample 2D CT plane in the same size and spatial location as the echocardiography image. Linear interpolation is the most popular technique of interpolation (Maes et al., 1997; Pluim et al., 2003; Zhu et al., 2002). To transform points from one image to another, the linear interpolation technique defines the intensity of a point as the weighted combination of the intensities of its neighbours and the weights are linearly dependent on the distance

between the point and its neighbours. The best matching interpolated 2D CT plane, and therefore the optimal alignment, was determined using normalized mutual information (NMI).

### 3.2.3.3 Normalized Mutual Information (NMI)

The mutual information metric,  $I(A, B)$  is given by Equation 3.10 and Equation 3.11:

$$I(A, B) = H(A) + H(B) - H(A, B) \quad (3.10)$$

$$I(A, B) = \sum_a \sum_b \rho_{AB}(a, b) \log \frac{\rho_{AB}(a, b)}{\rho_A(a) \rho_B(b)} \quad (3.11)$$

where  $H(A)$  and  $H(B)$  are the Shannon-Wiener entropies of cardiac CT and echocardiography images respectively whereas the joint entropy of the two images is given by  $H(A, B)$  (Faber et al., 1991). The  $H(A)$ ,  $H(B)$  and  $H(A, B)$  are defined by Equation 3.12, 3.13 and 3.14:

$$H(A) = -\sum_a \rho_A(a) \log \rho_A(a) \quad (3.12)$$

$$H(B) = -\sum_b \rho_B(b) \log \rho_B(b) \quad (3.13)$$

$$H(A, B) = -\sum_a \sum_b \rho_{AB}(a, b) \log \rho_{AB}(a, B) \quad (3.14)$$

where  $p_{AB}(a, b)$  is the joint probability of the two images, whereas  $p_A(a)$  and  $p_B(b)$  are the marginal probabilities of image A and B, respectively, which can be estimated from the normalized joint histogram.

NMI is arguably an excellent similarity metric and has shown to be robust and well-suited for multimodal image registration (D. Hill et al., 2000; Huang et al., 2009). This metric does not assume a linear relationship between image intensities of different modalities. The co-occurrence of the most probable values in the two modality images is maximized at the optimal registration (Kiss et al., 2013). Assuming  $A$  is the 2D interpolated CT plane and  $B$  the echocardiography image, the mutual information metric  $NMI(A, B)$  is given by Equation 3.15:

$$NMI(A, B) = \frac{1}{n} \sum_{j=1}^n \frac{H(A) + H(B_j)}{H(A, B_j)} \quad (3.15)$$

where  $n$  is the number of echocardiography frames used in the registration process.

### 3.2.3.4 Optimization

The image registration task was performed iteratively using a generalized pattern search (GPS) algorithm to find the optimal spatial transformation parameters that maximize the NMI measure of overlap image pixel intensities. The GPS algorithm (Momma et al., 2002) comes from a family of numerical optimization methods that do not involve gradient of the objective function to be optimized. Thus it is specifically suited for a function that is not differentiable such as mutual information in its usual form. GPS works by sampling points in a fixed pattern around the seed position (Dennis et al., 1994) provided from pre-procedural planning using CT.

During optimization, all transformation parameters were scaled to a range of -1 to 1 (except scaling from 0 to 1) to compensate for the difference in the order of magnitude between parameters and to improve convergence speed, as well as the accuracy of the output. The objective functions were evaluated using parallel processing, and the optimizer was iterated until the search step becomes sufficiently small and convergence

to a maximum NMI has been achieved. The optimal transformation found was subsequently applied to cardiac CT volume to create matching 2D CT planar image. This image can be fused with echocardiography image to create a composite image for surgical navigation.

### **3.3 Validation of registration accuracy**

The registration of the proposed method was analysed qualitatively and quantitatively as described in the next subsections.

#### **3.3.1 Qualitative assessment of registration accuracy**

The registration accuracy of the proposed method was compared against gold standard manual registration. The validation was performed on the short axis “*Mercedes Benz*”, long parasternal axis and four chamber views of ten patients. During temporal registration, three echocardiography frames of each views are interpolated to be registered to the cardiac CT of ten patients. The spatial registration on three different views were performed on 90 images in total.

##### **3.3.1.1 Defining the gold standard alignment**

Manual registration was performed by experts by manually manipulating the transformation parameters. To do this, the transformation parameters are estimated based on the expert’s knowledge of the echocardiography plane orientation with respect to the heart location within the patient body. The rotation, translation and scaling in x, y and z direction were used to align the echocardiography and cardiac CT and was considered the gold standard. This approach has been shown to produce less than one millimetre localization error (Hacihaliloglu et al., 2009).

### 3.3.1.2 Overall cardiac CT image quality

Overall interpolated cardiac CT image qualities by the proposed method were validated by two experts. They assessed the image quality of interpolated cardiac CT image and score the images from 1 to 4. The description of the score is as follows:

- Score 1: Excellent image quality. The image shows excellent visibility and differentiation of the anatomic details of the heart structure relevant for surgical treatment of heart valves. Very similar to the structure seen in echocardiography image.
- Score 2: Good image quality. The image shows good visibility of the relevant anatomic details for valve treatment. Quite similar to the structure seen in echocardiography image.
- Score 3: Poor but still diagnostic. The image shows poor visibility of the anatomic details. The plane seems to be slightly off from the intended valve plane as shown in echocardiography.
- Score 4: Bad. The image shows nondiagnostic image quality and delineation of anatomic structures and root not possible. The plane is completely off and different from the echocardiography image.

Interobserver agreement for image quality, cardiac structure morphology with CT were expressed as the Cohen  $\kappa$  statistic (Cohen, 1960).

### 3.3.2 Quantitative assessment of registration accuracy

To assess the registration accuracy quantitatively, expert segments the aortic valve annulus, aorta body, left atrium and left ventricle on both echocardiography and the best matching CT planes (obtained from manual and automatic registrations). Dice Similarity Coefficient (DSC) and Hausdorff Distance (HD) metric are calculated on contoured

region. Besides that, the diameter of aortic and mitral valves annulus are measured from both automatic and manually registered CT planes. Agreement in diameter measurements obtained from the two different registration mechanisms was subsequently compared using a Bland–Altman plot. Statistical differences between echocardiography-automatically registered CT (echo-autoCT) and echocardiography-manually registered CT (echo-manualCT) were also analysed using Student’s T test with p value set at 0.05. In addition, root mean square error (RMSE) was calculated to analyse the transformation parameters. Further details of each quantitative analysis are given in the next subsections.

### 3.3.2.1 Manual segmentation

Manual segmentation was performed by the expert on both CT image resulted from manual and automatic registration and the echocardiography images. In “Mercedes Benz” sign views, the cross section of aortic valve was contoured, whereas in long parasternal view, the long body of aorta was contoured. This views are essential view to diagnose for aortic valve disease particularly. Besides that, in 4 chamber view, expert contoured the LA and LV. LA and LV are two closest structures to mitral valve and are affected structures by mitral valve disease (Enriquez-Sarano & Frye, 2007; Turi, 2004).

### 3.3.2.2 Dice Similarity Coefficient (DSC)

DSC measures the spatial overlap between two contoured regions of interest (ROI) in the best matching 2D CT plane and echocardiography frames. This measure is sensitive to both location and size of the contoured ROI, and is defined by Equation 3.16.

$$DSC = \frac{1}{n} \sum_{j=1}^n \frac{2(R_A \cap R_{B_j})}{R_A + R_{B_j}} \quad (3.16)$$

where  $R_A$  and  $R_B$  are the contoured ROI in the 2D CT plane and the echocardiography frames, respectively.  $n$  is the number of echocardiography frame used in registration. DSC

ranges from 0 to 1, with DSC of 0 indicates no overlap and DSC of 1 indicates complete congruence between two ROIs.

### 3.3.2.3 Hausdorff distance (HD)

Hausdorff distance (HD), by contrast, is a distance measure to estimate the distance between two ROIs by the spatial distance of their contour points. This measure is defined by Equation 3.17 and 3.18.

$$H(A, B) = \frac{1}{n} \sum_{j=1}^n \max(h(A, B_j), h(B_j, A)) \quad (3.17)$$

$$h(A, B) = \max_{a \in A} \min_{b \in B} \|a - b\| \quad (3.18)$$

where  $A$  and  $B$  are two sets of contour points in the cardiac CT plane and echocardiography frames, respectively. It also means that HD computes the mutual proximity between two ROIs by indicating the maximal distance between any points of one ROI to the other ROI (Zou et al., 2004).

The DSC and HD metric are indirect assessment of the registration accuracy, in which the degree of area similarity and shape difference of the aortic and mitral valve between two comparing planes are assessed. These 2D measurement of aortic and mitral valves are considered reasonable measurement for assessing the registration accuracy of the proposed technique as the clinical intention is to fuse 2D echocardiography and 2D interpolated plane of CT.

### 3.3.2.4 Diameter of aortic and mitral valve annulus measurement

In addition, the diameters of the aortic and mitral valves annulus were measured from both automatic and manually registered CT planes. For the aortic valve, the diameter of the annulus was defined as the circumcircle diameter of the valve annulus due to the

noncircular shape of the aortic valve in the “*Mercedes Benz*” sign view. Whereas for the mitral valve annulus, the diameter of the annulus was defined in the four chamber view. The Bland-Altman plots were used to compare the agreement in diameter measurements obtained from the two different registration mechanisms. Statistical differences between registration of echocardiography to automatically registered CT (echo-autoCT) and echocardiography to manually registered CT (echo-manualCT) was also analysed using Student’s T-test with p-value set at 0.05.

### 3.3.2.5 Root mean square error (RMSE)

To perform quantitative analysis on the transformation parameter, the root mean square error (*RMSE*) was calculated to compare each of the transformation parameters between manual and automatic registration. This measure is defined in Equation 3.19.

$$RMSE = \sqrt{\frac{1}{n} \sum_{i=1}^n (\|T_{m_i} - T_{a_i}\|)^2} \quad (3.19)$$

where  $T_m$  is the transformation parameter (i.e. translation, rotation or scaling) obtained from expert’s manual registration and  $T_a$  is the corresponding transformation parameter resulted from the proposed algorithm.

## CHAPTER 4: RESULTS

In this chapter, various results generated by the proposed automatic registration pipeline are presented. The registration workflow is validated on ten patient data sets. In Section 4.1, resulted echocardiography from temporal registration and best matching CT plane of a patient is presented. These results include three views of echocardiography frames, which include the “*Mercedes Benz*” sign, long parasternal and four chamber views. In Section 4.2, the best matching plane resulted from the proposed method is compared to manual gold standard registration results. The overall quality image was validated by two experts and the interobserver agreement is expressed as the Cohen  $\kappa$  statistic.

In Section 4.3, the computation results of DSC and HD are presented. The quantitative metrics are calculated on contoured region of aortic valve, aorta body, left atrium and left ventricle of various views of image acquisition. The valves diameter measurements are presented in Section 4.4 where the agreement of measurement in both registration methods are analysed by Bland-Altman Plots. The quantitative error analysis of transformation parameters are presented in Section 4.5, which includes the RMSE of each transformation parameters. The fusion images of echocardiography and cardiac CT plane of the 3 views are presented in Section 4.6. While in Section 4.7, computation time of the image registration algorithm are presented.

#### 4.1 Automatic registration results

In this study, by using the proposed intensity-based registration algorithm, a rigid geometrical transformation was applied to the 2D planar echocardiography image to spatially maneuvered within the vicinity of the cardiac CT volume in search for the best matching cardiac CT plane. Figure 4.1 depicts the results of registering 3 different views in a patient. Row 1 shows the echocardiography images of the “Mercedes Benz” sign, long parasternal and four chamber views, which were extracted from the time series echocardiography data set at the temporal registration step. Whereas, row 2 displays the interpolated CT planes resulted from the proposed automatic registration method.

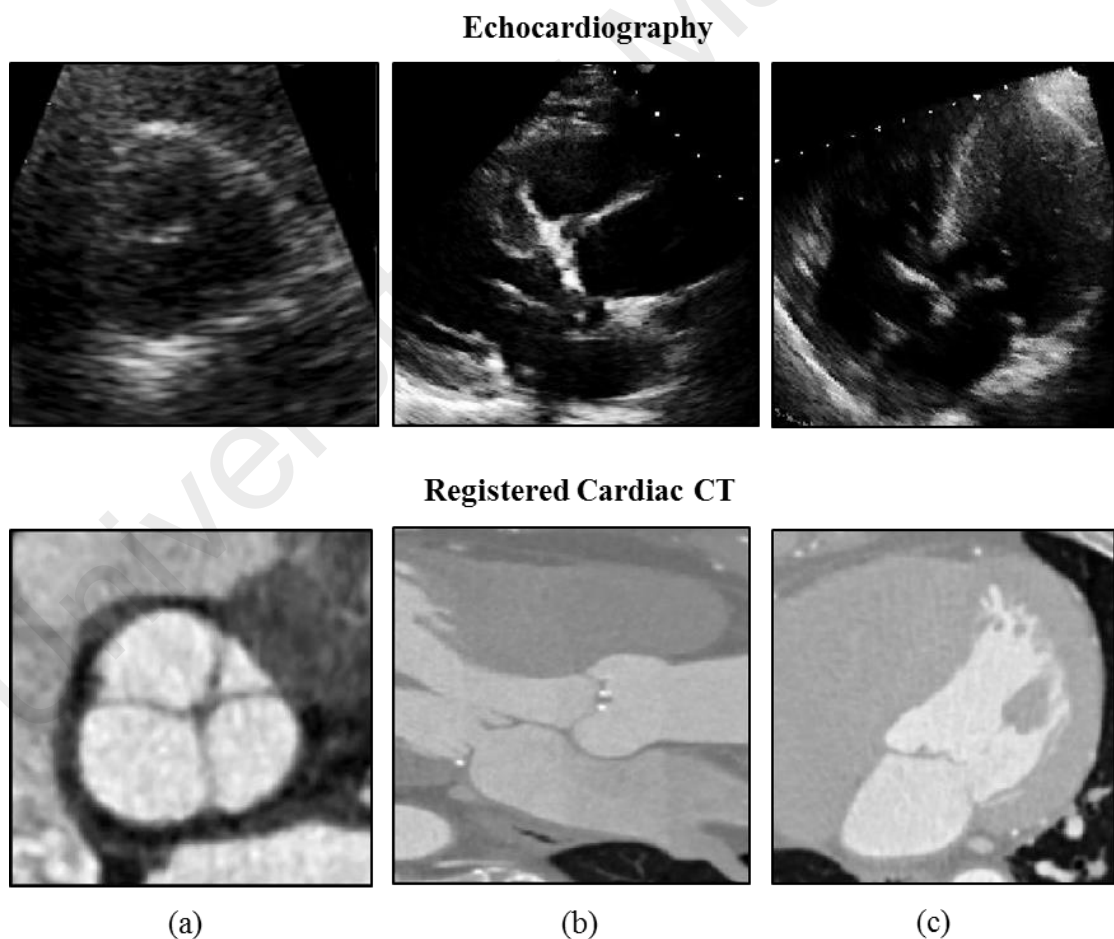


**Figure 4.1: Automatic registration result. (a) “Mercedes Benz”, (b) long parasternal axis, (c) four chamber views.**

## 4.2 Comparison between automatic registration and manual registration results

To validate the automatic registration algorithm, manual registration was performed by the expert. The transformation parameters were manually manipulated to obtain the views of the corresponding interpolated CT images which the expert found to resemble the 2D echocardiography image. Figure 4.2 presents the automatic registered CT (AutoCT) in row 1 while row 2 displays the manually registered CT (ManualCT) by the expert. The appearances of cardiac structures on registered AutoCT were found to resemble those manually collocated CT planes by the expert.

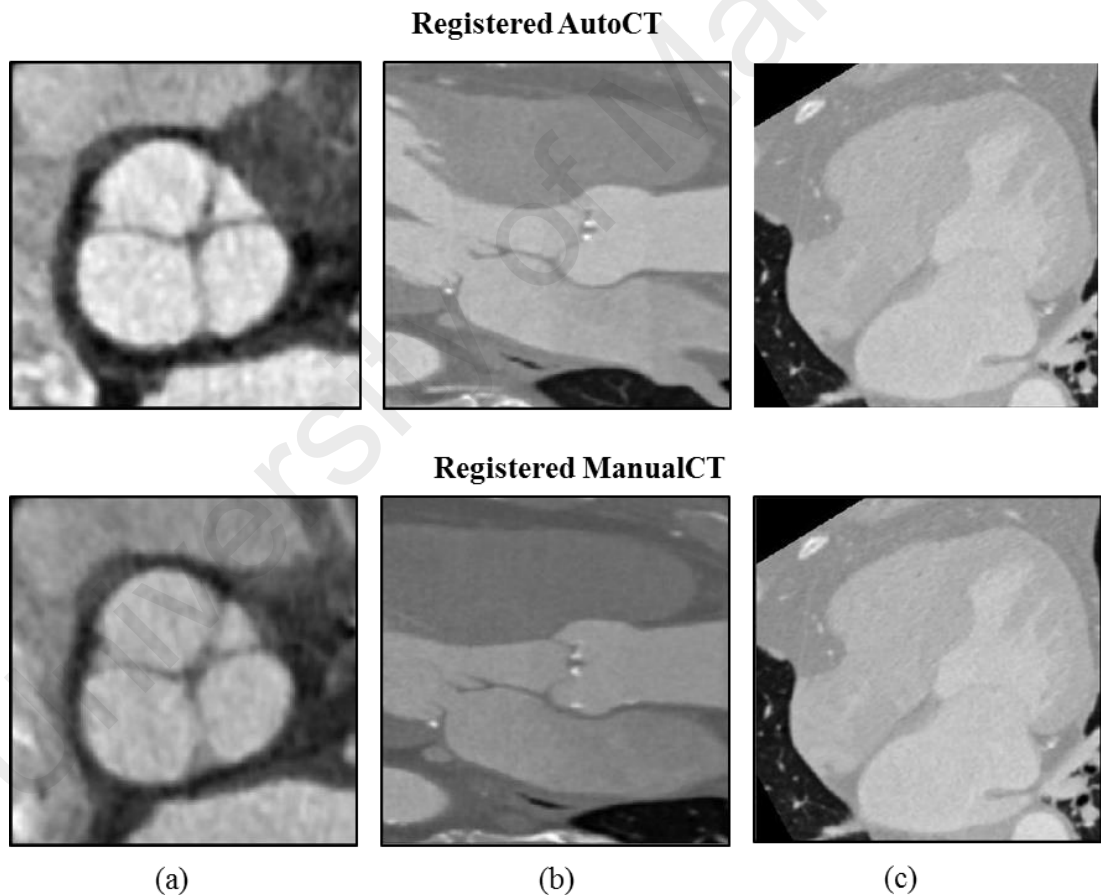


**Figure 4.2: Comparison between automatic registered CT and manually registered CT of three different views. (a) “Mercedes Benz”, (b) long parasternal axis, (c) four chamber views.**

Overall quality of CT images in all 10 patients was rated by both experts with good interobserver agreement ( $\kappa=0.86$ ), as grade 1 (excellent) in 39 images (43.3%) and as grade 2 (good) in 51 images (56.7%). No reader rated CT image quality as grade 3 (poor but still diagnostic) and grade 4 (bad and nondiagnostic).

### 4.3 DSC and HD results

The DSC and HD of the common features as delineated in both echocardiography and CT planes are tabulated in Table 4.1. Comparing both echo-autoCT and echo-manualCT in short axis “*Mercedes Benz*” sign views, both DSC values were comparable at 0.81 ( $\pm 0.08$ ) and 0.79 ( $\pm 0.09$ ), respectively. DSC value above 0.7 indicates that the contoured ROI in both types of images have considerable similarity in area size and spatial overlap [33]. Similar HD was also computed between the two pairs of registration, with the value of the former equal to 1.30 ( $\pm 0.13$ ) mm and the latter equal to 1.32 ( $\pm 0.04$ ) mm. This registration error was comparable in magnitude to about 3 to 4 pixels in the resolution of CT and echocardiography, which is acceptable in view of the much bigger field of view yielded by both imaging modalities (i.e. 0.4 x 0.4 x 0.4 mm for a CT volume and 0.3 mm x 0.3 mm for a 2D echocardiography plane).

The performance of the proposed algorithm was found consistent for the long parasternal axis view (as in Table 4.1). The long body of the aorta was contoured in the echocardiography and interpolated cardiac CTs by both methods. The DSC values was 0.79 ( $\pm 0.02$ ) for echo-autoCT pair, whereas for echo-manualCT was 0.73 ( $\pm 0.02$ ). Both image pairs have a similar area size and spatially overlap. HD between the two ROIs are comparable with the value for the echo-autoCT was equal to 1.19 ( $\pm 0.11$ ) mm and for the echo-manualCT was equal to 1.22 ( $\pm 0.08$ ) mm. This distance error was comparable in magnitude to about 3 to 4 pixels in the resolution of CT and echocardiography.

Consistent performance was also found in the four chamber view (as in Table 4.1). Here DSC and HD were calculated on two contoured structures, left atrium and left ventricle. DSC values for echo-autoCT and echo-manualCT for the left atrium were equal to  $0.87 (\pm 0.04)$  and  $0.86 (\pm 0.04)$ , respectively. Whereas, HD for the echo-autoCT was equal to  $1.23 (\pm 0.32)$  mm and  $1.24 (\pm 0.29)$  mm. This registration error is comparable in magnitude to about 3–4 pixels in the resolution of CT and echocardiography. The performance of the proposed algorithm was found consistent for the left ventricle structure too, where the DSC values were  $0.82 (\pm 0.07)$  and  $0.84 (\pm 0.06)$  for the echo-autoCT and echo-manualCT, respectively. While HD values for both pairs were  $1.14 (\pm 0.18)$  mm and  $1.09 (\pm 0.21)$  mm for echo-autoCT and echo-manualCT, respectively.

**Table 4.1: Registration accuracy as measured using DSC and HD.**

Plane	Measure	Echo –autoCT <sup>1</sup> (mean $\pm$ std)	Echo -manualCT <sup>2</sup> (mean $\pm$ std)
<sup>1</sup> Aortic valve	DSC	$0.81 \pm 0.08$	$0.79 \pm 0.09$
	HD	$1.30 \pm 0.13$ mm	$1.32 \pm 0.04$ mm
<sup>2</sup> Long body of aorta	DSC	$0.79 \pm 0.02$	$0.73 \pm 0.02$
	HD	$1.19 \pm 0.11$ mm	$1.27 \pm 0.08$ mm
<sup>3</sup> Left atrium	DSC	$0.87 \pm 0.04$	$0.86 \pm 0.04$
	HD	$1.23 \pm 0.32$ mm	$1.24 \pm 0.29$ mm
<sup>3</sup> Left ventricle	DSC	$0.82 \pm 0.07$	$0.84 \pm 0.06$
	HD	$1.14 \pm 0.18$ mm	$1.09 \pm 0.21$ mm

<sup>1</sup>DSC and HD resulted from contoured region in the “Mercedes Benz” sign view

<sup>2</sup>DSC and HD resulted from contoured region in the long parasternal view

<sup>3</sup>DSC and HD resulted from contoured region in the four chamber view

#### 4.4 Bland-Altman analysis

Diameters of aortic and mitral valve were measured from the automatically and manually registered CT planes. The agreement between the automatic registration method and the gold standard manual registration were assessed through the Bland-Altman analysis. By using this graphical approach the difference of two measurements against the mean of the same measurements was shown. This approach allowed a visualization of the extent to which the measurements differed from each other.

The Bland-Altman plot in Figure 4.3 demonstrates a good agreement in the diameter measurement of aortic valve annulus as obtained from the automatically and manually registered CT planes. The limit of agreement was about -2.83 to 3.07mm and the mean difference for aortic valve diameter measurement was found to be  $-0.12 \pm 1.50$  mm.

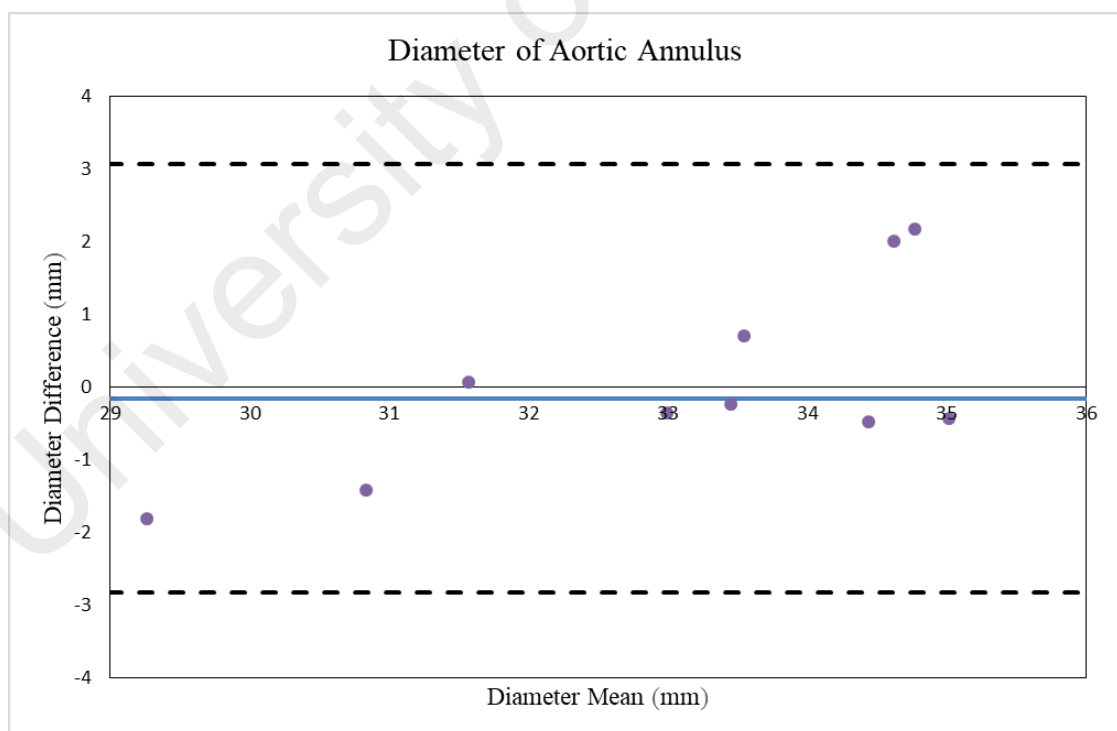


**Figure 4.3: Difference of aortic valve diameter measurement between CT plane from automatic and manual registration method, with 95% limits of agreement (black dotted line) and bias (blue line).**

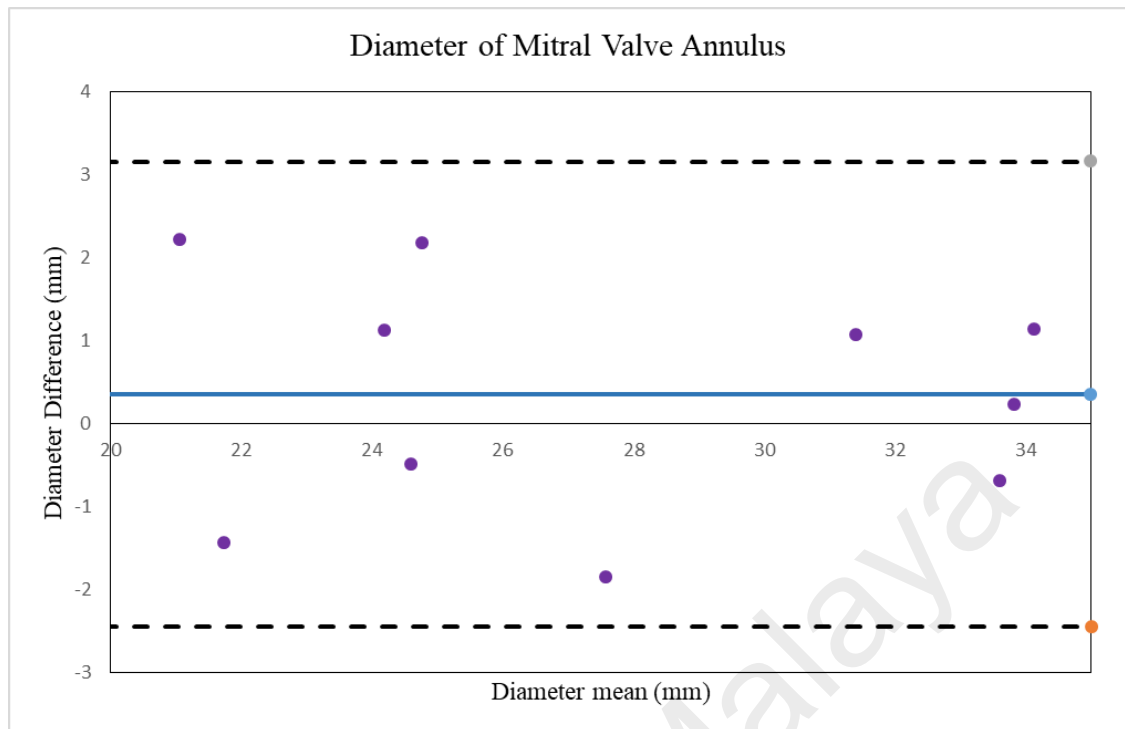


**Figure 4.4: Difference of mitral valve diameter measurement between CT plane from automatic and manual registration method, with 95% limits of agreement (black dotted line) and bias (blue line).**

Whereas for the mitral valve diameter measurement as in Figure 4.4, the limit of agreement was about -2.45 to 3.16 mm and the mean difference for mitral valve diameter measurement were found to be  $-0.35 \pm 1.43$  mm. Both Bland-Altman plots showed no significant bias for both registration methods.

#### 4.5 Transformation analysis

A quantitative analysis on the transformation was performed by computing the root mean square error (RMSE) for each transformation parameter. The quantitative error of the transformation parameters are tabulated in Table 4.2. The RMSE for translation is ranging from 0 to 2.12 mm which is comparable in magnitude to about 0 to 5 pixels of the resolution of cardiac CT and echocardiography. The angular deviation is less than  $3^\circ$  and minimal scaling deviation was tabulated.

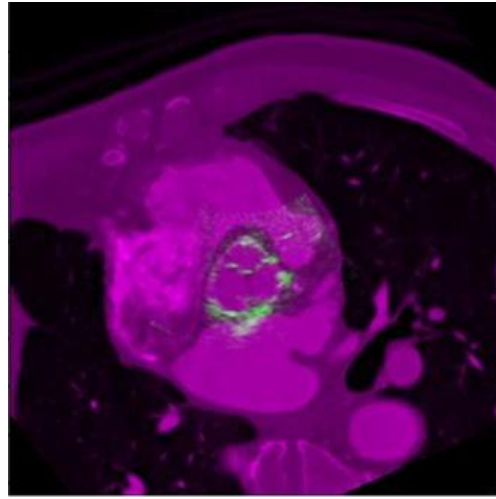
**Table 4.2: RMSE of transformation parameter between automatic and manual registration method.**

Patient #	Translation (mm)			Rotation (°)			Scaling	
	$\Delta tx$	$\Delta ty$	$\Delta tz$	$\Delta \alpha$	$\Delta \beta$	$\Delta \gamma$	$\Delta sx$	$\Delta sy$
1	0.02	0.27	0.01	0.24	0	0.53	0.01	0
2	0.14	0.28	0.42	1.89	0	0	0	0
3	0.22	0.04	0.02	0.03	0	0.18	0	0
4	0.42	1.13	0.78	0.47	0	0	0	0
5	0	0.07	0.06	0.03	0	0.24	0	0
6	1.69	2.12	0	0	2.67	2.54	0	0
7	1.7	2.12	1.70	2.95	0	2.83	0	0
8	1.91	2.12	0	0	0	0	0	0
9	0.42	1.13	0.78	0.47	0	0	0	0
10	0	0.07	0.068	0.03	0	0.24	0	0

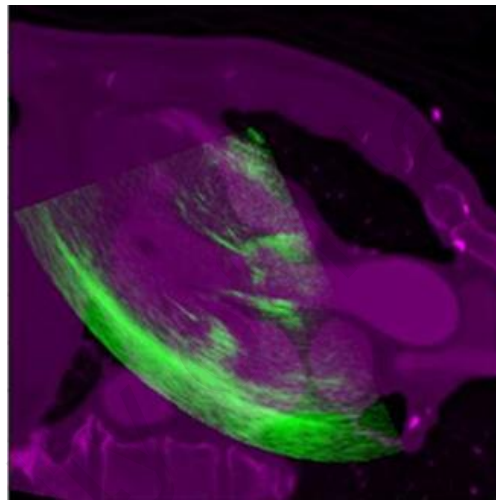
$\Delta tx$ ,  $\Delta ty$  and  $\Delta tz$  refer to the RMSE for the translation, while  $\Delta \alpha$ ,  $\Delta \beta$  and  $\Delta \gamma$  refer to the RMSE for rotation along the three axes. Whereas,  $\Delta sx$  and  $\Delta sy$  are RMSEs in scaling along both dimensions of the planar image.

#### 4.6 Echocardiography and cardiac CT fusion image

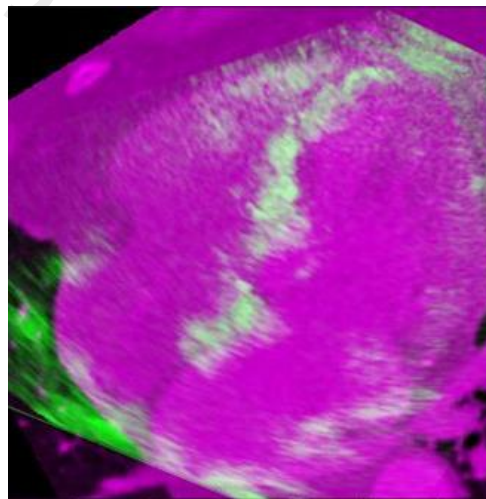
The echocardiography and the interpolated best matching plane of cardiac CT were fused during surgical guidance procedure. The fused images are shown in Figure 4.4. Figure 4.5 (a) shows the composite of echocardiography and auto-CT for short axis “Mercedes Benz” sign view. The aortic valves in both images are perfectly aligned. Whereas in Figure 4.5 (b), the fused image of the long parasternal view depicts the body of aorta and the adequately aligned surrounding structure in both images. Consistent performance is observed in Figure 4.5 (c) where the four chamber fused images show that features of both images were perfectly aligned. Expert’s visual inspection of overlapped cardiac structures divulges that the proposed registration method is capable to align the images successfully as desired in clinical applications.



(a)



(b)



(c)

**Figure 4.5: Fusion of echocardiography frame and cardiac CT at (a) short axis “Mercedes Benz” sign, (b) long axis parasternal and (c) four chamber views.**

#### 4.7 Registration computation time

The average computation time for the registration of 3 different views are tabulated in Table 4.3.

**Table 4.3: Average Computation Time for Automatic Registration of Different Views**

<b>Views</b>	<b>Average Computation Times (Seconds)</b>
<b>“Mercedes Benz” sign</b>	50 s
<b>Long parasternal</b>	48 s
<b>Four chamber</b>	46 s

University of Malaya

## CHAPTER 5: DISCUSSION

In this chapter, results of the proposed registration technique and its clinical impact are discussed. Section 5.1 covers the major findings of this research. A comparison to other previous similar studies is provided in Section 5.2. The clinical relevance of the proposed techniques is discussed in Section 5.3, whereas limitations are acknowledged and suggested for future improvement in Section 5.4 and Section 5.5, respectively.

### 5.1 Major findings of the study

In this study, a registration framework for fusing 3D cardiac CT images and 2D echocardiography frames at the absence of an optical tracking system has been presented. The applied registration procedure originates from the discipline of information theory, whereby the mutual information of two arbitrary datasets from different imaging modalities is maximized. Without an optical tracking system mounted on the echocardiography transducer, the proposed method has shown the practicability to be utilized during intraprocedural navigation during TVR and TVI.

In this study, a temporal registration was performed to align echocardiography and cardiac CT images in time since both modalities produce images of different sampling latencies and temporal resolution. The echocardiography image frames interpolated from the time series echocardiography recording were then subject to preprocessing procedure to reduce speckle noise. The visual inspection by experts reveals that the proposed temporal registration and noise reduction methods are capable of synchronizing the images in time with reduced speckle noise in the echocardiography images.

Currently, the proposed method is applied to the retrospective data. The automatic registered CT images are found to match its corresponding echocardiography's views which were extracted out from the time series data set at the temporal registration step.

Besides that, the proposed spatial registration method was evaluated by comparing it against gold standard manual registration. The appearance of cardiac structures on automatic registered CT planes was found to resemble those in the manually collocated CT planes by the expert. Moreover, the automatically registered CT image has shown good agreement with the manually selected CT image by expert, in terms of insignificant visual appearance as well as quantitative assessment of aortic and mitral valve diameter between the corresponding interpolated planes.

Cohen statistics show good interobserver agreement for the overall quality of registered CT images in all ten patients. In addition, the reported DSC values were above 0.7. This indicates that the contoured ROI in both types of images have considerable similarity in area size and spatial overlap. Whereas, the reported HD shows a distance error that was comparable in magnitude to about three to four pixels in the resolution of CT and echocardiography. This is acceptable in view of the much bigger field of view yielded by both imaging modalities (i.e.,  $0.4 \times 0.4 \times 0.4$  mm for a CT volume and  $0.3$  mm  $\times$   $0.3$  mm for a 2D echocardiography plane). The Bland-Altman plots demonstrate good agreement in the diameter measurement of the valves annulus as obtained from the automatically and manually registered CT planes. Besides that, the RMSE of transformation parameters for translation, rotation and scaling were found minimal.

These validation results, therefore, show a promising accuracy of the proposed technique to be applied for navigation during TVR and TVI procedures. The proposed method has shown feasibility in visualizing the anatomical structures of the heart such as aortic valves, long body of aorta, mitral valve, left atrium and left ventricles which are vital during TVR and TVI procedures.

## 5.2 Comparison with previous similar studies

In this study, the reported distance error in terms of HD measurement of the registration method was between  $1.14 \pm 0.18$  mm and  $1.30 \pm 0.13$  mm (Table 5.1). This error could be caused by several factors, including the spatial registration errors between echocardiography and cardiac CT images, the physical variations of the same structure as imaged by echocardiography and cardiac CT, as well as the variation in manual delineation of cardiac structure for comparison. Currently, to the author's knowledge, no similar study has been published so far. Therefore no comparable error values could be found in the literature. However, in this subsection, a comparison of registration accuracy based on the distance error between multimodal registrations of some related works on cardiac registration are discussed and presented in Table 5.1.

Huang et al. (2009) reported a TRE of  $1.7 \pm 0.4$  mm using a phantom for their 2D echocardiography to cardiac CT registration. Besides, the registration framework of echocardiography to CT by Lang et al. (2011) resulted in a TRE of  $2.15 \pm 0.6$  mm for inner left ventricular wall and  $1.5 \pm 0.45$  mm for the aortic root. Meanwhile, the registration frameworks proposed by Linte et al. (2007) reported a TRE of 5.2 mm for the left ventricle registration between TEE and MRI modalities. The CT to TEE registration proposed by F. P. Li et al. (2015) resulted in a TRE of  $2.68 \pm 0.94$  mm for mitral valve annulus. All these studies utilized optical tracking systems in their registration frameworks. Comparatively, the accuracy of the registration method proposed by this research has shown the lowest TRE in the literature despite of the absence of an optical tracker for the registration.

Table 5.1 summarizes the related studies, their region of interest (ROI) and the reported distance error in comparison to current study. Based on Table 5.1, it can be observed that the distance error of the proposed approach is the lowest of all compared results from other studies.

**Table 5.1: Comparison of distance errors in related studies on multimodality registration.**

Previous Similar Studies			Current Study	
Studies	ROI	Distance Error (mm)	ROI	Distance Error (mm)
(Huang et al., 2009)	Phantom	$1.7 \pm 0.4$	Aortic valve	$1.32 \pm 0.04$
(Lang et al., 2011)	Left ventricle Aortic root	$2.15 \pm 0.6$ $1.5 \pm 0.45$	Long body of aorta	$1.27 \pm 0.08$
(Linte et al., 2007)	Left ventricle	5.2	Left atrium	$1.24 \pm 0.29$
(F. P. Li et al., 2015)	MVA	$2.68 \pm 0.94$	Left ventricle	$1.09 \pm 0.21$

### 5.3 Clinical relevance of the study

Cardiovascular imaging plays an important role in the diagnosis and surgical planning of many cardiac diseases. During cardiac intervention, image registration could offer invaluable solution to the physician in terms of integrating complementary information from multiple modalities. Modern technology such as CT and MRI provides excellent image quality for structural and functional assessment but lacks in real time capability. In addition, it comprises expensive solutions requiring a special sitting facility. Echocardiography is low cost, portable and allows real-time imaging. However, it is confounded by speckle noise. Nevertheless, 2D intraoperative echocardiography images could be more easily interpreted if they would be used in conjunction with good contrast, preoperative images from cardiac CT. Integrating 2D echocardiography and cardiac CT

could overcome the limitations of an individual modality and would be potentially useful for TVR or TVI guidance. 2D echocardiography and cardiac CT are the two most common, minimally invasive treatment procedures indicated for patients with aortic and mitral valve diseases.

In this thesis, a novel image registration framework for information fusion between 2D echocardiography and 3D cardiac CT was introduced to guide TVR and TVI procedures. Compared to previous studies (Huang et al., 2009; Lang et al., 2011; F. P. Li et al., 2015; Linte et al., 2007; Sandoval & Dillenseger, 2013; Sun et al., 2007; Zhong et al., 2006), where optical tracking systems were employed to provide image localization, the proposed method has shown feasibility in the absence of such tracking technology. The proposed registration framework targets to establish a direct spatial relationship between anatomical and functional information from both imaging modalities for a rapid and accurate assessment of the aortic and mitral valve structures. These information are crucial for procedural planning, potentially reducing the risk and morbidity associated with the treatment intervention. Within the high quality dynamic 3D anatomical context provided by CT images, interpretability of intraoperative 2D echocardiography images has shown to significantly improve. In addition, this multimodality registration method also provides other potential advantages including the assessment of the left ventricular motion and thickness as well as ventricular hypertrophy condition, which are not available in either echocardiography or cardiac CT images alone.

## **5.4 Study limitations and suggestion for improvement**

A few limitations in the research were observed and are summarized in the following subsections. Proposals for improving current limitations are also provided.

### **5.4.1 The heart as rigid body structure**

Currently, the heart is assumed to be rigid with periodic heart motions throughout the imaging process. Therefore, the current techniques employed a rigid spatial transformation in the registration process. The rigid spatial transformation in the registration framework is commonly used in clinical practice and is considered to be acceptable for reaching the correct diagnosis (Marinelli et al., 2012). Although this hypothesis is valid in some surgical scenarios, the heart is indeed nonrigid but a dynamic structure. Deformation of the heart inevitably occurs during the pumping cycle. Other factors such as respiration as well as probe and surgical instruments pressure on the skin can also contribute to the deformation of heart. These factors would jeopardize the accuracy of image registration during real time imaging.

Though the proposed registration method is based on a rigid spatial transformation, the validation results nevertheless have shown a promising accuracy of the proposed technique to be applied for intraprocedural surgical guidance. The registration technique may be further improved with the use of nonrigid registration methods (Ledesma-Carbayo et al., 2005) to compensate for such deformation. However, this may add more complexity to the registration process, and the speed of registration could be compromised.

In the temporal registration process, a linear interpolation with the aid of the ECG signal was utilized to achieve temporal synchronization between echocardiography and cardiac CT, since there was no significant variation of the heart rate between the imaging

sessions. However, in cases where heart rate changes significantly between cardiac procedures, a nonlinear temporal scaling of ECG may be required.

#### **5.4.2 Seed position**

The proposed technique requires a priori knowledge of the rough position and orientation of the 2D echocardiography image with respect to the 3D axes of the patient body in order to initialize the registration search space. This information is currently estimated during treatment planning by the clinician before the actual surgical procedure. Inaccurate positioning of the initial plane (seed) by the physician may jeopardize the accuracy of the final CT plane inferred through the optimization process. The accuracy of this seed placement could depend on the experts' knowledge on how the echocardiography views are being acquired from patient. Special training to the physician may be required for the application of such a registration technique in clinical scenario.

Our current results indicate a small distance between the positions of the seed plane and the correctly registered plane. When tested against large displacement of a few centimeters offset, the resulting interpolated CT plane may show a low degree of area similarity (DSC) and huge shape difference (HD) to the echocardiography image. In case prior knowledge of the seed plane is unavailable, a feature-based method (Mikic et al., 1998; Zheng et al., 2012) may be incorporated into the current framework to provide a rough estimation of the initial valve plane before fine tuning with intensity-based registration. Other than that, the robustness of the algorithm to large displacement may be improved by using a multiresolution scheme, which hierarchically refines the accuracy through coarse-to-fine registration (Gong et al., 2014) or by using a multistart optimization scheme (Song et al., 2007).

### **5.4.3 Computation speed**

One notable limitation of the proposed method is the computation time. The proposed technique has yet to include speed optimization. While there is a difference in the computational time between different views as given in Table 4.3, it is difficult to assess whether the computation time is the sole result of the registration algorithm. The differences in size of the data sets, the varying amount of noise in echocardiography images and the initial seed plane position may also have contributed to the differences in computation time.

Implementation in other programming platform such as ITK when used as standalone software may provide higher image processing speed for a real-time application. Furthermore, the registration speed may be further improved via a pyramid or multi-resolution implementation (Zheng et al., 2012).

### **5.5 Suggestions to improve the current technique**

In improving the proposed registration techniques for echocardiography and CT, a few additional processing steps will be required. In the temporal registration process, to achieve temporal synchronization between echocardiography and cardiac CT, a linear interpolation with the aid of the ECG signal still could be utilized for the patient with a periodic motion heart rate. However, in the case where the heart rate significantly changes between the cardiac procedures, a nonlinear temporal scaling of ECG will be required. Figure 5.1 shows the new scheme incorporated for temporal registration to improve the current study.

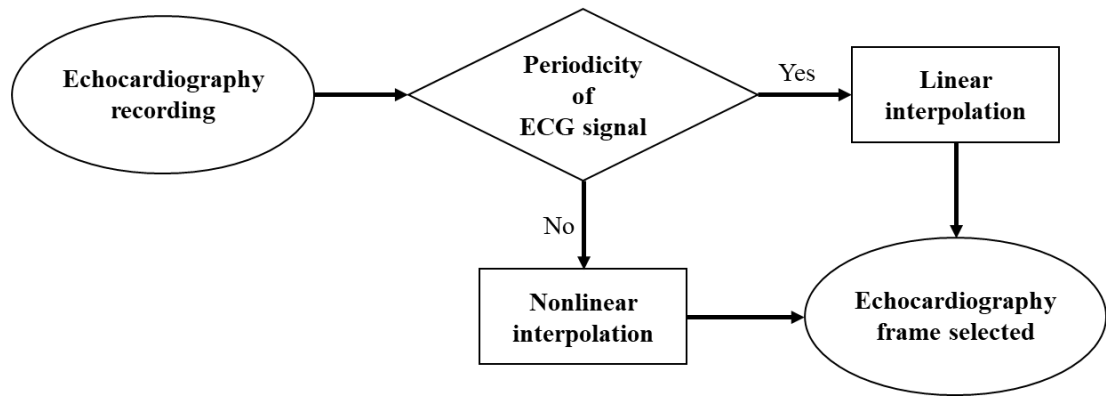


**Figure 5.1: New registration scheme to improve temporal registration.**

In the spatial registration process, where the echocardiography frame is spatially aligned with cardiac CT, a registration with a hybrid method could be employed to improve the proposed technique to be applied during real time imaging. This hybrid method is a combination of a feature based and an intensity based scheme. The feature based method (Mikic, Krucinski, & Thomas, 1998; Zheng et al., 2012) could provide a rough estimation of the initial valve plane seed position before fine tuning with intensity-based registration.

Besides, a nonrigid transformation scheme with speed optimization could be implemented in the spatial registration scheme to improve the proposed techniques. As the heart contracts during its cycle, a free-form deformations scheme based on *B*-spline method and the maximization of NMI can be employed so that the accuracy of the registration scheme is improved. In addition, a multistart or multiresolution optimization method could be utilized to the registration workflow. These methods are one way to explore the transformation parameter space. They could be combined with other local optimization methods. It restarts the search, for the global optimum from a new solution once a region (or a path) has been explored by local optimization. The new start position is uniformly sampled from the transformation parameter space. Figure 5.2 shows the new scheme incorporated for temporal registration to improve the current proposed study.

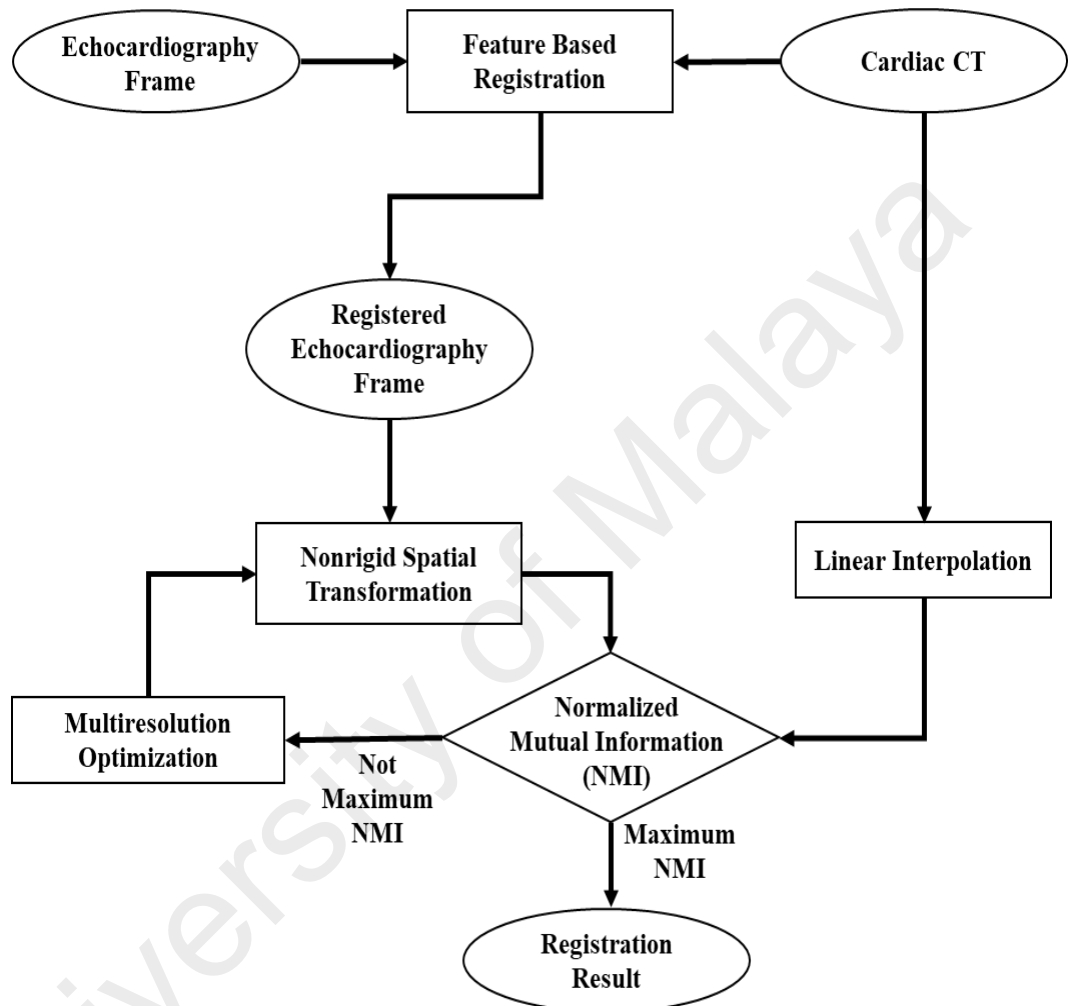


**Figure 5.2: New registration scheme to improve spatial registration.**

## CHAPTER 6: CONCLUSION AND FUTURE WORK

This chapter presents the contribution of this thesis, conclusions and suggestions for future research.

### 6.1 Thesis contribution

The principal contribution of this thesis is the development of an automatic registration framework for the fusion of preoperative 3D cardiac CT and intraoperative 2D echocardiography images, which could potentially be utilized during intraprocedural navigation for TVR and TVI. In this thesis, a registration pipeline consisting of three main steps: temporal registration, preprocessing and spatial registration is presented and validated on three different cardiac views: 1. “*Mercedes Benz*” sign, 2. long parasternal axis and 3. four chamber views of real clinical data. The temporal registration step allows the usage of an echocardiography image frame at a similar cardiac phase as that of the cardiac CT to be automatically chosen for spatial registration. In the second step, preprocessing of echocardiography images from temporal registration step was performed to reduce the speckle noise. The third step involves spatial registration, which was performed using a rigid geometrical transformation and intensity-based registration algorithm to spatially align 2D planar echocardiography image with the static 3D cardiac CT volume. The presented registration algorithm has the ability to correct temporal and spatial misalignment between preoperative cardiac CT and intraoperative echocardiography images.

In brief, the contribution of this thesis is twofold. On one hand, this thesis introduces a multimodal registration framework to guide intraprocedural navigation during TVR and TVI for aortic and mitral valve diseases. On the other hand, the presented algorithm was performed with no optical tracking device. Therefore an augmentation to the echocardiography transduce probe is not necessary. Careful inspection of the proposed

algorithms would reveal their advantages in comparison to the state-of-the art as previously discussed in Chapter 3.

## **6.2 Conclusions**

The fusion of 2D echocardiography and 3D cardiac CT plays an integral role in enhancing the physician's capability to utilize medical imagery information for cardiac surgery involving aortic and mitral valves. The principal objective of this thesis was to achieve fusion of the 2D planar echocardiography images with 3D cardiac CT volume. To the best of the authors' knowledge, this is the first discussion of image fusion for aortic and mitral valve registration with no optical tracking information provided to aid the process. As an alternative, to initialize the registration search, the orientation of echocardiography image was determined from the preprocedural planning. The spatial registration method consists of an intensity-based registration algorithm, which utilizes normalized mutual information (NMI) and a pattern search optimization algorithm. The interpolated cross-sectional view from the cardiac CT volume which matches the echocardiography image during the navigation process is produced during the image registration process. The proposed registration framework could potentially be applied in the diagnosis and image guidance procedure for TVR and TVI as commonly indicated for the treatment of aortic and mitral valve diseases. Results on ten patients indicate encouraging accuracy of the proposed method to be applied clinically.

Future research should investigate the speeding up of the computational time via a pyramid or multi-resolution image registration approach and GPU processing. The current registration framework could also include a feature-based method to facilitate the physician to estimate the initial point of the echocardiography views.

### **6.3 Future work**

A number of interesting and worth pursuing research that could be used to extend the work in this thesis are described in the following subsections.

#### **6.3.1 Intraoperative guidance of cardiac treatment using echocardiography and cardiac CT fusion**

Application of the framework for real time guidance of minimally invasive treatment of other cardiac diseases is also of interest and will be left for future work.

Other than TVR/TVI for aortic and mitral valve disease, there are other minimally invasive treatment for cardiac diseases. For example, for atrial septal defect (ASD) or an opening between the right atrium and the left atrium, a minimally invasive atrial septal defect closure procedure is usually prescribed (Linte et al., 2009). Instead of open heart surgery, which is prone to high risk for the patient, the minimally invasive procedure involves physician making a small (4-6 cm) incision on the right side of the chest. The heart-lung machine is inserted via a small incision in the groin, allowing the heart to be stopped for the sewing of the patch. A soft retractor is inserted, which gently opens the narrow space between the ribs, enabling the surgeon to insert the specialized minimally invasive instruments. Here, an image guidance system such as echocardiography enhanced with cardiac CT plays a vital role to provide the physician with high resolution images of the heart and the ASD.

Meanwhile, for the patient suffering from atrial fibrillation or an irregular heartbeat (arrhythmia) which can lead to blood clots, stroke, and heart failure, a catheter radiofrequency ablation is typically be prescribed (Pankratov et al., 2005). During catheter radiofrequency ablation, a small area of heart tissue that is causing rapid and irregular heartbeats is destroyed by radiofrequency energy, thus restoring the heart's regular rhythm. The ablation procedure itself is performed under 2D echocardiography

guidance whereas the ablation route is determined in a preoperative stage on 3D cardiac CT images. Therefore, the registration of 2D intraoperative echocardiography images to the preoperative cardiac CT images is then necessary in order to transfer and follow the ablation path in the preoperative context.

### **6.3.2 Comparison of echocardiography-cardiac CT fusion with echocardiography-MRI fusion**

Similar to Cardiac CT, cardiac MRI can also provide 3D cross sectional images of the heart. MRI images provide high resolution image quality with high tissue contrast that enables the assessment and measurement of different heart structures (Chambers et al., 2016). However, there are limitations on MRI as compared to cardiac CT such as contraindicated to metal implant patient, and it is a more expensive procedure. Nevertheless, for the patient who undergoes this procedure and is prescribed with minimally invasive treatment, the MRI images can be registered to echocardiography using the proposed registration and fusion method.

In addition, up to date, there is no comparative study of echocardiography-CT and echocardiography-MR fusion in literature. Thus, it may be worth to pursue registration on these modalities, and validate the techniques based on clinical indices. The challenges and registration speed between both fusion techniques can be studied.

### **6.3.3 US-CT image fusion for other anatomical structures**

The method proposed by this thesis could also be applied to fuse dynamic 2D ultrasound images with 3D preoperative CT images of other body parts such as for liver and lung surgeries, where the structure are subject to approximately periodic respiratory motion.

In the field of hepatic intervention, ultrasonography (US) can provide real-time anatomical and functional information with no radiation hazard (Yamashita et al., 1995). Meanwhile, CT or MRI examinations are performed preoperatively. During minimally invasive US-guided procedures, such as biopsy and radiofrequency ablation for percutaneous hepatic intervention, the physician has to correlate the US images of the liver to its 3D anatomical context using CT or MR images. The liver cannot be scanned by echocardiography with orthogonal transverse, sagittal, or coronal planes, which are frequently used for the interpretation of CT or MR images in the daily practice, thus making the visual registration a challenging task. The sonographic window of the scanning is sometimes limited by the rib cage, intestines, or omental fat adjacent to the liver. Therefore, the registration of US to the corresponding 3D CT images during US guided hepatic interventions may assist physician during the procedure, in order to avoid injuries to the surrounding normal tissue structures.

On the other hand, brachytherapy is the radiation therapy to treat patient with lung cancer. This treatment procedure requires the US to guide the physician in applying the radioactive source at the tumor site (Stock et al., 1996). Due to the inferior image quality of US, the US-CT fusion may provide better visualization for navigation during the procedure.

## REFERENCES

- Acker , M. A., Parides , M. K., Perrault , L. P., Moskowitz , A. J., Gelijns , A. C., Voisine , P., Smith , P. K., Hung , J. W., Blackstone , E. H., Puskas , J. D., Argenziano , M., Gammie , J. S., Mack , M., Ascheim , D. D., Bagiella , E., Moquete , E. G., Ferguson , T. B., Horvath , K. A., Geller , N. L., Miller , M. A., Woo , Y. J., D'Alessandro , D. A., Ailawadi , G., Dagenais , F., Gardner , T. J., O'Gara , P. T., Michler , R. E., & Kron , I. L. (2014). Mitral-Valve Repair versus Replacement for Severe Ischemic Mitral Regurgitation. *New England Journal of Medicine*, 370(1), 23-32. doi:10.1056/NEJMoa1312808
- Ahemad, M., & Narayanan, S. (1999). Rheumatic chorea in children: a study of prevalence of clinical and echocardiographic valvular involvement. *Indian Heart J*, 51(694), 8.
- Ahmed, J., Mostafa Zaman, M., & Monzur Hassan, M. (2005). Prevalence of rheumatic fever and rheumatic heart disease in rural Bangladesh. *Tropical doctor*, 35(3), 160-161.
- Aladl, U. E., Hurwitz, G. A., Dey, D., Levin, D., Drangova, M., & Slomka, P. J. (2004). Automated image registration of gated cardiac single - photon emission computed tomography and magnetic resonance imaging. *Journal of Magnetic Resonance Imaging*, 19(3), 283-290.
- Alexander, R. W., Schlant, R. C., & Fuster, V. (1998). Hurst's the heart, arteries and veins: *McGraw-Hill, Health Professions Division*.
- Alraies, M. C., Garry, D. J., & Garry, M. G. (2017). Physiology of the Normal and Failing Heart *Congestive Heart Failure and Cardiac Transplantation* (pp. 21-37): Springer.
- Applegate, E. (2013). The Sectional Anatomy Learning System-E-Book: Concepts and Applications 2-Volume Set: *Elsevier Health Sciences*.
- Audette, M. A., Ferrie, F. P., & Peters, T. M. (2000). An algorithmic overview of surface registration techniques for medical imaging. *Medical Image Analysis*, 4(3), 201-217.
- Ballinger, J. R. (2015). Pitfalls and limitations of SPECT, PET, and therapeutic radiopharmaceuticals. *Paper presented at the Seminars in nuclear medicine*.
- Betancur, J., Simon, A., Tavard, F., Langella, B., Leclercq, C., & Garreau, M. (2012). Segmentation-free MRI to CT 3D registration for Cardiac Resynchronization

Therapy optimization. *Paper presented at the Computing in Cardiology (CinC), 2012.*

Brown, L. G. (1992). A survey of image registration techniques. *ACM computing surveys (CSUR)*, 24(4), 325-376.

Budoff, M. J., & Shinbane, J. S. (2016). *Cardiac CT imaging: diagnosis of cardiovascular disease: Springer.*

Bushberg, J. T. (2002). *The essential physics of medical imaging: Lippincott Williams & Wilkins.*

Carabello, B. A. (2007). Aortic valve disease *Cardiovascular Medicine* (pp. 381-392): Springer.

Chambers, J. B., Myerson, S. G., Rajani, R., Morgan-Hughes, G. J., & Dweck, M. R. (2016). Multimodality imaging in heart valve disease. *Open heart*, 3(1), e000330.

Chan, K.-L., Liu, X., Ascah, K. J., Beauchesne, L. M., & Burwash, I. G. (2004). Comparison of real-time 3-dimensional echocardiography with conventional 2-dimensional echocardiography in the assessment of structural heart disease. *Journal of the American Society of Echocardiography*, 17(9), 976-980.

Chen, J. J., Manning, M. A., Frazier, A. A., Jeudy, J., & White, C. S. (2009). CT angiography of the cardiac valves: normal, diseased, and postoperative appearances. *Radiographics*, 29(5), 1393-1412.

Chun, E. J., Choi, S. I., Lim, C., Park, K.-H., Chang, H.-J., Choi, D.-J., Kim, D. H., Lee, W., & Park, J. H. (2008). Aortic stenosis: evaluation with multidetector CT angiography and MR imaging. *Korean journal of radiology*, 9(5), 439-448.

Cohen, J. (1960). A coefficient of agreement for nominal scales. *Educational and psychological measurement*, 20(1), 37-46.

Cremer, P., Hachamovitch, R., & Tamarappoo, B. (2014). Clinical Decision Making With Myocardial Perfusion Imaging in Patients With Known or Suspected Coronary Artery Disease. *Seminars in nuclear medicine*, 44(4), 320-329.

Dennis, J., & Torczon, V. J. (1994). Derivative-free pattern search methods for multidisciplinary design problems. *Paper presented at the The Fifth AIAA/USAF/NASA/ISSMO Symposium on Multidisciplinary Analysis and Optimization.*

- Driscoll, D. J. (2016). Normal Cardiac Anatomy and Clinical Evaluation *Congenital Heart Diseases: The Broken Heart* (pp. 11-21): Springer.
- Dymarkowski, S., & Bosmans, H. (2005). Cardiac MRI physics *Clinical Cardiac MRI* (pp. 1-31): Springer.
- Enriquez-Sarano, M. L., & Frye, R. L. (2007). Mitral Valve Diseases. In J. T. Willerson, H. J. J. Wellens, J. N. Cohn, & D. R. Holmes (Eds.), *Cardiovascular Medicine* (pp. 397-430). London: Springer London.
- Evangelista, A., Flachskampf, F. A., Erbel, R., Antonini-Canterin, F., Vlachopoulos, C., Rocchi, G., Sicari, R., Nihoyannopoulos, P., Zamorano, J., & Reviewers:, D. (2010). Echocardiography in aortic diseases: EAE recommendations for clinical practice. *European Journal of Echocardiography*, *11*(8), 645-658.
- Faber, T. L., McColl, R. W., Opperman, R. M., Corbett, J. R., & Peshock, R. M. (1991). Spatial and temporal registration of cardiac SPECT and MR images: methods and evaluation. *Radiology*, *179*(3), 857-861.
- Feuchtner, G. (2013). Imaging of cardiac valves by computed tomography. *Scientifica*, *2013*.
- Fox, J., Pandit-Taskar, N., & Strauss, H. W. (2013). Cardiac anatomy and pathophysiology of coronary circulation as a basis for imaging *From Basic Cardiac Imaging to Image Fusion* (pp. 1-14): Springer.
- Frost, V. S., Stiles, J. A., Shanmugan, K. S., & Holtzman, J. C. (1982). A model for radar images and its application to adaptive digital filtering of multiplicative noise. *IEEE Transactions on pattern analysis and machine intelligence*(2), 157-166.
- Fung, Y.-c. (2013). Biomechanics: circulation: *Springer Science & Business Media*.
- García-Fernández, M. A., & Caso, P. (2009). Echocardiography: Basic Principles. In J. L. Zamorano, J. J. Bax, F. E. Rademakers, & J. Knuuti (Eds.), *The ESC Textbook of Cardiovascular Imaging* (pp. 1-38). London: Springer London.
- Gardner, T. J., Horneffer, P. J., Manolio, T. A., Pearson, T. A., Gott, V. L., Baumgartner, W. A., Borkon, A. M., Watkins, L., & Reitz, B. A. (1985). Stroke Following Coronary Artery Bypass Grafting: A Ten-Year Study. *The Annals of thoracic surgery*, *40*(6), 574-581.
- Gilardi, M. C., Rizzo, G., Savi, A., Landoni, C., Bettinardi, V., Rossetti, C., Striano, G., & Fazio, F. (1998). Correlation of SPECT and PET cardiac images by a surface

matching registration technique. *Computerized Medical Imaging and Graphics*, 22(5), 391-398.

- Gong, M., Zhao, S., Jiao, L., Tian, D., & Wang, S. (2014). A novel coarse-to-fine scheme for automatic image registration based on SIFT and mutual information. *IEEE Transactions on Geoscience and Remote Sensing*, 52(7), 4328-4338.
- Grau, V., Becher, H., & Noble, J. A. (2007). Registration of multiview real-time 3-D echocardiographic sequences. *Medical Imaging, IEEE Transactions on*, 26(9), 1154-1165.
- Grewal, J., Mankad, S., Freeman, W. K., Click, R. L., Suri, R. M., Abel, M. D., Oh, J. K., Pellikka, P. A., Nesbitt, G. C., & Syed, I. (2009). Real-time three-dimensional transesophageal echocardiography in the intraoperative assessment of mitral valve disease. *Journal of the American Society of Echocardiography*, 22(1), 34-41.
- Guéziec, A., Kazanzides, P., Williamson, B., & Taylor, R. H. (1998). Anatomy-based registration of CT-scan and intraoperative X-ray images for guiding a surgical robot. *Ieee Transactions on Medical Imaging*, 17(5), 715-728.
- Hacihaliloglu, I., Hodgson, A., Abugharbieh, R., & Rohling, R. (2009). Assessing surface localization accuracy in 3D local phase ultrasound images using CT reference images. *Computer Assisted Orthopaedic Surgery (CAOS)*, 137-140.
- Hahn, R. T. (2013). Use of imaging for procedural guidance during transcatheter aortic valve replacement. *Current opinion in cardiology*, 28(5), 512-517.
- Healthwise-Incorporated. (2016). Aortic Valve Stenosis. Retrieved from <https://myhealth.alberta.ca/Health/pages/conditions.aspx?hwid=hw179837>
- Heart Valve Society of America. (2017). Retrieved from <http://www.heartvalvesocietyofamerica.org/more.html>
- Hill, D., & Hawkes, D. (2000). Handbook of Medical Imaging: Processing and Analysis, chapter Across-modality registration using intensity-based cost functions. *New York: Academic*, 537-553.
- Hill, D. L., Batchelor, P. G., Holden, M., & Hawkes, D. J. (2001). Medical image registration. *Physics in medicine and biology*, 46(3), R1.
- Hipwell, J. H., Penney, G. P., McLaughlin, R. A., Rhode, K., Summers, P., Cox, T. C., Byrne, J. V., Noble, J. A., & Hawkes, D. J. (2003). Intensity-based 2-D-3-D registration of cerebral angiograms. *Ieee Transactions on Medical Imaging*, 22(11), 1417-1426.

- Ho, S. Y. (2002). Anatomy of the mitral valve. *Heart*, 88(suppl 4), iv5-iv10.
- Huang, X., Moore, J., Guiraudon, G., Jones, D. L., Bainbridge, D., Ren, J., & Peters, T. M. (2009). Dynamic 2D Ultrasound and 3D CT Image Registration of the Beating Heart. *Ieee Transactions on Medical Imaging*, 28(8), 1179-1189.
- Ibanez, L., Schroeder, W., Ng, L., & Cates, J. (2015). The insight segmentation and registration toolkit. *Software Guide*.
- Iung, B., Baron, G., Butchart, E. G., Delahaye, F., Gohlke-Bärwolf, C., Levang, O. W., Tornos, P., Vanoverschelde, J.-L., Vermeer, F., Boersma, E., Ravaud, P., & Vahanian, A. (2003). A prospective survey of patients with valvular heart disease in Europe: The Euro Heart Survey on Valvular Heart Disease. *European Heart Journal*, 24(13), 1231-1243.
- Kawakita, S. (1986). Rheumatic fever and rheumatic heart disease in Japan. *Japanese circulation journal*, 50(12), 1241-1245.
- Kenny, T. (2013). Cardiovascular anatomy and physiology. *The Nuts and Bolts of Implantable Device Therapy Pacemakers*, 1-14.
- Khalil, A., Faisal, A., Lai, K. W., Ng, S. C., & Liew, Y. M. (2016). 2D to 3D fusion of echocardiography and cardiac CT for TAVR and TAVI image guidance. *Medical & Biological Engineering & Computing*, 1-10.
- Khalil, A., Faisal, A., Lai, K. W., Ng, S. C., & Liew, Y. M. (2017). Multimodality Registration of 2D Echocardiography and Cardiac CT for the Mitral Valve Diagnosis and Surgical Planning. *Journal of Medical Imaging*.
- Khurshid, K., McGough, R. J., & Berger, K. (2008). Automated cardiac motion compensation in PET/CT for accurate reconstruction of PET myocardial perfusion images. *Physics in medicine and biology*, 53(20), 5705.
- Kiss, G., Ford, S., Claus, P., D'hooge, J., & Torp, H. (2013). *Fusion of 3D echo and cardiac magnetic resonance volumes during live scanning*. Paper presented at the 2013 IEEE International Ultrasonics Symposium (IUS).
- Klein, S., Staring, M., & Pluim, J. P. (2007). Evaluation of optimization methods for nonrigid medical image registration using mutual information and B-splines. *IEEE Transactions on image processing*, 16(12), 2879-2890.
- Korpas, D. (2013). Heart Anatomy and Physiology *Implantable Cardiac Devices Technology* (pp. 13-18): Springer.

- Kühl, H. P., Schreckenber, M., Rulands, D., Katoh, M., Schäfer, W., Schummers, G., Bücken, A., Hanrath, P., & Franke, A. (2004). High-resolution transthoracic real-time three-dimensional echocardiography: quantitation of cardiac volumes and function using semi-automatic border detection and comparison with cardiac magnetic resonance imaging. *Journal of the American College of Cardiology*, 43(11), 2083-2090.
- Lang, P., Rajchl, M., Li, F., & Peters, T. M. (2011). *Towards model-enhanced real-time ultrasound guided cardiac interventions*. Paper presented at the Intelligent Computation and Bio-Medical Instrumentation (ICBMI), 2011 International Conference on. IEEE.
- Lazo, D. (2014). *Fundamentals of sectional anatomy: an imaging approach*: Nelson Education.
- Ledesma-Carbayo, M. J., Kybic, J., Desco, M., Santos, A., Suhling, M., Hunziker, P., & Unser, M. (2005). Spatio-temporal nonrigid registration for ultrasound cardiac motion estimation. *Ieee Transactions on Medical Imaging*, 24(9), 1113-1126.
- Lee, J.-S. (1980). Digital image enhancement and noise filtering by use of local statistics. *IEEE Transactions on pattern analysis and machine intelligence*(2), 165-168.
- Leon, M. B., Smith, C. R., Mack, M., Miller, D. C., Moses, J. W., Svensson, L. G., Tuzcu, E. M., Webb, J. G., Fontana, G. P., & Makkar, R. R. (2010). Transcatheter aortic-valve implantation for aortic stenosis in patients who cannot undergo surgery. *New England Journal of Medicine*, 363(17), 1597-1607.
- Lester, H., & Arridge, S. R. (1999). A survey of hierarchical non-linear medical image registration. *Pattern recognition*, 32(1), 129-149.
- Levick, J. R. (2013). *An introduction to cardiovascular physiology: Butterworth-Heinemann*.
- Li, F., Lang, P., Rajchl, M., Chen, E. C., Guiraudon, G., & Peters, T. M. (2012). Towards real-time 3D US-CT registration on the beating heart for guidance of minimally invasive cardiac interventions. *Paper presented at the Proc. SPIE*.
- Li, F. P., Rajchl, M., White, J. A., Goela, A., & Peters, T. M. (2013). Generation of synthetic 4D cardiac CT images for guidance of minimally invasive beating heart interventions. *Paper presented at the International Conference on Information Processing in Computer-Assisted Interventions*.

- Li, F. P., Rajchl, M., White, J. A., Goela, A., & Peters, T. M. (2015). Ultrasound Guidance for Beating Heart Mitral Valve Repair Augmented by Synthetic Dynamic CT. *Medical Imaging, IEEE Transactions on*, 34(10), 2025-2035.
- Liew, Y., McLaughlin, R., Chan, B., Aziz, Y. A., Chee, K., Ung, N., Tan, L., Lai, K., Ng, S., & Lim, E. (2015). Motion corrected LV quantification based on 3D modelling for improved functional assessment in cardiac MRI. *Physics in medicine and biology*, 60(7), 2715.
- Linte, C. A., Moore, J., Wedlake, C., Bainbridge, D., Guiraudon, G. M., Jones, D. L., & Peters, T. M. (2009). Inside the beating heart: An in vivo feasibility study on fusing pre-and intra-operative imaging for minimally invasive therapy. *International Journal of Computer Assisted Radiology and Surgery*, 4(2), 113.
- Linte, C. A., Wierzbicki, M., Moore, J., Guiraudon, G., Jones, D. L., & Peters, T. M. (2007). On enhancing planning and navigation of beating-heart mitral valve surgery using pre-operative cardiac models. *Paper presented at the Engineering in Medicine and Biology Society, 2007. EMBS 2007. 29th Annual International Conference of the IEEE*.
- Maes, F., Collignon, A., Vandermeulen, D., Marchal, G., & Suetens, P. (1997). Multimodality image registration by maximization of mutual information. *Ieee Transactions on Medical Imaging*, 16(2), 187-198.
- Maffessanti, F., Addetia, K., Murtagh, G., Weinert, L., Patel, A. R., Lang, R. M., & Mor-Avi, V. (2014). Fusion imaging of computed tomography and 3D echocardiography: Combined assessment of coronary anatomy and myocardial function. *Paper presented at the Computing in Cardiology Conference (CinC), 2014*.
- Mahesh, M., & Cody, D. D. (2007). Physics of cardiac imaging with multiple-row detector CT. *Radiographics*, 27(5), 1495-1509.
- Maintz, J. A., & Viergever, M. A. (1998). A survey of medical image registration. *Medical Image Analysis*, 2(1), 1-36.
- Mäkelä, T., Clarysse, P., Sipilä, O., Pauna, N., Pham, Q. C., Katila, T., & Magnin, I. E. (2002). A review of cardiac image registration methods. *Medical Imaging, IEEE Transactions on*, 21(9), 1011-1021.
- Manning, W., & Pennell, D. (2002). Cardiovascular Magnetic Resonance Churchill Livingstone. *New York*.

- Marijon , E., Ou , P., Celermajer , D. S., Ferreira , B., Mocumbi , A. O., Jani , D., Paquet , C., Jacob , S., Sidi , D., & Jouven , X. (2007). Prevalence of Rheumatic Heart Disease Detected by Echocardiographic Screening. *New England Journal of Medicine*, 357(5), 470-476.
- Marinelli, M., Positano, V., Tucci, F., Neglia, D., & Landini, L. (2012). Automatic PET-CT Image Registration Method Based on Mutual Information and Genetic Algorithms. *The Scientific World Journal*, 2012, 567067.
- Marzullo, P., & Mariani, G. (2016). From Basic Cardiac Imaging to Image Fusion: *Springer*.
- Messika-Zeitoun, D., Serfaty, J.-M., Laissy, J.-P., Berhili, M., Brochet, E., Iung, B., & Vahanian, A. (2006). Assessment of the Mitral Valve Area in Patients With Mitral Stenosis by Multislice Computed Tomography. *Journal of the American College of Cardiology*, 48(2), 411-413.
- Mikic, I., Krucinski, S., & Thomas, J. D. (1998). Segmentation and tracking in echocardiographic sequences: Active contours guided by optical flow estimates. *Ieee Transactions on Medical Imaging*, 17(2), 274-284.
- Momma, M., & Bennett, K. P. (2002). A pattern search method for model selection of support vector regression. *Paper presented at the Proceedings of the 2002 SIAM International Conference on Data Mining*.
- Morris, M. F., Maleszewski, J. J., Suri, R. M., Burkhart, H. M., Foley, T. A., Bonnicksen, C. R., Anavekar, N. S., Young, P. M., Williamson, E. E., & Glockner, J. F. (2010). CT and MR Imaging of the Mitral Valve: Radiologic-Pathologic Correlation 1. *Radiographics*, 30(6), 1603-1620.
- Moscucci, M. (2013). Grossman & Baim's cardiac catheterization, angiography, and intervention: *Lippincott Williams & Wilkins*.
- Newman, M. F., Mathew, J. P., Grocott, H. P., Mackensen, G. B., Monk, T., Welsh-Bohmer, K. A., Blumenthal, J. A., Laskowitz, D. T., & Mark, D. B. (2006). Central nervous system injury associated with cardiac surgery. *The Lancet*, 368(9536), 694-703.
- Nishimura, R. A. (2002). Aortic valve disease. *Circulation*, 106(7), 770-772.
- Nobuyoshi, M., Arita, T., Shirai, S.-i., Hamasaki, N., Yokoi, H., Iwabuchi, M., Yasumoto, H., & Nosaka, H. (2009). Percutaneous Balloon Mitral Valvuloplasty. *A Review*, 119(8), e211-e219.

- O'Connor, M. K. (2000). Evaluation of motion-correction techniques in cardiac SPECT. *The Journal of Nuclear Medicine*, 41(7), 1298.
- Omran, A. S., Arifi, A. A., & Mohamed, A. A. (2010). Echocardiography of the mitral valve. *Journal of the Saudi Heart Association*, 22(3), 165-170.
- Osnabrugge, R. L., Mylotte, D., Head, S. J., Van Mieghem, N. M., Nkomo, V. T., LeReun, C. M., Bogers, A. J., Piazza, N., & Kappetein, A. P. (2013). Aortic stenosis in the elderly: disease prevalence and number of candidates for transcatheter aortic valve replacement: a meta-analysis and modeling study. *Journal of the American College of Cardiology*, 62(11), 1002-1012.
- Otto, C. M. (2012). The practice of clinical echocardiography: *Elsevier Health Sciences*.
- Pallotta, S., Gilardi, M., Bettinardi, V., Rizzo, G., Landoni, C., Striano, G., Masi, R., & Fazio, F. (1995). Application of a surface matching image registration technique to the correlation of cardiac studies in positron emission tomography (PET) by transmission images. *Physics in medicine and biology*, 40(10), 1695.
- Pankratov, M., Benetti, F., & Vivian, J. (2005). Method for non-invasive heart treatment: *Google Patents*.
- Perona, P., & Malik, J. (1990). Scale-space and edge detection using anisotropic diffusion. *IEEE Transactions on pattern analysis and machine intelligence*, 12(7), 629-639.
- Pluim, J. P., Maintz, J. A., & Viergever, M. A. (2003). Mutual-information-based registration of medical images: a survey. *Ieee Transactions on Medical Imaging*, 22(8), 986-1004.
- Rafael Gonzalez, C., & Woods, R. (2002). Digital image processing. *Pearson Education*.
- Sandoval, Z. L., & Dillenseger, J.-L. (2013). Evaluation of computed tomography to ultrasound 2D image registration for atrial fibrillation treatment. *Paper presented at the Computing in Cardiology Conference (CinC), 2013*.
- Shekhar, R., & Zagrotsky, V. (2002). Mutual information-based rigid and nonrigid registration of ultrasound volumes. *Ieee Transactions on Medical Imaging*, 21(1), 9-22.
- Singh, J. P., Evans, J. C., Levy, D., Larson, M. G., Freed, L. A., Fuller, D. L., Lehman, B., & Benjamin, E. J. (1999). Prevalence and clinical determinants of mitral, tricuspid, and aortic regurgitation (the Framingham Heart Study). *The American journal of cardiology*, 83(6), 897-902.

- Sinha, S., Sinha, U., Czernin, J., Porenta, G., & Schelbert, H. (1995). Noninvasive assessment of myocardial perfusion and metabolism: feasibility of registering gated MR and PET images. *AJR. American journal of roentgenology*, 164(2), 301-307.
- Slogoff, S., Reul, G. J., Keats, A. S., Curry, G. R., Crum, M. E., Elmquist, B. A., Giesecke, N. M., Jistel, J. R., Rogers, L. K., & Soderberg, J. D. (1990). Role of perfusion pressure and flow in major organ dysfunction after cardiopulmonary bypass. *The Annals of thoracic surgery*, 50(6), 911-918.
- Song, G., Avants, B. B., & Gee, J. C. (2007). Multi-start method with prior learning for image registration. *Paper presented at the Computer Vision, 2007. ICCV 2007. IEEE 11th International Conference on*.
- Stock, R. G., Stone, N. N., DeWyngaert, J. K., Lavagnini, P., & Unger, P. D. (1996). Prostate specific antigen findings and biopsy results following interactive ultrasound guided transperineal brachytherapy for early stage prostate carcinoma. *Cancer*, 77(11), 2386-2392.
- Suetens, P. (2017). *Fundamentals of medical imaging*: Cambridge university press.
- Sun, Y., Kadoury, S., Li, Y., John, M., Resnick, J., Plambeck, G., Liao, R., Sauer, F., & Xu, C. (2007). Image guidance of intracardiac ultrasound with fusion of pre-operative images. *Medical Image Computing and Computer-Assisted Intervention–MICCAI 2007*, 60-67.
- Szpala, S., Wierzbicki, M., Guiraudon, G., & Peters, T. M. (2005). Real-time fusion of endoscopic views with dynamic 3-D cardiac images: a phantom study. *Ieee Transactions on Medical Imaging*, 24(9), 1207-1215.
- Tabrizi, M. H., Dong, K., & Movahed, A. (2001). Performance comparison of different motion correction algorithms used in cardiac SPECT imaging. *Paper presented at the Information Technology: Coding and Computing, 2001. Proceedings. International Conference on*.
- Tavard, F., Simon, A., Leclercq, C., Donal, E., Hernández, A. I., & Garreau, M. (2014). Multimodal registration and data fusion for cardiac resynchronization therapy optimization. *Medical Imaging, IEEE Transactions on*, 33(6), 1363-1372.
- Tsang, M. Y., Choi, J.-O., Borlaug, B. A., Greason, K. L., Cha, S. S., Nishimura, R. A., & Oh, J. K. (2015). Low-Flow, Low-Gradient Severe Aortic Stenosis in the Setting of Constrictive Pericarditis Clinical Characteristics, Echocardiographic Features, and Outcomes. *Circulation: Cardiovascular Imaging*, 8(7), e002812.

- Turgeon, G. A., Lehmann, G., Guiraudon, G., Drangova, M., Holdsworth, D., & Peters, T. (2005). 2D - 3D registration of coronary angiograms for cardiac procedure planning and guidance. *Medical Physics*, 32(12), 3737-3749.
- Turi, Z. G. (2004). Mitral Valve Disease. *Circulation*, 109(6), e38-e41.
- Weese, J., Penney, G. P., Desmedt, P., Buzug, T. M., Hill, D. L., & Hawkes, D. J. (1997). Voxel-based 2-D/3-D registration of fluoroscopy images and CT scans for image-guided surgery. *IEEE transactions on information technology in biomedicine*, 1(4), 284-293.
- Welsh, J. (2013). Heart, circulation and blood cells. *Physiology of mollusca*, 2, 125-174.
- Wu, W., Acton, S. T., & Lach, J. (2006). Real-time processing of ultrasound images with speckle reducing anisotropic diffusion. *Paper presented at the Signals, Systems and Computers, 2006. ACSSC'06. Fortieth Asilomar Conference on*.
- Yamashita, Y., Matsukawa, T., Arakawa, A., Hatanaka, Y., Urata, J., & Takahashi, M. (1995). US-guided liver biopsy: predicting the effect of interventional treatment of hepatocellular carcinoma. *Radiology*, 196(3), 799-804.
- Yoon, H. S., Park, M. Y., Shin, W. Y., Sco, B. S., & Cho, S. H. (1995). Changes of Clinical Patterns of the Acute Rheumatic Fever in Korea (Compared report of 1973-1985 with that of 1986-1992). *Korean Journal of Pediatrics*, 38(4), 470-481.
- Yu, Y., & Acton, S. T. (2002). Speckle reducing anisotropic diffusion. *IEEE Transactions on image processing*, 11(11), 1260-1270.
- Zheng, Y., John, M., Liao, R., Nottling, A., Boese, J., Kempfert, J., Walther, T., Brockmann, G., & Comaniciu, D. (2012). Automatic aorta segmentation and valve landmark detection in C-arm CT for transcatheter aortic valve implantation. *Ieee Transactions on Medical Imaging*, 31(12), 2307-2321.
- Zhimin, W., Yubao, Z., Lei, S., Xianliang, Z., Wei, Z., Li, S., Hao, W., Jianjun, L., Detrano, R., & Rutai, H. (2006). Prevalence of chronic rheumatic heart disease in Chinese adults. *International journal of cardiology*, 107(3), 356-359.
- Zhong, H., Kanade, T., & Schwartzman, D. (2006). "virtual touch": An efficient registration method for catheter navigation in left atrium. *Medical Image Computing and Computer-Assisted Intervention-MICCAI 2006*, 437-444.

Zhu, Y.-M., & Cochoff, S. M. (2002). Influence of implementation parameters on registration of MR and SPECT brain images by maximization of mutual information. *Journal of nuclear medicine*, 43(2), 160-166.

Zitova, B., & Flusser, J. (2003). Image registration methods: a survey. *Image and vision computing*, 21(11), 977-1000.

Zou, K. H., Warfield, S. K., Bharatha, A., Tempany, C. M., Kaus, M. R., Haker, S. J., Wells, W. M., Jolesz, F. A., & Kikinis, R. (2004). Statistical validation of image segmentation quality based on a spatial overlap index 1: Scientific reports. *Academic radiology*, 11(2), 178-189.

University of Malaya

## LIST OF PUBLICATIONS AND PAPERS PRESENTED

### Article in Academic Journals

Khalil, A., Faisal, A., Lai, K. W., Ng, S. C., & Liew, Y. M. (2016). 2D to 3D fusion of echocardiography and cardiac CT for TAVR and TAVI image guidance. *Medical & Biological Engineering & Computing*, 1-10. (ISI-Indexed)

Khalil, A., Faisal, A., Lai, K. W., Ng, S. C., & Liew, Y. M. (2017). Multimodality Registration of 2D Echocardiography and Cardiac CT for the Mitral Valve Diagnosis and Surgical Planning. *Journal of Medical Imaging*. (ISI – Indexed)

### Proceeding

Khalil, A., Faisal, A., Ng, S.-C., Liew, Y. M., & Lai, K. W. (2016, 14-16 Sept. 2016). Echocardiography to cardiac CT image registration: Spatial and temporal registration of the 2D planar echocardiography images with cardiac CT volume. *Paper presented at the 2016 IEEE 18th International Conference on e-Health Networking, Applications and Services (Healthcom)*. (ISI-Indexed)

Khalil, A., Faisal, A., Ng, S.-C., Liew, Y. M., & Lai, K. W. (2017). Mitral valve rigid registration using 2D echocardiography and cardiac computed tomography. *Paper presented at the Applied System Innovation (ICASI), 2017 International Conference on*. (ISI-Indexed)